Characterization of Junctional Proteins in the Dorsal Root Ganglion of Rats with Traumatic Nerve Injury

Charakterisierung von Junktionsproteinen im
Spinalganglion von Ratten mit traumatischer Nervenverletzung

Doctoral thesis for a medical doctoral degree
at the Graduate School of Life Sciences,
Julius-Maximilians-Universität Würzburg,
Section Neuroscience

submitted by
Thomas Joachim Lux

from
Frankfurt am Main

Würzburg……..

Submitted on: ……..……..

Office stamp

Members of the Thesis Committee:

Chairperson: Prof. Dr. Philip Tovote

Primary Supervisor: Prof. Dr. Heike L. Rittner

Supervisor (Second): Prof. Dr. Robert J. Kittel

Supervisor (Third): PD Dr. Robert Blum

Supervisor (Fourth): Dr. Jeremy T.-C. Chen

Date of Public Defence: ……..……

Date of Receipt of Certificates: …….

Acknowledgements

Firstly, I want to thank my parents and my sister who always supported me. Without you I would not have been able to achieve this.
Secondly, I am grateful for my supervisors and co-workers. Prof. Rittner had the patience to let me try things my way and always helped me as soon as I got stuck. Dr. Chen spent endless time trying to figure out where we could optimize our experiments and always helped me out.
Thanks to you and my fellow students, special thanks to you Christina and Carla, I had a great time working with you.

And lastly, always think of these wise words:

"Everything not saved will be lost."
- Nintendo "Quit Screen" message

Affidavit

I hereby confirm that my thesis entitled "*Characterization of Junctional Proteins in the Dorsal Root Ganglion of Rats with Traumatic Nerve Injury*" is the result of my own work. I did not receive any help or support from commercial consultants. All sources and / or materials applied are listed and specified in the thesis.

Furthermore, I confirm that this thesis has not yet been submitted as part of another examination process neither in identical nor in similar form.

Place, Date Signature

Eidesstattliche Erklärung

Hiermit erkläre ich an Eides statt, die Dissertation "*Charakterisierung von Junktionsproteinen im Spinalganglion von Ratten mit traumatischer Nervenverletzung*" eigenständig, d.h. insbesondere selbständig und ohne Hilfe eines kommerziellen Promotionsberaters, angefertigt und keine anderen als die von mir angegebenen Quellen und Hilfsmittel verwendet zu haben.

Ich erkläre außerdem, dass die Dissertation weder in gleicher noch in ähnlicher Form bereits in einem anderen Prüfungsverfahren vorgelegen hat.

Ort, Datum Unterschrift

1 Inhalt

2 Introduction

This work characterizes the expression pattern of the adhesion G protein-coupled receptors (aGPCR) latrophilin-1 (Adgrl1) and latrophilin-3 (Adgrl3), as well as the tight junction proteins claudin-1, claudin-5, claudin-12, claudin-19, and the tight junction associated protein ZO-1 in the dorsal root ganglion of rats with and without traumatic mononeuropathy.

2.1 Neuropathic Pain

The International Association for the Study of Pain defines neuropathic pain as a ”pain caused by a lesion or disease of the somatosensory nervous system”. This definition includes a multitude of aetiologies, which range from metabolic conditions to blunt trauma, as well as their wide range of clinical manifestations. If pain originates from a lesion or disease of the somatosensory system, it is classified as neuropathic pain. Therefore, neuropathic pain is defined as a clinical syndrome, rather than a specific disease. Conventional analgesics like non-steroidal anti-inflammatory drugs have a limited effect on patients' symptoms and current therapy relies mostly on antidepressants, antiepileptics, and opioids [1]. Despite medication and physical therapy, patients often report a significant negative impact of their disease on their life quality [1, 2].

2.1.1 Clinical Relevance

According to the definition of the International Association for the Study of Pain, pain is a subjective sensation. This sensation combines input from the sensory system, past experiences, as well as emotional components. Its evolutionary importance lies in its warning function, which informs an organism of actual or potential tissue damage. The sensory component of pain perception is called nociception and is mediated by polymodal sensory neurons, the nociceptors. These nociceptors are connected to the sensory cortex, as explained in chapter 2.1.2, but they are also linked to the limbic system causing acute and chronic affective reactions. These reactions severely influence and shape an organism's behaviour, well-being and functionality [3].

The estimated global prevalence of chronic pain varies between 1 and 18 %. Due to the lack of objective measurement or quantification of pain, inclusion criteria vary between studies [4]. Physicians may quantify heat, cold, and mechanical pain threshold as well as other sensory qualities often affected in neuropathic conditions utilizing sophisticated methods like quantitative sensory testing. Nevertheless, they are often time-consuming, require a high level

of expertise, and do not measure spontaneous pain [5, 6]. Besides the obvious ethical responsibility to prevent pain and due to the high prevalence, as well as the severe and very individual impact of chronic pain on patients, the economic and social consequences on society must be noticed. While the direct cost of chronic pain treatment is one factor, a Swedish study revealed 91% of socioeconomic costs originating from chronic pain related to production loss due to sick leave [7].

Therefore, ways to understand and consequently reduce this highly prevalent cause of suffering and socioeconomic deficits must be the focus of further research efforts.

2.1.2 Physiology of Pain Sensation

Neuropathic pain originates from lesions or diseases of the somatosensory system. Depending on time-course (acute, sub-acute, chronic), localisation (symmetric, asymmetric, and mono-, polyneuropathy) as well as electrophysiological test results (axonal, demyelinating), a list of possible differential diagnoses is made, and they are usually classified into several categories.

Sensory neurons *somata* reside in the neuron rich region of the dorsal root ganglion. The axons of pseudo-unipolar neurons form the second distinct region of the dorsal root ganglion, the fibre rich region. Additionally, first morphological studies divided the dorsal root ganglia's cell population into groups of large and small cells.

A primary sensory neuron whose activity leads to the sensation of pain is called a nociceptive neuron and their afferences lead to the spinal cord or the brain stem where they form synapses. Primary nociceptive afferents are part of the posterior root and enter the spinal cord with fibres of other primary sensory neurons. In contrast to mechanosensory and proprioceptive neurons', thermosensitive and nociceptive neurons' fibres cross to the contralateral side of the spinal cord before ascending the in the *tractus spinothalamicus anterior* and *lateralis* (anterolateral system). The axon enters the ventral posterior nucleus of the thalamus and is connected to the third neuron whose axon is connected to the somatosensory cortex located in the *gyrus postcentralis*. Central mechanisms are also able to inhibit nociceptive neurons via descending pathways in the *periaqueductal grey.* Another relevant pathway of nociception activates the reticular formation and subsequently the ascending reticular activating system. As a result, the whole cortex's activation level and the organism's attention level rises. Figure 1 (adapted from [8]) illustrates a schematic of the signal transduction needed for perception of a noxious stimulus.

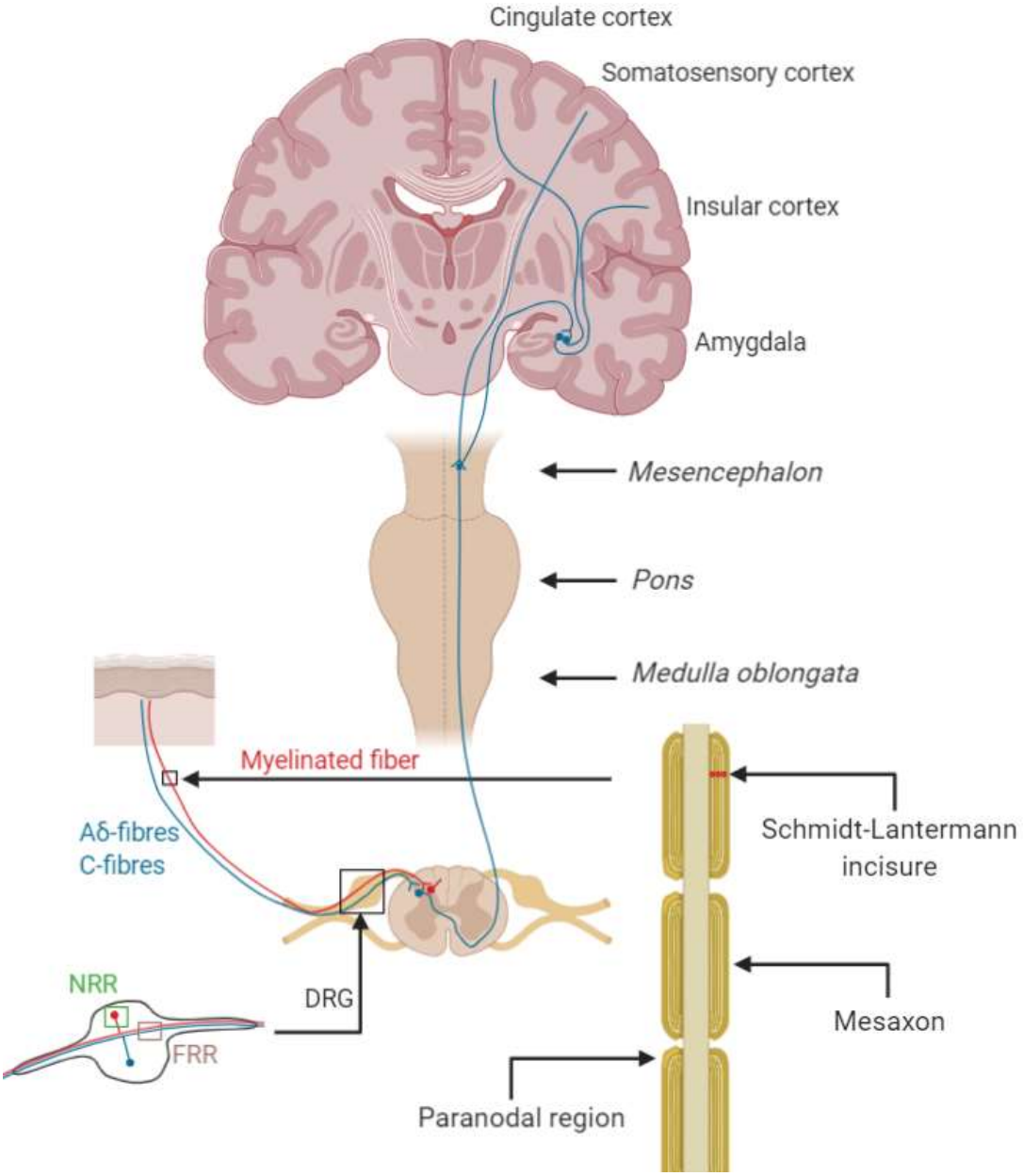

Figure 1. The pain pathway. Noxious stimuli are detected by nociceptors and transmitted to the somatosensory, insular cingulate gyrus. This causes pain perception as well as autonomous reactions. Pain is perceived by the pseudo unipolar first order neurons, whose somata reside in the dorsal root ganglion's neuron rich region (NRR, exemplary region framed in green). The somata are connected to the fibres in the fibre rich region (FRR, exemplary region framed in red) with a T-stem like structure. Depending on fibre type, the fibre's myelination and tight junction protein expression differs. After signal transmission to the second-order neuron, the fibres cross to the spinal cords contralateral side via the commisura anterior and ascend in the tractus spinothalamicus anterior and lateralis composing the extralemniscal system. The third-order neuron's cell body is in the thalamus. Besides the somatosensory cortex for pain localization and conscious feeling, target neurons of the pain pathway include the cingulate cortex, the amygdala, the insular cortex, and the formatio reticularis for emotional and autonomous reaction. (Created with bioRender®)

Cellular signal transduction relies on metabotropic and ionotropic signalling. Alterations regarding any component of these mechanisms may increase or decrease cell sensitivity on almost all levels of the somatosensory pathway. Exemplary, a single loss of function mutation in a nociceptor-specific sodium channel might disable the organism to feel pain [9]. Furthermore, central sensitization caused by lack of inhibitory neurotransmitters may lead otherwise sub-threshold signals to cause pain sensation [10, 11]. As these mechanisms may cause states of pain, they may also harbour answers to the question of novel therapeutic strategies. Detailed knowledge regarding nociceptors and their physiology exceed this thesis' scope but can be found in an excellent review by Dubin et al. [12].

Traumatic nerve injury causes Wallerian degeneration, resulting in demyelination, axon degeneration and phagocytosis [13]. This process, the focus of the next chapter, is associated with blood-nerve-barrier breakdown, which in turn is accompanied by the emergence of neuropathic pain [14].

2.1.3 Animal Models of Neuropathic Pain

Several neuropathic pain animal models are known. Models mimicking metabolically and chemotherapy-induced as well as traumatic neuropathy have been established in the past [15]. For traumatic mononeuropathy, commonly used models are nerve crush, spared nerve injury, and chronic constriction injury (CCI) [16-18]. As this thesis' experiments utilize CCI, Figure 2 demonstrates the outcome of the surgical procedure: The sciatic nerve is ligated loosely, which causes nerve irritation, intraneural oedema, inflammation and neurodegeneration [19, 20].

The early phase of a traumatic mononeuropathy includes the first seven days. During this week animals develop increasing thermic and mechanical hypersensitivity, allodynia and spontaneous pain associated behaviour. These reach their maximum seven days after the procedure. The early phase is followed by the recovery phase. Until three to six weeks after CCI nociceptive thresholds typically return to normal.

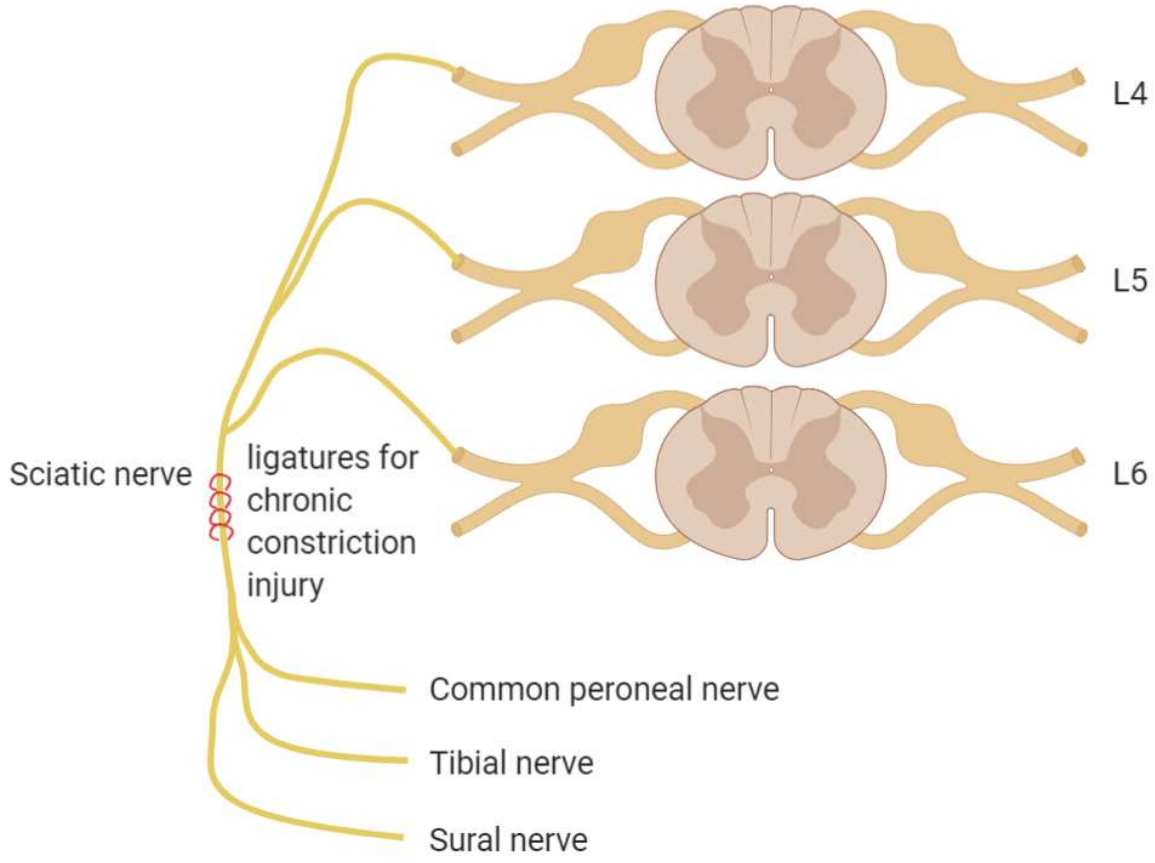

Figure 2. The CCI model. After anaesthesia, the sciatic nerve is exposed and loose silk ligatures are applied, causing tissue damage to the peripheral nerve, but not complete necrosis. The ligatures affect nerve fibres from segments L4-6. (Created with bioRender®)

2.2 The Dorsal Root Ganglion

The nervous system is divided into its central and peripheral nervous part. The dorsal root ganglion is a component of the peripheral nervous system and harbours the *somata* of the pseudo unipolar primary sensory neurons. Neurons in the dorsal root ganglion are arranged in a rough somatotopy [21]. Signal transmission is achieved through action potential generation and is characterized by membrane depolarisation carried by a sodium current. Repolarization of these neurons is driven by a potassium current. The pseudounipolar neurons' T-junction can intervene in signal propagation by acting as a filter [22-24].

Nerve fibres are divided into myelinated fibres surrounded by Schwann cells and non-myelinated fibres. Multiple nerve fibres are embedded in the endoneurium and sheathed by the perineurium to form a nerve fascicle. During development of the nervous system, nerves sprout from the spinal canal to the periphery and are still surrounded by extensions of the *dura mater*. This layer of protection is the epineurium. It embeds multiple nerve fascicles with its inner layer

and sheathes them with its mechanically strong outer layer, completing the structure of the peripheral nerve [25]. According to morphological features the dorsal root ganglion is divided into neuron rich and fibre rich regions. The neuron rich region possesses a leaky vascular barrier but has similar perineural barrier permeability. Furthermore, the neuron rich region has a higher vessel density compared to the peripheral nerve. To our current knowledge the fibre rich region's barriers are similar to that of the peripheral nerve [26-28].

2.2.1 Cell Populations of the Neuron Rich Region

Classification of nerve fibres by Erlanger and Gasser discriminates fibre types by myelination and conduction velocity. It includes A (Aα, Aβ, Aγ, Aδ), B and C type fibres [29]. Since the original work in 1927, scientists have adapted the classification to integrate specific differences between species. Perception of thermal, itch and noxious stimuli primarily relies on signal transduction by unmyelinated C- and, in low quantity, on myelinated Aβ-, as well as Aδ-fibres [30]. These sensations, physiologically, warn the organism of immediate danger. Literature distinguishes between uni- and polymodal nociceptors, with the estimated proportions considerably varying in literature [12]. Silent nociceptors are a subpopulation of nociceptors not depolarizing under normal conditions but only after sensitization (e.g. inflammation) [12, 31].

The neuron rich region of dorsal root ganglia harbours vessels, neuron cell bodies, as well as satellite cells. After early volumetric assessment of the rat lumbar dorsal root ganglion's neurons, they were divided into large (~57,200 μm^3) and small (~10,700 μm^3) cells. Also, the number of myelinated fibres correlates closely with the amount of large cells, whereas the number of unmyelinated fibres correlates closely with the amount of small cells [32]. Furthermore, *in vitro* studies observed a loose positive correlation between conduction velocity and cross-sectional cell area at nuclear level [33]. Aβ-fibres and Aδ-fibres may be associated with large neurons, while C-fibres mostly belong to the small dorsal root ganglion neurons in mice [34]. Other than by size and myelination, neuronal populations may be defined by using immunohistochemical markers. Three of the most commonly used markers are NF200 (neurofilament heavy polypeptide), IB4 (isolectin B4), and CGRP (calcitonin gene-related peptide). While NF200 is associated with large myelinated mechanosensors, IB4 is associated with non-peptidergic nociceptors and CGRP with peptidergic nociceptors. Advances in the field of immunohistochemistry and single cell RNA sequencing led to a more detailed distinction: Cells are clustered using protein markers and their gene expression profile. Thereby, the

classification based on gene ontological studies has been linked to the physiological characteristics of neurons [35].

Usoskin et al. established a classification based on single-cell RNASeq in the dorsal root ganglion of mice (**Figure 3**). By correlation of gene expression profile, the authors were able to distinguish 11 subtypes with profiles for sensory neurons that cause pain, pressure, temperature, proprioceptive, and touch sensation [35].

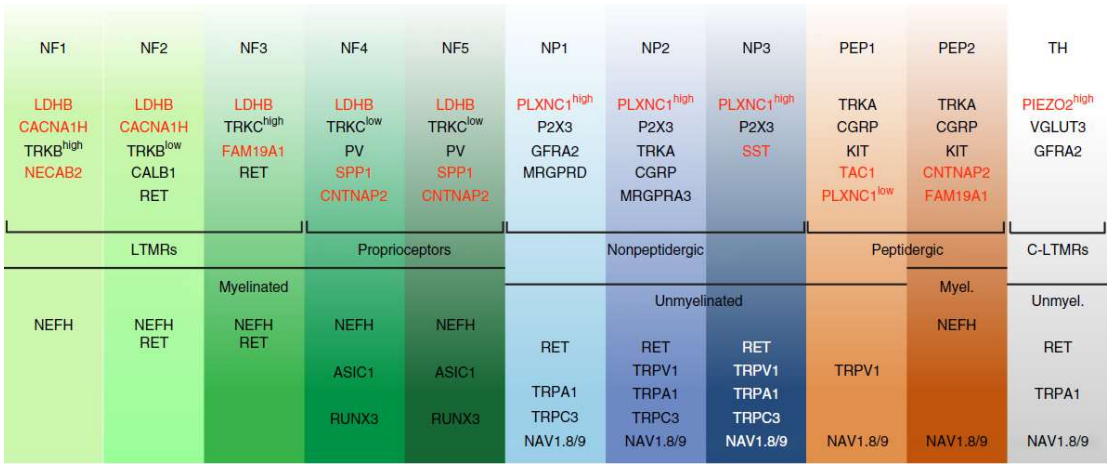

Figure 3. Classification of 11 distinct neuron types in the DRG of mice. New proposed immunohistochemistry markers in red, previously used markers in black (top). NF200+ cells include groups NF1-NF5, IB4+ cells include groups NP1-NP3 and CGRP+ cells include groups PEP1 and PEP2. Brackets indicate proposed function based on the cluster's gene profile. NF: neurofilament, NP: non-peptidergic, PEP: peptidergic, LTMR: low-threshold mechanoreceptor. (Reprinted by permission from Copyright Clearing Center: Springer Nature, Nature Neuroscience, Unbiased classification of sensory neuron types by large-scale single-cell RNA sequencing, Figure 4b, Usoskin et al. Copyright 2014; License Number: 4957601156764 [35])

2.2.2 Tight Junction Proteins in the Dorsal Root Ganglion

The blood-dorsal-root-ganglion-barrier (blood-DRG-barrier) has yet to be evaluated thoroughly. Vessel density and permeability of small and large molecules in the neuron-rich region within the dorsal root ganglion are higher than in peripheral nerve fibres. Nevertheless, studies of tight junction protein expression patterns *in situ* are still lacking sufficient evidence [26]. Studies in patients with neuropathic diseases, e.g. Fabry's disease or chemotherapy-induced neuropathy, have shown changes in dorsal root ganglion volume. This indicates that oedema and the blood-DRG-barrier may be involved in the pathogenesis of neuropathic pain [36-38]. Furthermore, macrophage infiltration into the dorsal root ganglion, e.g. during paclitaxel-induced neuropathy, is still of unclear origin and function. Unravelling these events might yield new therapeutic options [39]. Lastly, the blood-DRG-barrier's leakiness in healthy condition still poses a mystery in terms of physiological function. Therefore, it is valuable to

study and evaluate the blood-DRG-barrier's tight junction distribution, organization, and regulation.

2.2.3 Barriers of the Peripheral Nervous System

Since little information regarding the blood-DRG-barrier is available, the closely related blood-nerve-barrier is particularly important to understand. Sensory neurons are the gate to our perception and need a strictly regulated environment to serve their function reliably. Too high as well as too low activity results in functional impairment, greatly influencing the well-being and functionality of an organism. As described later (chapter 2.4.3), the composition of tight junctions greatly affects the permeability and selectivity of the barrier and significantly alters the resulting extracellular environment. The most dominant tight junction proteins in peripheral nerval barriers are *Tjp1, Cldn1, Cldn3, Cldn19, Ocln*, and *MarvelD2* [40, 41]. Crucial component of the nerve's barriers is the perineurium, composed of a mesenchymal barrier (*pars fibrosa*) for mechanical and an epithelial barrier (*pars epitheloidea*) for chemical protection. Furthermore, the endoneural vessel barrier limits entry of noxious blood borne stimuli into the nerve from the inside [42]. Like the central nervous system, the peripheral nerves are embedded in spinal fluid. Even though the compartments containing these fluids are connected, it is called endoneural fluid in the peripheral nervous system. Endoneural cells produce and maintain the endoneural fluid [43].

Several laminar layers make up the *pars epitheloidea* of the perineurium, all of which have their own basal lamina. The epithelioid myofibroblasts of this tissue originate from the central nervous system's glial cells, which migrate into the peripheral nervous system during embryonic development. The barrier-forming cells are connected to each other via gap junctions, adherence junctions and tight junctions. *Tjp1*, *Cldn1*, *Cldn3*, *Cldn19*, *Ocln,* and *MarvelD2* are the dominant components of these inter-cellular connections [43].

Schwann cells wrap around the nerve fibres to fulfil their function of regulating the microenvironment. This isolating structure enables saltatory excitation transmission, increasing the fibre's conductance velocity. While wrapping around an axon, the spread volume of Schwann cell cytoplasm grows rapidly and increases the diffusion and transport distances. A special feature of Schwann cells are Schmidt-Lanterman incisures, which seal the myelin sheath together with tight junctions and connect the cytoplasm of the different layers. This allows for faster diffusion and transport in the widely spread cytoplasm of the Schwann cells. These incisures predominantly express the tight junction proteins *Cldn1*, *Cldn3, Cldn12*, *Ocln,* and *Tjp1*. The zone of two adjacent myelinating Schwann cells almost connecting forms a node of

Ranvier. This gap of myelination is the key feature of saltatory excitation, allowing a new spike of depolarization between the isolated regions of the axon. Adjacent to these gaps lies the paranodal region in which tight junctions seal the Schwann cells' myelin barrier. *Cldn1*, *Cldn19*, *Ocln*, *Tjp1* and *MarvelD2* are the main components of these tight junctions. Disruption of the Schwann cells' tight junctions may result in impaired sensation [43].

Vessels in nerve tissues are challenged to deliver adequate nutrition while maintaining the environment free of blood-borne toxins. The predominant tight junction components in the blood-nerve-barrier are *Cldn5*, *Tjp1* and *Ocln*. The blood-nerve-barrier is rather leaky in the postnatal period, and as the organism matures, the endothelial vessel barrier strengthens its barrier function [43].

For the blood-DRG-barrier, Hirakawa et al. demonstrated an interesting deviation to the otherwise strictly regulated neural barriers: vascular permeability for intravenously injected fluorescent Evans-blue albumin in the dorsal root ganglion is significantly higher than in other neuronal tissues [26]. Furthermore, high permeability was only observed in the neuron rich but not in the fibre rich region of the dorsal root ganglion.

2.2.4 The Dorsal Root Ganglion in Neuropathic Pain

While the dorsal root ganglion is not involved in basic therapeutic algorithms, its role in pain development has been implicated. Physicians may use interventional therapies like spinal ganglia block or neurostimulation, for example in severe cases of chronic regional pain syndrome [44-48]. Furthermore, an inflammatory reaction like that of the peripheral nerve may occur in the dorsal root ganglion following nerve injury [49, 50]. This reaction is accompanied by up- or downregulation of genes relevant for signal transmission and results in hyperexcitability of neurons [51-53]. The regional sympathetic nervous system, also involved in some neuropathic conditions like complex regional pain syndrome, is connected to the dorsal root ganglion via the *rami communicantes* [54, 55]. Lastly, excitation of other closely located neurons may, in some cases, partially depolarize adjacent cell bodies. While it rarely reaches the threshold for action potential generation. The process called "cross-excitation" is not fully understood yet, but may be related to sensitization [56].

Nerve transection proximal to the dorsal root ganglion (or other forms of dorsal root ganglion destruction) can alleviate pain and rescue the neuropathic phenotype. Interestingly, nerve injury distal to the dorsal root ganglion causes neuropathic pain and is a common element of neuropathic pain models as shown in Figure 4 [57, 58]. The consistent anatomic location and specific regional innervation turn the dorsal root ganglion into an attractive and specific target

for pain treatment. Use cases include pain in the groin or feet in which dorsal column fibres are hardly accessible for spinal cord stimulation. Segmental conditions like discogenic pain, post-herpetic neuralgia or phantom limb pain may also be indications [55, 57, 59-61].

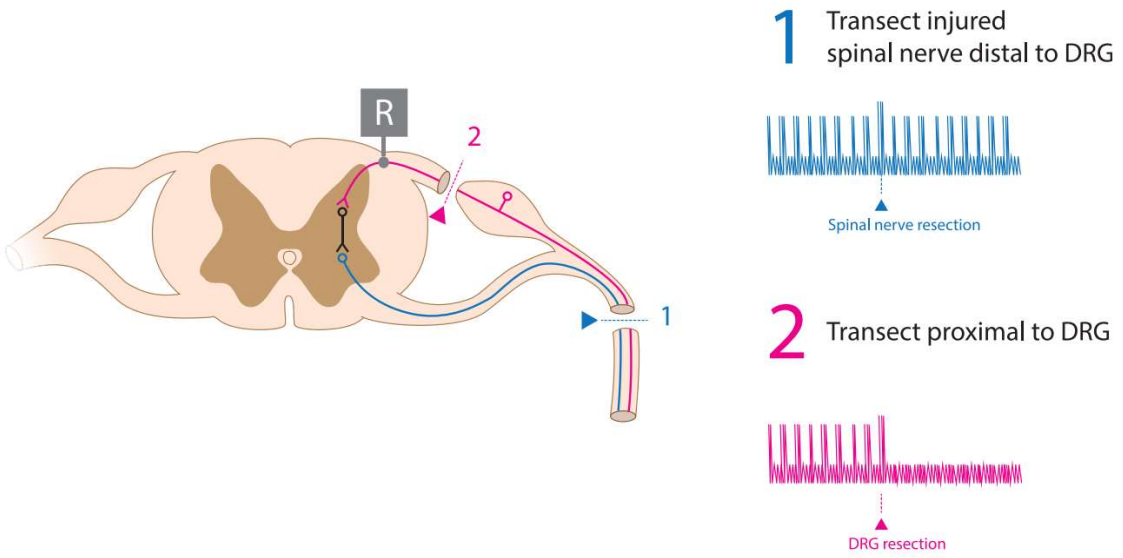

Figure 4. Dorsal root ganglion resection alleviates ectopic excitation. Animals with ectopic action potential generation and a neuropathic phenotype underwent nerve transections proximal or distal to the dorsal root ganglion. Dorsal root ganglion resection rescued the behavioural and electrophysiological phenotype. Therefore, the dorsal root ganglion might have a significant role in ectopic signal generation. (Reprinted by permission from Copyright Clearing Center: Oxford University Press, Pain Medicine, Unique Characteristics of the Dorsal Root Ganglion as a Target for Neuromodulation, Figure 4, Esposito et al. Copyright 2019; License Number: 4957610299880 [58]).

The dorsal root ganglion is target of therapies: evidence strongly suggests a key-role in spontaneous pain generation after nerve injury. Peculiarities like the t-stem structure of pseudounipolar neurons and the leakiness of the blood-DRG-barrier have been observed. Nevertheless, the physiological function of these features is unknown. We currently do not know why or how the dorsal root ganglion is involved in transmission, alteration, or generation of sensory signals. Is it a mere relay station for signals, does it act as signal filter or enhancer? Is it a physiological sensor comparable to the *area postrema* in the brain, due to the leakiness of its' barrier? Diagnostics as well as therapeutics of neuropathic conditions might greatly advance if we continue to understand more about the dorsal root ganglion.

2.3 Adhesion G Protein-Coupled Receptors

Latrophilins are aGPCR [62], which form an own subclass within the Class-B G protein-coupled receptors (GPCR). Almost all receptors of this subfamily have a proteolytic site as distinct feature [63]. The human genome analysis foretells 800 proteins of the GPCR family and about 34% of therapeutic drugs target them, for example angiotensin receptor blockers, ß-blockers, opioid agonists, and histamine receptor blockers [64, 65]. Diseases like hypertension, diabetes, and sepsis are associated with GPCR dysfunction [66]. This underlines the physiological and therapeutic importance of this receptor class in modern medicine.

The latrophilin subfamily was originally discovered due to their capability to bind to α-latrotoxin, a component of the black widow spider's venom. Its ability to activate the pre-synapse independently of other neurotransmitters makes α-latrotoxin a strong neurotoxin. While neurexins may also bind α-latrotoxin, they need a calcium rich environment for activation. The aGPCR lathrophilin-1, also called Adgrl1, on the other hand does not depend on calcium levels and is therefore called calcium-independent receptor of α-latrotoxin. [67]

2.3.1 Introducing: Adhesion G Protein-Coupled Receptors

The family of GPCRs comprises of six subfamilies based on similarities in sequence and function [63].While GPCR make up the greatest protein class in the human genome, aGPCR are the second largest group within them. 33 receptor genes in the human genome are classified as aGPCR based on their resembling structure. Based on current literature, they are the least understood ones [68, 69]. Figure 5 illustrates the structural characteristics of aGPCR, including the GPCR autoproteolysis-inducing domain [70].

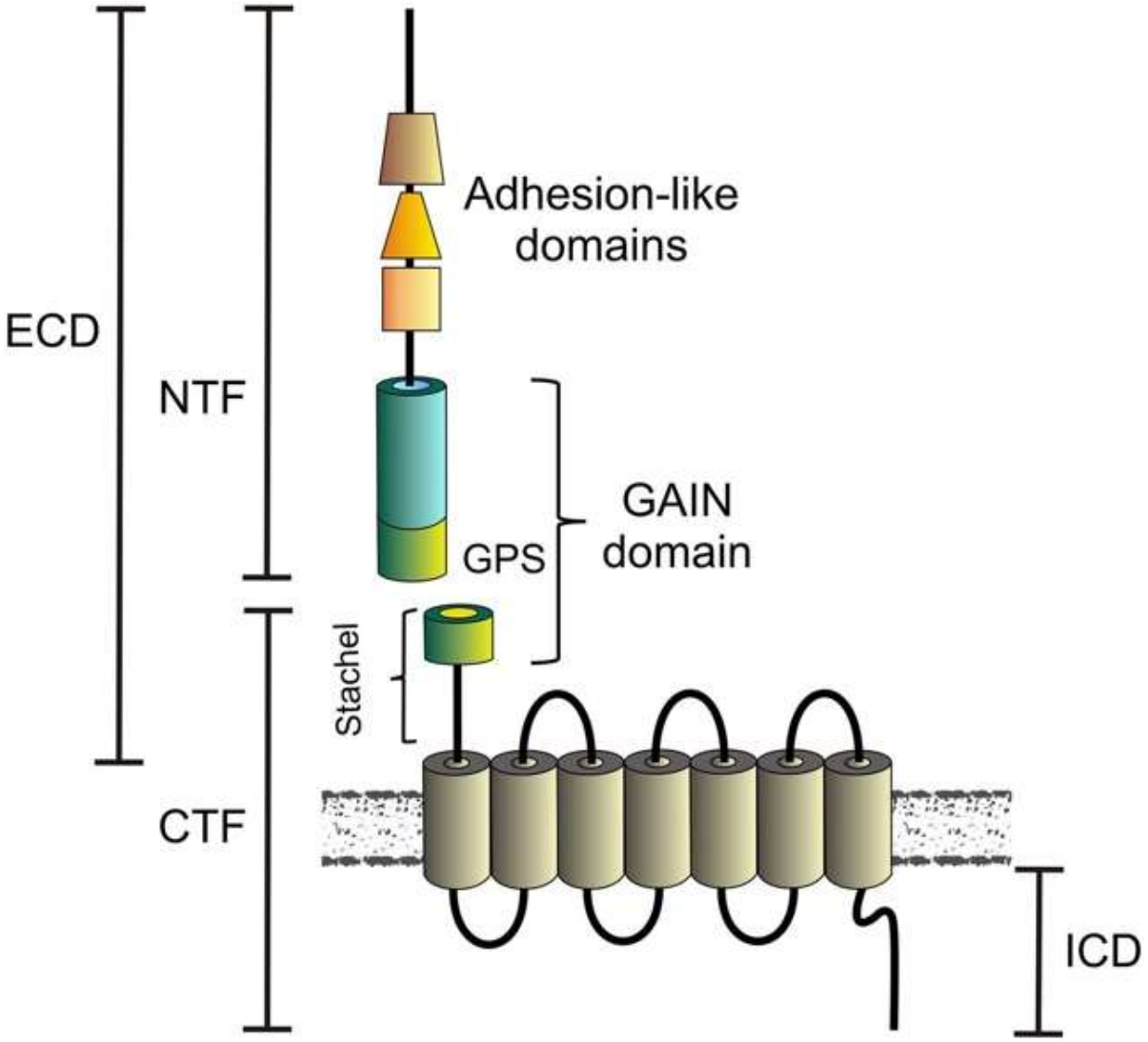

Figure 5. Structure of aGPCRs. AGPCRs possess adhesion folds for mechanical interaction as well as a GPCR autoproteolysis-inducing (GAIN) domain containing the GPCR proteolytic site (GPS). The GPCR proteolytic site divides the receptor into a N-terminal (N-terminal fragment, NTF) and a C-terminal fragment (C-terminal fragment, CTF). The Stachel sequence, which may modulate the receptor's behaviour, is in the GPCR autoproteolysis-inducing domain. ECD: extracellular domain; ICD: intracellular domain; (Figure taken from Monk et al. 2015 [71], Reprinted by permission from Copyright Clearing Center: John Wiley and Sons, Annals of the New York Academy of Sciences, New functions and signaling mechanisms for the class of adhesion G Protein-coupled receptors, Liebscher et al. Copyright 2014; License Number: 4960060713047)

The aGPCR family is divided into nine subfamilies according to structural differences between its 7-transmembrane domains and extracellular termini [68]. The first recognized member of this protein family, also a seven transmembrane domain receptor, is the epidermal growth factor like molecule containing mucin-like hormone receptor 1. Shortly after, *Adgrl1* was discovered [72]. Initially, aGPCRs were thought to be closely related to Class B GPCR [73]. Further research, also involving the human genome project, led to the receptors being categorized as their own class: 7-transmembrane domain receptors containing a long N-terminal extracellular

region related to class B. The especially long extracellular domain may mechanically interact with the extracellular environment due to its adhesion motifs, coining the term adhesion G protein-coupled receptors.

The N-terminal end of transmembrane domain 1 extends far into the extracellular space and contains the characteristic GPCR autoproteolysis-inducing domain: this aGPCR specific region contains both the GPCR proteolytic site and the stalk region. The stalk region is of special interest, as it may autoactivate or autoinhibit the putative receptor as an endogenous ligand. For many aGPCR, an endogenous ligand other than their own stalk region is unknown to this date [74].

The detection of extracellular signals and the following cellular response is the fundamental mechanism for inter-cellular communication. Fulfilling this purpose, GPCR have an influence on local as well as systemic signalling and are common targets for pharmaceutical applications, even though the physiological function of many GPCR is still uncertain [65]. As the name suggests, all GPCR bind to a G protein. The coupled G protein causes an intracellular effect after activation [75]. The exact function of a G protein depends on the arrangement of different α-, β- and -γ subunits. There are four classes of α-subunits. This division is based on sequence similarities and distinguishes α_s, $\alpha_{i/o}$, $\alpha_{q/11,}$ and $\alpha_{12/13}$ classes. With their unique features, aGPCR build a fascinating bridge between mechanical interaction and metabotropic signalling.

Hamann et al. reviewed aGPCRs tissue distribution in rodents, and **Table 2-1** summarizes the latrophilin specific content [74]. While the many blank spaces symbolize the need for further research, most of the analysed tissues expressed *Adgrl2*, while *Adgrl1* and *Adgrl3* were mainly expressed in neuronal tissue. The ubiquitous expression of *Adrgl2* suggests a rather unspecific housekeeping function. Therefore, current neuroscience research focusses largely in *Agrgl1* and *Agrl3*.

Table 2-1. *Adgrl* expression patterns in rodents. (Table adapted from Hamann et al. 2015 [74])

Structure	Adgrl1	Adgrl2	Adgrl3
Bone marrow – Hematopoietic stem/progenitor cells			
Erythrocytes			
Platelets			
Lymphocytes			
Granulocytes			
Monocytes/Macrophages/Dendritic cells			
Myocytes (heart)			
Pneumocytes			
Hepatocytes			
Exocrine cells (pancreas)			
Mesangial cells (kidney, glomerulus)			
Adrenal Gland (medulla)			
Placenta			
Epithelial cells (mammary gland)			
Skeletal muscle (myocytes)			
Neurons (central nervous system)			
Astrocytes			
Oligodendrocytes			
Microglia			
Neurons (peripheral nervous system)			
Schwann cells			

unknown, mRNA expression, protein +, protein ++, protein +++

2.3.1.1 Nomenclature of adhesion G protein-coupled receptors

In 2015, the aGPCR consortium established a new nomenclature as the field progressed and confusion due to inconsistent nomenclature grew [74]. Now, all names start with the abbreviation "ADGR" for **Ad**hesion **G** protein-coupled **R**eceptor, followed by the first letter of the most prominent former name of the receptor or alphabetically if they were classified as

"GPR" until now. For example, Adgrl for adhesion G protein coupled receptor latrophilin, is followed by a number specifying the subtype. According to this new nomenclature, the latrophilins, formerly also known as Calcium-Independent Receptor of α-Latrotoxin Cirl, Lectomedin, or latrophilin, are referred to as Adgrl. The names for the arthropod's latrophilins, dCirl, and *C. elegans'* latrophilins, lat-1, and lat-2, are still commonly used.

2.3.1.2 Structure of aGPCR

AGPCRs have several distinct features separating them from other GPCRs. The 33 known human homologs of aGPCRs exhibit a large extracellular domain and a GPCR proteolytic site (except for ADGRA1, which does not contain a GPCR proteolytic site) in addition to the 7-transmembrane domains, a feature of all GPCR. The GPCR proteolytic site is located within the GPCR autoproteolysis-inducing domain and posttranslational cleavage at the GPCR proteolytic site splits the receptor into a N-terminal and a C-terminal fragment. It is not entirely clear whether and to what extend this cleavage is necessary for proper function. Depending on the specific receptor, splice variant, and context the impact of this cleavage differs and is therefore still subject of current research. Some studies report that the N-terminal fragment and C-terminal fragment may have biological functions in addition to regular receptor activity [71, 76].

The structural components of aGPCRs may be divided either by topography or by the self-cleavage of these receptors at the GPCR proteolytic site. Looking at the topography, the receptor's components are classified into an extracellular domain, a 7-transmembrane domain, and an intracellular domain. After cleavage of the large extracellular domain at the GPCR proteolytic site the receptor is built into the cell membrane as a heterodimer in most cases. It consists of its large N-terminal fragment, containing diverse adhesion motifs and therefore varying in size between 200 to 5600 amino acids in mammals [70]. The adhesion motifs vary from receptor to receptor and are highly specific regarding ligand recognition. Splice variants and glycosylation patterns may cause alterations [68, 77]. The resulting receptor variety and their functional differences are still subject of extensive research. The mechanical interaction via adhesion motifs poses a possible mechanism for tissue-specific cell guidance in the development of an organism by the same receptor through tissue specific splice and glycosylation variants. Neural development research in *C. elegans*, *D. melanogaster* and mice strongly supports this hypothesis [78, 79].

The GPCR autoproteolysis-inducing domain is located behind the adhesion motifs, following the direction to the C-terminus. This domain is highly conserved in most aGPCRs, suggesting

relevance regarding receptor functionality [80]. Grey et al. demonstrated this first in Adgre5 [81], shortly followed by Adgrl1 [72]. In mammals, the GPCR autoproteolysis-inducing domain is about 320 residues long and contains subdomains A and B. The GPCR proteolytic site motif is in the C-terminal β strands of subdomain B and is embedded into multiple β-strands and α-helices. Both the GPCR autoproteolysis-inducing domain and the GPCR proteolytic site motif are required for autoproteolysis. The steric configuration of the GPCR autoproteolysis-inducing domain affects the affinity for ligands and therefore their function [82]. Occurrence of N-glycosylation of the GPCR-induced proteolytic site in the endoplasmic reticulum controls the probability of proteolysis [81, 83]. After cleavage, the N-terminal fragment and the C-terminal fragment remain as a heterodimer, connected by non-covalent hydrophobic bonds. Some studies implicate a loss of correct membrane translocation in cleavage-deficient aGPCR mutants [84], while others show normal membrane trafficking [85]. This concludes that the relevance of cleavage is heterogenous within the family of aGPCR. It might not be imperative for correct membrane trafficking and function for all aGPCR. Although some aGPCR may function correctly after loss of GPCR proteolytic site cleavage, functional destruction of the GPCR autoproteolysis-inducing domain leads to loss of function in most aGPCR [76, 86]. This indicates that the steric function of this domain is more important than cleavage.

While recent research focussed on the physiological function of *dCirl*, little is known about function of this receptor family in vertebrates [70, 78, 87-89]. To the best of current knowledge neural tissue is most dominant regarding *Adgrl1* and *Adgrl3* expression, both of which are highly conserved in vertebrates. Nevertheless, the exact spatial distribution in the peripheral nervous system of vertebrates is still unknown [90, 91].

The structure of aGPCR with its specialized extracellular domain allows interaction with the extra cellular matrix. While the precise mechanisms of action of this family are still the subject of current research, Scholz et al. proposed interactions between the extracellular matrix and neurons after studies in *Drosophila* [88, 89].

2.3.1.3 Split Personality Hypothesis

In normal cell surface presentation, the N-terminal and the C-terminal fragments of the aGPCRs are seldomly connected covalently, but through hydrophobic bonds. The plasma of mammals contains trace amounts of some aGPCRs' N-terminal fragments under physiological conditions. Given the high conservation of the GPCR autoproteolysis-inducing domain, the question arises whether the N-terminal fragment of one aGPCR may bind to the C-terminal fragment of another. This question led to the split personality hypothesis, which states that the N-terminal

fragment of one aGPCR may bind non-covalently to another aGPCRs C-terminal fragment after shedding [92, 93]. While the physiological and experimental relevance of this observation has yet to be elucidated, this poses another feature of aGPCR which raises questions. Furthermore, following up on this research topic is important to correctly plan future experiments including ligand and antibody binding studies.

2.3.2 *Adgrl1* and *Adgrl3*

The latrophilin receptor family was first discovered while looking into the mechanism of action behind α-latrotoxin's strong poisonous effect: pain and paralysis but without structural damage or an inflammatory reaction – nevertheless potentially lethal in humans. This suggests that the poison directly interacts with the peripheral nervous system. Further research revealed that *α*-latrotoxin may activate neurons in the vertebrate organism in both a calcium dependent and calcium independent fashion. While both mechanisms coexist in inter-neuronal synapses, *α*-latrotoxin activates the neuromuscular junction via the calcium dependent pathway [67].

Adgrl1 and *Adgrl3* are abundantly expressed in brain tissue of adult animals and maturing brain. Expression patterns during the embryonic and postnatal period in rats and mice are different but not always conclusive. New studies revealed a high number of splicing variants as well as a functional difference between them giving a potential explanation for some of the conflicting data. Nevertheless, regulation of latrophilin expression was detected in almost every study during brain maturation and neuron cultures from mice suggest latrophilin's interactions are critical for synapse maintenance [67].

While arthropods express only one isoform of the latrophilin family, *dCirl*, vertebrates have three different isotopes with different tissue distribution across species [67], suggesting different physiological functions. While both *Adgrl1* and *Adgrl3* are highly expressed in brain tissue of rats, *Adgrl2* expression is hardly observed in brain tissue. *Adgrl2* has a more ubiquitous distribution and is expressed evenly over most other tissues. Except for expression in the central nervous system, *Adgrl1* is also found in kidneys, spleen, and lungs. *Adgrl3* expression has been observed in heart, kidneys, placenta, pancreas, and testes [90, 94]. *ADGRL1* and *ADGRL3* are also enriched in the human brain [95] and studies revealed significant differences between specific brain regions regarding *ADGRL3* expression [96]. Concluding this, *Adgrl2's* ubiquitously expression across tissues makes it probable that it serves a more general purpose. Furthermore, Usoskin et al. reported low *Adgrl2* expression in the dorsal root ganglion [35]. *Adgrl1* and *Adgrl3* are primarily expressed in neural tissues and neuron specific functions have

already been demonstrated. This suggests a more neuron specific role like in axon sprouting. Therefore, neuroscience and this thesis, focus on *Adgrl1* and *Adgrl3*.

Previous α-latrotoxin binding studies revealed pre- and postsynaptic binding sites. While neurexins, the calcium dependent receptors of α-latrotoxin, are predominantly expressed pre-synaptically, there is currently no consensus about latrophilins. Pre- and postsynaptic expression have been observed. This implies high variability of the latrophilins signal transduction. *Adgrl1* is expressed in vertebral tissue but it is absent in glial cells. Northern Blot analysis revealed highest *Adgrl3* levels in the central nervous system, with especially high expression in the caudate nucleus, amygdala, prefrontal cortex, and cerebellum and lower expression in the hippocampus, corpus callosum, occipital pole, frontal lobe, temporal lobe, and putamen. *Adgrl3* is absent in the medulla, the thalamus, or the spinal cord [67, 78, 91].

Little is known about the physiological functions of the aGPCRs, and latrophilins are no exception. While the overall picture remains blurry, some hints to unravel the latrophilins' functions have been acquired: The counterpart to vertebrate *Adgrls* in *Drosophila* is *dCirl*. Knockout (ko) of *dCirl* revealed a modulatory function for mechanosensation [88, 89]. The tethered agonist of *dCirl*, its stachel sequence, may auto-activate the receptor and modulate the action potential frequency of the chordotonal organs via cAMP quenching [88, 89]. In neurons which detect light mechanical stimuli, reduced *dCirl* activity increased the sensory threshold for action potential generation. In neurons detecting coarse mechanical stimuli, which one might correlate with vertebrates' nociceptors, reduced *dCirl* activity decreased the threshold for action potential generation. Therefore, a role in conditions associated with painful hypersensitivity should be investigated. Gene modification studies proved the interaction of receptor and activation threshold to be dependent on the length of the N-terminal fragment. These experiments simulated mechanical stress by expressing shorter N-terminal fragments. Both, mechanical stress, and a short N-terminal fragment cause the endogenous ligand to be more exposed. The exposed ligand now causes increased receptor activity. Therefore, the experiments suggest signal modulation depending on mechanical stress exposure. Inactivation of the GPCR autoproteolysis-inducing domain prevents autoproteolysis, which in some aGPCR causes loss of functionality or incorrect membrane presentation. For *dCirl*, membrane placement and receptor function are unaltered if autoproteolysis is inhibited [84, 89]. While these results must be confirmed in vertebrates, this evidence suggests an interaction between receptors of the *Adgrl* family and somatosensation.

Adgrl1 ko mice show abnormal maternal behaviour [97]. *ADGRL1* mutations in humans are associated with neuropsychiatric disorders [98] as well as late-onset retinal degeneration [99]. A mutation of an *ADGRL1* transmembrane residue necessary for basal receptor activity has been associated with cancer [100]. *Adgrl3* interacts with *Flrt3* as an endogenous ligand and affects the formation and regulation of excitatory synapses during development [101]. Mice and zebrafish *Adgrl3* ko studies observed disturbed dopaminergic homeostasis and a hyperactive as well as impulsive phenotype. This phenotype may be reversed by anti-attention deficit hyperactivity disorder drugs [102-106]. Genetic analysis studies of patients suffering from attention deficit hyperactivity disorder have also shown that *ADGRL3* mutations are positively associated with the development of attention deficit hyperactivity disorder [96, 107, 108]. Additionally, it was computationally predicted that the mutants expressed in lung cancer would lose their function, also exhibiting a significantly higher frequency of *ADGRL3* copy loss than copy gain. These facts indicate a role as tumour suppressor for *ADGRL3* and have been discussed for other aGPCR [109].

Summarizing the current knowledge, *dCirl* was identified as modulator of somatosensation in *Drosophila*, where it causes hyposensitivity for light and hypersensitivity for coarse mechanical stimuli. *DCirl's* correlate in vertebrates is the latrophilin family. Of this family *Adgrl1* and *Adgrl3* are highly expressed in neuronal tissues. Animal studies for both receptors already observed behavioural changes, experiments addressing the somatosensory system have not been performed yet.

2.4 Tight Junction Proteins

The structural and functional integrity of tissues relies on cellular junctions for mechanical stability, cell polarity, management of correct composition, and compartmentalization of the extracellular environment. The most common and physiologically obvious tissues relying on tight junction proteins are epithelial cells of skin, kidney, gut, and vascular endothelial cells. Nevertheless, other tissue compartments like e.g. perineural cells also depend on precisely regulated cellular junctions [110]. As shown in **Table 2-2**, the proteins composing cellular junctions consist of adhesion contacts, communication junctions, signalling junctions, and tight junctions. Depending on the type of cellular contact, the proteins have specific distributions: they are either arranged in small spots, *maculae*, or circumferential around the whole cell, *zonulae.* These *zonulae* also divide the putative cell's membrane into apical and basolateral. Tight junctions form a belt-like structure around each cell in a tissue, which enables them to act as a barrier, allowing only specific molecules to pass through. Depending on the tissue, breakdown of the tight junctions in a barrier may lead to changes in electrolyte and cytokine balance as well as cellular invasion (i.e., immune cells or bacteria).

The tight junction proteins with transmembrane domains have extracellular domains and intracellular domains. The extracellular domains form homo- or heterodimers with tight junction proteins of adjacent cells. On the other side, the intracellular domains are connected to the actin skeleton via *zonula occludens* proteins. Considering the number of tight junction protein's transmembrane domains, the literature distinguishes between members of these protein family: tight junction proteins with one transmembrane domain (coxsackie and adenovirus receptor); junctional adhesion molecule, crumbs protein homolog 3, blood vessel epicardial substance with three transmembrane domains and tight junction proteins with four transmembrane domains (claudins, tight junction-associated MARVEL proteins). [110]

Table 2-2. Cellular junctions and their physiological function.

Junction	Function	Examples
Adhesion contacts	Mechanical anchor to the extracellular domain or neighbouring cells	Adherens junctions Desmosomes Hemidesmosomes
Communication junctions	Direct chemical or electrical connection to the neighbouring cell	Gap Junctions Electrical Synapses
Tight junctions	Separates compartments acting as a barrier and limiting chemical and cellular trespassing	
Signalling junctions	Indirect chemical connection between cells	Chemical synapses

Claudins, as integral membrane proteins, are key components of tight junctions. Depending on the member of the claudin family, they can either form very tight, selectively permeable, or leaky barriers. All of these serve their purpose in the complex organization of an organism. Being the major component for permeability regulation in tight junctions, the claudins play a particularly important role in upholding homeostasis in environmentally sensitive tissues. Current evidence suggests that there are 27 human claudins with molecular weights of 21-34 kDa [110, 111].

2.4.1 Structure of Claudins

The human claudin genes encode proteins with 207 to 305 amino acids, forming four transmembrane domains. Most claudins exhibit a PSD95, a Dlg1 or a ZO-1 PDZ-binding motif. The PDZ motif was first observed and the three name-giving proteins were studied. Other proteins expressing this motif, and therefore interacting with the PDZ-binding motif, are ZO-2 and -3, MAGI-1, -2 and -3, and MUPP1. These proteins function as adapter proteins, anchoring claudins to the intracellular cortical actin skeleton [110].

Splice variants of the first coding exon of *Cldn10*, *Cldn11,* and *Cldn18,* as well as splice variants of internal exons of *Cldn10* and *Cldn18* and splice variants of the last exon of *Cldn7* and *Cldn19* have been reported. While possible functional differences between the splice variants are obvious, it is also important to keep in mind the different primer and antibody affinities while studying genes and their respective proteins [110].

2.4.2 Expression Patterns of Claudins

Tight junctions are key components of epithelial and endothelial tissues and claudins are expressed in all known human epithelial and endothelial tissues. Vascular endothelial cells have strictly regulated tight junctions. In the context of neuronal tissues, they form the blood-brain-barrier and the blood-nerve-barrier. Both barriers have been the subject of extensive research over the past few years, while the blood-DRG-barrier has only been focussed on in few publications. The predominant claudins in vascular endothelia are *Cldn5*, *Cldn1,* and *Cldn12*. Besides epithelia and endothelia, Schwann cells in the peripheral nerve also express claudins (*Cldn11* and *Cldn19*) and even neurons may express tight junction proteins under certain conditions [110, 112, 113].

2.4.3 Physiological Functions of Claudins

Three main functions of tight junctions have been proposed: the barrier function that regulates paracellular transport, the fence function that separates the cell surface with its proteins into apical and basolateral, and the pore function that exceeds a simple barrier because of selective permeability. Tight junctions are often impermeable even for small ions. Measuring tissue conductance, comparing tissues with different protein expression, and ultimately correlating both with the tight junction proteins expression visible in electron microscopy enables electrophysiological quantification. Such studies show significant conductance differences between similar numbers of tight junction strands with differing claudin compositions. The key difference between tight junctions with a tight barrier and a leaky barrier is the claudin composition. Downregulation or replacement of a barrier-forming tight junction protein by a pore-forming tight junction protein causes decreased tissue resistance. Utilizing only electrophysiological experiments, separating the sole loss of tight junction proteins from their replacement by another one poses a challenge. Nevertheless, both states have significantly different effects *in vivo*. Pore-forming tight junction proteins are still a selective filter of the paracellular transport, especially for macromolecules, while fewer tight junction strands increase permeability non-selectively. **Table 2-3** summarizes the current knowledge of pore- and barrier-forming claudins, many of which are found to depend on specific interactions. These findings indicate a high variability of selective paracellular transport depending on the tissue specific expression patterns. Regarding selectivity, charge selectivity by forming small pores (r = 5 Å) and size selectivity of paracellular transport can be distinguished. By forming larger pores (r = 14 Å), claudins increase tight junction permeability for macromolecules [114, 115]. The exact pore size depends on the claudin composition.

Claudin-Claudin interactions of homo- and heteromeric peptides, interactions of *cis* and *trans* nature, as well as interactions of claudins with other tight junction proteins have been described in the past. This results in many possible combinations, each with its own unique properties and barrier function for differently charged ions as well as macromolecules. This enables organisms to regulate the extracellular environment in a very flexible way. An exemplary tissue for this behaviour is the peripheral nerve, requiring a tightly regulated environment for proper electric signal transmission in a healthy state. Tight junction protein expression, the permeability of the blood-nerve-barrier as well as the molecular composition of the extracellular environment change rapidly during traumatic nerve injury [14, 116]. Following these findings, a causal relation between barrier breakdown and altered sensation after nerve injury has been postulated.

Table 2-3. Charge selectivity of claudins. (* = data conflicting to the assignment in the table has been observed under certain conditions. Based on a metanalysis and adapted from [110]).

Cation selective claudins		**Anion-selective claudins**	
Predominantly pore-forming	Predominantly barrier-forming	Predominantly pore-forming	Predominantly barrier-forming
claudin-2	claudin-7	claudin-7	claudin-1
claudin-10b	claudin-19*	claudin-10a	claudin-3
claudin-15*		claudin-17	claudin-4*
claudin-16*			claudin-5
			claudin-6
			claudin-8*
			claudin-9
			claudin-11*
			claudin-14
			claudin-18-2

2.4.4 Regulation of Claudin Expression

In general, changes in transcription or translation rates, post-translational modifications, or interaction with cytoplasmatic scaffolding proteins may alter protein levels. Posttranslational modifications like palmitoylation, phosphorylation, and ubiquitinoylation also greatly affect the function and further placement of claudins. As an example, the phosphorylation of claudin-1 leads to insertion of tight junction strands, whereas dephosphorylation results in removal [117]. Similar observations have been observed with claudin-2 and claudin-4, while the opposite has been described for claudin-3 and a different phosphorylation site of claudin-4 [118, 119]. This

indicates a cellular routine in which changes in intracellular phosphorylation probabilities, for example in an inflammatory state, leads to a fast and efficient change of paracellular transport. After traumatic nerve injury phosphorylation of claudin-5 leads to insertion into tight junction strands but simultaneously causes dysfunction and thereby poses a third interesting outcome of phosphorylation [120, 121]. Other post-translational modifications, like the involvement of microRNA as post transcriptional regulators, show no easily recognizable pattern in the resulting reaction. This implies a highly versatile paracellular permeability regulation, which has yet to be understood [110, 122].

2.4.5 Specific Tight Junction Proteins in Detail

Claudin-1, as a barrier-forming tight junction protein, is expressed ubiquitously throughout the body and plays a critical role in the regulation of skin permeability. *Cldn1* ko mice die from dehydration and downregulation leads to dry skin associated diseases [123]. Other prominent sites of claudin-1 expression besides the skin are the liver as well as the intestines, but also the barriers of the central nervous system and peripheral nervous system. *Cldn1* expression in the peripheral nerve is mainly observed in the perineurium, endoneural vessels, nodes of Ranvier, Schmidt-Lanterman incisures, and the mesaxon [43]. The intracellular domain of claudin-1 expresses a PDZ binding motif which associates with ZO-1 and anchors the protein to the cytoskeleton. The extracellular domain of claudin-1 dimerizes as homodimers and heterodimers with other tight junction proteins of adjacent cells, i.e., claudin-2 and claudin-3 [43]. Several regulators of *Cldn1*, such as serine-threonine-kinases (i.e. glycogen synthase kinase 3 induces expression) and micro-RNAs (micro-RNA-183 can reduce *Cldn1* mRNA and protein expression) have been described [43]. Genomic studies in patients have shown neonatal sclerosing and cholangitis with ichthyosis to be associated with *CLDN1* mutations [123, 124].

Claudin-5 is commonly expressed in vascular endothelia. Two forms differing in the length of their N-terminus due to two start codons in the *Cldn5* gene have been observed so far [110, 125]. In the peripheral nerve, *Cldn5* expression is mainly observed in endothelial cells of vessels, the Schmidt-Lanterman incisures and the mesaxon [43]. The importance of vascular tight junctions has been demonstrated in studies of the blood-nerve-barrier and blood-brain-barrier. Therefore, its role in the blood-DRG-barrier should also be evaluated. Downregulation of *Cldn5* results in leaky vessels, allowing molecules of up to 800 Da to extravasate into the brain. *Cldn5* ko mice die shortly after birth with no specific macroscopic phenotype [126]. In the clinical context, the congenital DiGeorge and velo-cardio-facial syndromes have been associated with *CLDN5* mutations [43, 127].

Claudin-12 lacks a PDZ-binding domain, which makes it one of the few exceptions in the claudin family [110]. Furthermore, it seems to be only in a distant phylogenetical relation with the rest of the claudins. The central nervous system as well as the peripheral nervous system show *Cldn12* expression mainly in capillary cells, but mRNA expression is significantly lower compared to *Cldn5* [128]. After *Cldn5* downregulation, *Cldn12* is upregulated and functions as molecular sieve limiting permeation to a molecular size less than 800 Da [126].

Claudin-19 is predominantly expressed in the peripheral nervous system as well as the kidney and the retina but shows no expression in the central nervous system. It acts as a barrier-forming tight junction protein, but its ion-selectivity varies in different tissues. In the peripheral nervous system, claudin-19 forms interlamellar tight junctions in Schwann cell [110]. Interestingly, *Cldn19* ko mice show the phenotype of a peripheral neuropathy and nerve biopsies revealed a total reduction of tight junctions in Schwann cells, but no deficiency in formation of nodes of Ranvier as well as correct wrapping of Schwann cells around the axons [43].

2.5 Hypotheses

The dorsal root ganglion is one possible target for treatment of peripheral neuropathies. The exact mechanism behind ectopic excitation in the dorsal root ganglion and the nature of its leaky barrier in the neuron rich region are unknown. Nevertheless, the leaky barrier makes the dorsal root ganglion easily accessible for intravenously injected drugs. While blood-nerve-barrier breakdown after nerve injury has been characterized, little is known about the composition and possible alterations of the blood-DRG-barrier in neuropathy.

Secondly, latrophilins, receptors of the aGPCR family, increase the threshold for sensing light and decrease the threshold for sensing coarse mechanical stimuli in *Drosophila.* This makes the latrophilins a novel candidate to evaluate during neuropathy and the blood-DRG-barrier the pharmaceutically relevant structure for drug distribution. We aim to establish basic knowledge of the blood-DRG-barrier composition and distribution of latrophilins in the dorsal root ganglion of rats with neuropathy versus controls. Therefore, we evaluated the following hypotheses:

1. The expression of claudin-1, claudin-5, claudin-12, claudin-19, and/or ZO-1 expression in normal dorsal root ganglia is region specific because of their different permeabilities. In CCI, the expression of claudin-1, claudin-5, claudin-12, claudin-19, and/or ZO-1 is reduced, and the permeability of the blood-DRG-barrier increased.
2. $NF200^+$, $IB4^+$, and/or $CGRP^+$ primary sensory neurons express *Adgrl1* and *Adgrl3* and Adgrl1 and Adgrl3. Their expression is downregulated in CCI and recovers in the time course. ADGRL1 and ADGRL3 are also detectable in human dorsal root ganglia.

3 Material and Methods

3.1 Animals

For the conducted experiments, twenty male Wistar rats (Janvier) aged eight to twelve weeks were kept in cages of six in a 12-hour/12-hour light cycle with food and water *ad libitum*. All animal protocols were approved by the local authorities (Regierung von Unterfranken, RUF55.2.2-2532-2-612-16, 2-733 and 2-264). All Protocols were in accordance with the international guidelines for the care and use of laboratory animals (EU Directive 2010/63/EU for animal experiments). Criteria for termination of the experiments and humane endpoints with approved score sheets were defined. The animals were treated accordingly and all animal studies were reported following the ARRIVE guidelines [129].

Equal test groups were assigned, and experiments were conducted during the light phase. Surgery was performed by my supervisor, Dr. Jeremy Chen, under deep isoflurane anesthesia (1.8 Vol. % FiO_2). If paw withdrawal was absent, surgical tolerance was assumed. For CCI, the sciatic nerve was exposed by blunt preparation after skin incision and four loose silk ligatures with approximately 1 mm spacing in between were applied [130].

After the procedure, the skin was sutured. Sham operated animals received the same treatment, but no ligations were applied. The animals were euthanized with CO_2 at the defined endpoints or if abortion criteria were met.

3.2 Reverse Transcription qPCR

Tissue was harvested after euthanizing the animals. The samples were frozen with liquid nitrogen and stored at -80 °C until further usage. Quantification of *Adgrl1* and *Adgrl3* mRNA expression in different tissues was performed using reverse transcription qPCR. Using the TRIzol™ reagent, RNA was extracted and analyzed for yield and purity using the NanoDrop2000®. Afterwards, it was transcribed to cDNA using the High capacity cDNA Reverse Transcriptase Kit according to manufacturer's instructions, always including controls without RNA and reverse transcriptase ensuring a specific reaction. The rt-qPCR for quantification was performed with the PowerUp™ SYBR Green Master Mix following manufacturer's instructions.

Table 3-1. Primers

Gene	Primer Sequence (5' to 3')
***Gapdh*-fw**	AGTCTACTGGCGTCTTCAC
***Gapdh*-rev**	TCATATTTCTCGTGGTTCAC
***Adgrl1*-fw**	GCAGAAAGTCTTCGTGTGCC
***Adgrl1*-rev**	CGTAGATACGGTCACCTGCC
***Adgrl2*-fw**	ATGACACCGTGAGGAAGCAG
***Adgrl2*-rev**	TAGGGGTTGTTAGTGCCGTG
***Adgrl3*-fw**	CGTCCGAAAGCAGTCAGAGT
***Adgrl3*-rev**	CTGGCATTGTTCAGAAGCCC

3.3 Antibodies

The Anti-NF200 antibody (commercial) was obtained by immunizing the host organism with the C-terminal segment of enzymatically dephosphorylated pig neurofilament 200 and displays a broad species crosstalk, recognizing both the phosphorylated and non-phosphorylated forms of this antigen. The according gene in *Rattus norvegicus* is *Nefh* and expression is primarily found in neurons. While anti-NF200 antibodies primarily target larger neurons, there is no accurate association with functionality. An attempt to differentiate the $NF200^+$ cluster into five subpopulations has been performed and shows different transcriptomes and cell sizes [35]. The same work also attempted to make functional associations using gene ontology databases, identifying low threshold mechanoreceptors and proprioceptors as main constituents of the $NF200^+$ cluster. Studies in rats lumbar dorsal root ganglia observed ~40 % of the neurons to be $NF200^+$ with a mean cross-sectional area of ~930 µm² for L4 and L5, but ~660 µm² for L6 [33]. $NF200^-$ neurons had no area differences between L4/5 (~ 325 µm²) and L6 (~327 µm²).

The Anti-CGRP antibody (commercial) was obtained by immunizing goats with a synthetic peptide corresponding to a C-terminal sequence of rats' calcitonin gene-related peptide. $CGRP^+$ neurons either secrete CGRP or express it in the endoplasmic reticulum. CGRP is, commonly used for identifying dorsal root ganglion neurons of the peptidergic nociceptor cluster.

Isolectin B4 (commercial) is a glycoprotein of the tetrameric type I isolectin family and binds to α-Galactose. It is obtained from *Bandeiraea simplicifolia* and commonly used to identify the conventional non-peptidergic nociceptor cluster in dorsal root ganglion neurons. While mainly C-fibre neurons are $IB4^+$, some $IB4^+/NF200^+$ neurons as well as $IB4^+$ A-fibre neurons were observed in past studies [131]. Of lumbar rat dorsal root ganglia cells, ~60 % of the neurons are

$IB4^+$ and consist of small (< 400 µm²) and large (> 800 µm²) neurons with a median cross sectional cell area between 200 and 300 µm² [132].

The Anti-ADGRL1 antibody (supplied by Prof. Ushkaryov) was obtained by immunizing rabbits with the N-terminal domain of ADGRL1 (protein sequence: YAFNTNANREEPVSLAFPNP). The antibody was purified before usage: Blots including the 100 – 140 kDa regions of rats' dorsal root ganglions were blocked overnight in 5% non-fat dry milk blocking solution. Subsequently the blot was incubated with the ADGRL1 antibody overnight at 4 °C. Afterwards, the blot was thoroughly washed, and antibodies were eluted with 100 mM triethylamine (pH = 11.5) and immediately neutralized with 1 M HEPES buffer (pH = 7.5). IgG concentration was verified using the Nanodrop2000 machine (10 µm/ml).

Due to post-translational proteolysis, we expect bands of ~ 120 kDa N-terminal fragment (our target) and ~85 kDa for the C-terminal fragment.

The Anti-ADGRL3 antibody (commercial) was obtained by immunizing rabbits with a synthetic peptide of the C-terminal domain of ADGRL3. Before usage, the same purification procedure as for the ADGRL1 antibody was performed, but we used the 70 – 100 kDa range. For ADGRL3, we also expect bands of ~ 120 kDa N-terminal fragment and ~85 kDa (our target) for the C-terminal fragment.

3.4 Western Blot

Protein extraction was performed using the TRIZOL™ reagents according to manufacturer's instructions. Yield and purity were determined using the NanoDrop2000. The separation gel was prepared with 3.35 ml H_2O, 4 ml Acrylamid/bis (30:2), 2.5 ml 3 M Tris (pH 8.8), 100 μl 10% sodium dodecyl sulfate (SDS), 100 μl 10% ammonium persulfate (APS) and 6 μl tetramethylethylenediamine. The collection gel was prepared with 3.48 ml H_2O, 0.8 ml Acrylamid/bis (30:2), 0.625 ml 1 M Tris (pH 6.8), 50 μl 10% SDS, 50 μl 10% ammonium persulfate and 5 μl tetramethylethylenediamine. For SDS-polyacrylamide gel electrophoresis, the protein concentrates were denaturized by adding β-mercaptoethanol and applying heat (50 °C). SDS inhibits protein-protein interactions by charging proteins strongly negative, masking the proteins' own charge. A voltage of 50 V was applied for 30 min for clustering of the protein mixture in the collection gel. Subsequently, the voltage was increased to 120 V until the smallest proteins reached the desired distance.

Proteins were blotted from the gel to a nitrocellulose-membrane overnight at 40 mA in Towbin-Buffer (3.03 g/l Tris, 14.415 g/l Glycine, 0.375 g/l SDS in a mixture of 200 ml methanol and 800 ml distilled water).

Membranes were blocked with 2.5% milk and 2.5% bovine serum albumin in phosphate buffer solution (PBS) for 1 h at room temperature. Rabbit anti-ADGRL1 and rabbit anti-ADGRL3 antibodies were applied at a dilution of 1:1000 in 1% bovine serum albumin in PBS overnight at 4 °C. The membranes were washed and incubated with horse radish peroxidase conjugated sheep anti-rabbit antibodies (1:3000) for 1 h at room temperature. Afterwards, the membranes were thoroughly washed (three times 10 min at room temperature) in 0.1% Tween in PBS.

For signal detection, ECL-I and ECL-II solutions (containing luminol) were mixed 1:1 and incubated for 2 min at room temperature. The oxidation caused light emission (428 nm) which was captured with a chemo-luminescence detector.

3.5 Immunofluorescence and Immunohistochemistry

3.5.1 General Preparation

Tissue was harvested by a Dr. Chen after euthanizing the animals. The samples were embedded in Tissue Tek O.C.T. Compound and snap frozen in liquid nitrogen. Samples were stored at -80 °C for RNA*ish* and -20 °C for regular immunohistochemistry. Cryosections (10 µm) were prepared at -20 °C in a cryostat and stored at -80 °C until further usage.

3.5.2 RNAish

Tissue sections were incubated in precooled 4% paraformaldehyde (PFA) in diethyl pyrocarbonate (DEPC) treated, distilled water for 15 min. Until RNAscope probes were added, washing steps were performed with DEPC treated reagents to prevent RNA degradation. After fixation, the samples were dehydrated in ethanol (50%, 70%, 100%, 100%; 5 min each at room temperature). Hydrophobic barriers of approximately equal area were drawn around the tissue sections. As barriers had dried completely, sections were incubated with two drops of RNAscope Protease IV reagent (15 min, room temperature). Subsequently, RNAscope fluorescent multiplex assay or chromogenic assay was performed according to manufacturer's instructions, using probes for rat *Adgrl1* and *Adgrl3*. *Adgrl1* mRNA was visualized with Cy3 and *Adgrl3* with Cy3 or Cy5 dye.

After the RNAscope assay, further preparations were performed under minimal light exposure. Samples were washed, blocked in 10% donkey serum in PBS (1 h, room temperature), and counterstained with neuronal markers: for peptidergic nociceptors mouse anti-CGRP antibodies

(1:150), for large myelinated mechanosensors and proprioceptors rabbit anti-NF200 antibodies (1:200) and for non peptidergic nociceptors IB4-FITC conjugate (1:200) was added over two nights at 4 °C. All antibodies were diluted in 10% donkey serum in PBS. After incubation, the sections were thoroughly washed in PBS, and appropriate secondary antibodies were added if necessary. All secondary antibodies were diluted in PBS (1:1,000) and incubated for 1 h at room temperature. Before mounting the slides using Vectashield Hardset Antifade Mounting Medium, the slides were washed and counterstained with DAPI or Hoechst 33342 solution. The slides were stored at 4°C for a maximum of 24 h until imaging.

3.5.3 Protein Staining Protocols

Immunofluorescence

For fixation, sections were immersed in 4% PFA for 15 min at 4 °C and blocked with 10% donkey serum in 0.3% Triton X-100 in PBS for 1 h at room temperature. Afterwards, slides were incubated with the respective antibodies for 16 h at 4 °C: rabbit claudin-1 antibody (1:100), mouse claudin-5-Alexa488 conjugate antibody (1:200), claudin-12 (1:100), rabbit claudin-19 (1:100, gifted by Prof. Hou, St. Louis, USA [133]), mouse ZO-1-Alexa488 conjugate antibody (1:200) and rabbit von Willebrandt Factor antibody (1:100). Following primary antibody incubation, the samples were thoroughly washed in PBS and incubated with a suitable secondary antibody for 1 h at room temperature if needed. Finally, the samples were counterstained for nuclei with DAPI or Hoechst 33342 solution according to manufacturer's instructions and washed before mounting with Vectashield Antifade Mounting Medium. The slides were stored at 4 °C until imaging.

For anti-ADGRL/3 antibodies, the sections were fixed with 4% PFA and 1% glutaraldehyde in distilled water (15 min, 4 °C). The samples were treated with 0.3% H_2O_2 in distilled water for 10 min at room temperature and rinsed with PBS afterwards. Before applying the primary antibodies, sections were blocked with 10% donkey serum in 0.3% Triton-X in PBS for 1 h at RT. The rabbit ADGRL1 or rabbit ADGRL3 antibodies (1:200, Centennial, Colorado, USA; NLS1138) were applied as co-stainings with the respective neuronal marker (NF200, IB4, CGRP). The following steps of secondary antibody incubation, nuclear counterstaining and mounting were performed as described above.

Immunohistochemistry

Human dorsal root ganglion samples were obtained from the Netherlands brain bank. All tissues were donated for science with explicit consent. Therefore, no further ethical vote was required. Cryosections (d = 10 µm) were prepared after embedding the samples in O.C.T. Tissue Tek®. After PFA fixation (4% in distilled water, 15 min, 4 °C), samples were blocked 10% donkey serum in 0.3% Triton X in PBS for 1 h at RT. Samples were treated with eluted ADGRL1 (1:200) and ADGRL3 (1:200) antibodies overnight at 4 °C. After thorough washing horseradish peroxidase conjugated donkey anti-rabbit antibodies were incubated for 1 h at room temperature. Sequentially, slides were stained utilizing the 3,3'-diaminobenzidine peroxidase substrate kit following manufacturer's instructions. Signal was detected using bright field microscopy.

Studies on autofluorescence reduction were conducted chemically or via photo bleaching. The chemical approach was performed with the TrueVIEW® Autofluorescence Quenching Kit following manufactures instructions. For photo bleaching, tissue sample were exposed to daylight for up to 24 h or to a daylight lamp (TL 80, Breuer, Ulm, Germany) for up to 48 h.

3.5.4 Imaging

For evaluation, images of the fluorophore labelled samples were taken within one session using the same settings for each antibody on either a regular fluorescence microscope (Biorevo BZ-9000-E, Keyence, Osaka, Japan) or a confocal microscope (Olympus FV1000 confocal laser scanning microscope, Shinjuku, Japan). For semiquantitative *Adgrl1/3* RNA*ish*, 12-bit image analysis, stacks with a step size of 1 µm and a resolution of 1600 x 1600 pixels covering 424 µm² were acquired.

3.5.5 Image Analysis

Images were analysed with Fiji/ImageJ (Version 1.52o, Open Source). Brightfield images were used to distinguish the distinct areas of the dorsal root ganglion as demonstrated in **Figure 18** whenever required. For cell type specific analysis, putative counter-stainings (vessels: von Willebrandt Factor; neuron subpopulations: NF200, IB4, CGRP) were used to identify regions of interest. If z-Stacks were acquired, maximum projection images were calculated before further processing. Area and sum intensity of all regions of interest (ROI) were determined for further analysis. Furthermore, at least three background regions were also marked as ROI and measured to account for individual noise in later calculations.

For unbiased and repeatable dot segmentation during RNA*ish* semi-quantification, an ImageJ script was established, processing as following: The z-stack was converted into a maximum

projection image and a threshold mask was applied (grey value >=1200 for the Cy3 and >= 1150 for the Cy5 channel). The mask was then filtered for elements with a pixel size between 3 and 22 pixels, the resulting ROIs were measured in the putative channel.

3.5.6 Computational Image Segmentation

For unbiased verification of the manual image segmentation during RNA*ish* semi-quantification, an experimental approach with segmentation by a computational neural network (DeepFLaSH [134]) was performed. Training images were exported as 1024 x 1024 pixel, 8-bit images and labels were provided as 1024 x 1024 pixel binary images. The network was trained with six manually segmented images for each neuronal marker, training for 75 epochs. None of the RNA*ish* images were used for training. Subsequently, the network was used to segment the images for semi-quantification of mRNA expression.

3.5.7 Calculations

To approximate the number of RNAscope dots per cell, the following calculations were performed for each cell in each channel:

1. **Mean determined intensity of background ($mIntD_{BG}$):**

$$\mathrm{mIntD_{BG}} = \frac{\sum_{i=1}^{n_{BG}} \frac{Intensity_{BG_i}}{Area_{BG_i}}}{n_{BG}}$$

2. **Corrected determined intensity of a cell:**

$$cIntD_{cell} = IntD_{cell} - (Area_{cell} * mIntD_{BG})$$

3. **Corrected determined intensity of a single dot:**

$$c\mathrm{IntD_{Dot}} = \mathrm{IntD_{Dot}} - (\mathrm{Area}_{Dot} * m\mathrm{Int}D_{BG})$$

4. **Approximated dot number per cell (dpc):**

$$dpc = \frac{cIntD_{cell}}{\frac{\sum_i n_{Dots}(cIntD_{Dot_i})}{n_{Dots}}}$$

The mean dpc value of all measured cell ROIs is the dpc value of the sample; n_{dots} represents the count of all dots in one image; n_{BG} represents the three measured background areas.

3.6 Statistical Analysis

R Studio (Version 1.1447, Open Source) was used for statistics and plot generation with the plugins indicated in Table 3-2. For analysis of normality the Shapiro Wilk test and for analysis of variance homogeneity, Levene's Test of Equality was used if not stated otherwise. Further statistical analysis was performed as indicated in each experiment's result section. Whiskers in figures mark compared groups with statistical significance and stars represent the level of significance measured by p value (*: $p < 0.05$; **: $p < 0.01$; ***: $p < 0.001$).

Table 3-2. R Studio Plugins

Plugin	Version
ggplot2	3.2.1
ggpubr	0.2.3
readr	1.3.1
FSA	0.8.25
devEMF	3.7
officer	0.3.5
rvg	0.2.1
tidyverse	1.2.1
extrafont	0.17
readxl	1.3.1
lawstat	3.3
data.table	1.12.2

3.7 Material Lists

Table 3-3. Chemicals

Chemical	Manufacturer	Catalogue Number
4,6-diamidin-2-phenylindol (DAPI)	Roche	10 236 276 001
Acetone	Sigma Aldrich	W33261
Acrylamide / Bis 30%	Roth	A3574
Bromphenolblue	Sigma Aldrich	B0126
Diethylpyrocarbonate	Sigma Aldrich	D5758

Dimethyl sulfoxide	Sigma Aldrich	D4540
Tissue-Tek O.C.T. Compound	Sakura	4583
Vectashield Mounting Medium	Vector Labs	H-1400
Ethanol absolute	Th. Geyer	32205
Ethylenediaminetetraacetate	SERVA	11280
Glycerol	Invitrogen	11514011
Isopropanol	Sigma Aldrich	I9516
Non-Fat Dry Milk Powder	AppliChem	A0830,1000
Sodium chloride	Sigma Aldrich	31434
Sodium chloride (1 mol/l)	Roth	K025.1
Sodium hydroxide (1 mol/l)	Merck	1.09137.1000
Phosphate Buffered Saline Solution	Sigma Aldrich	D8537-1L
PageRuler^{TM} Plus Prestained Protein Ladder (10-250 kDa)	Thermo Scientific	26619
QIAzol Lysis Buffer	Qiagen	1023537
Bovine Serum Albumin	Sigma Aldrich	A2153
RNase Away	Sigma Aldrich	83931
RNase-free Water	Invitrogen	AM9937
IB4-FITC Conjugate	Sigma Aldrich	L2895
Tris(hydroxymethyl)aminomethane	Roth	5429.3
Triton X-100	Sigma Aldrich	X100
Tween-20bn	Sigma Aldrich	P1379
Distilled Water	Braun	0082479E
Hydrogen peroxide	Sigma Aldrich	216763
β-Mercaptoethanol	Sigma Aldrich	M6250
Hoechst 33342 solution	ThermoFisher Scientific	62249

Table 3-4. Primary Antibodies

Target Protein	Host Organism	Manufacturer	Catalogue Number
ADGRL1	Rabbit	Prof. Yuri Ushkaryov	
ADGRL3	Rabbit	Novus Biologicals	NLS1138
Claudin-1	Rabbit	Invitrogen	51-9000
Claudin-5 (Alexa 488 conjugate)	Mouse	ThermoFisher Scientific	352588
Claudin-12	Rabbit	IBL	#18801
Claudin-19	Rabbit	Prof. Hou, St. Louis, USA	
CGRP	Mouse	Abcam	Ab81887
Glutamine Synthetase	Mouse	BD Biosciences	610517
CD68 (FITC conjugate)	Mouse	Bio-Rad	MCA341F
MBP	Mouse	Sigma Aldrich	AMAB91062
S100b	Mouse	Sigma Aldrich	AMAB91038
NF200	Mouse	Sigma Aldrich	N0142
NF200	Rabbit	Sigma Aldrich	N4142
Pan-Sodium	Mouse	Sigma Aldrich	S8809
ZO-1 (Alexa 488 conjugate)	Mouse	Invitrogen	331594

Table 3-5. Secondary Antibodies

Species	Target Protein	Conjugate	Manufacturer	Catalogue Number
Donkey	Goat IgG	Alexa Fluor 405	Invitrogen	A-31553
Donkey	Goat IgG	Alexa Fluor 488	Invitrogen	A-11058
Donkey	Goat IgG	Alexa Fluor 594	Invitrogen	A-11055
Donkey	Goat IgG	Alexa Fluor 647	Invitrogen	A-21447
Donkey	Mouse IgG	Alexa Fluor 408	Invitrogen	A-31553
Donkey	Mouse IgG	Alexa Fluor 488	Invitrogen	A-21202
Donkey	Mouse IgG	Alexa Fluor 594	Invitrogen	A-21203
Donkey	Mouse IgG	Alexa Fluor 647	Invitrogen	A-31571
Goat	Rabbit IgG	Alexa Fluor 405	Invitrogen	A-31553
Donkey	Rabbit IgG	Alexa Fluor 488	Invitrogen	A-21206
Donkey	Rabbit IgG	Alexa Fluor 594	Invitrogen	A-21207
Donkey	Rabbit IgG	Alexa Fluor 647	Invitrogen	A-31573
Sheep	Rabbit IgG	HRP	Roche	12-015-215-001

Table 3-6. Solutions

Solution	Composition
DEPC-treated water	0.1% DEPC in distilled water
ECL solution I	250 mM luminol 90mM and p-Coumaric acid in DMSO, 10% tris
ECL solution II	10% Tris, 0.64% H_2O_2

Table 3-7. Commercially available kits

Kit	Manufacturer	Catalogue Number
RNAscope 2.5 HD Assay RED kit	ACD Bio	322350
RNAscope Fluorescent Multiplex kit	ACD Bio	320850
High Capacity cDNA Reverse Transcription Kit	Thermo scientific	4368814
Power Up SYBR Green Master Mix	Applied Biosystems	A25778
DAB Peroxidase (HRP) Substrate kit	Vector Laboratories	SK-4100
TrueVIEW® Autofluorescence Quenching Kit	Vector Laboratories	SP-8400

Table 3-8. Machines

Machine	Manufacturer	Catalogue Number
Real-time Thermocycler	Applied biosystems	272007446
Fluorescence microscope	Keyence	Biorevo BZ-9000-E
FV1000 confocal laser scanning microscope	Olympus	FV1000
Microtome	Leica	CM 3050S
Centrifuge (cooled)	BECKMAN	Avanti J-30I
Centrifuge (table)	Eppendorf	5418R
Tissue-Lyser	Qiagen Retsch	85220
HybEZ II Oven	Advanced Cell Diagnostics	240200ACD-2
Mixer Uzusio VTX-3000	Laboratory and Medical Supplies	VTX-3000L
Chemo-luminescence detector	Alpha Innotech	FluorChem FC2

Table 3-9. Miscellaneous material

Material	Manufacturer	Catalogue Number
Prolene 5.0	Ethicon Inc	Prolene 5.0
Nitrocellulose membrane	Fisher Scientific	10401396
Object slides ”SuperFrost Plus”	R. Langenbrinck GmbH	03-0060
Perma Silk 6.0	Ethicon Inc.	Perma Silk 6.0

Table 3-10. RNAscope Probes

Gene	Ref. Number
Hs-*ADGRL1*	547061
Hs-*ADGRL3*	547071
Rn-*ADGRL1*	520421
Rn-*Adgrl3*	520431
Rn-*Adgrl3*	520431-C3
Positive Control Probe (*Rn-Ppib*)	313921
Negative Control Probe (*DapB*)	310043
3-Plex Negative Control Probe (*Rn-Ppib* / *Hs-PPIB*)	320871
3-Plex Positive Control Probe (*DapB*)	320891

Table 3-11. Software

Software	Distributor	Version
Fiji/ImageJ	Wayne Rasband, NIH, USA	1.52o
R	The R Project	3.5.3
RStudio	RStudio, Boston, USA	1.1.447

4 Results

Firstly, I established and verified the RNA*ish* protocols as well as the quantification of the resulting images. My work further characterizes the mRNA level of *Adgrl1/3* in the neuronal subpopulations of lumbar dorsal root ganglia in rats ($NF200^+$, $IB4^+$, $CGRP^+$) before and after CCI using RNA*ish* combined with immunofluorescence. Furthermore, I demonstrated ADGRL1/3 expression at protein level within rat and human dorsal root ganglia by using antibodies, but with limited certainty regarding specificity. The mRNA study revealed a transient downregulation of *Adgrl1* in $IB4^+$ neurons one week after CCI and its recovery after 3 and 6 weeks.

In the second part, the spatial distribution of tight junction proteins in the neuron rich region as well as the fibre rich region and their putative epi-/perineural regions in lumbar dorsal root ganglia was characterized before and after CCI in an immunofluorescence study. I demonstrated a region-specific distribution of the tight junction proteins claudin-1, mainly expressed in the epi-/perineural region, and claudin-19, mainly expressed in the fibre rich region, as well as the tight junction associated protein ZO-1, which was mainly expressed in the epi-/perineural part of the fibre rich region. One week after CCI induced traumatic mononeuropathy, we observed a downregulation of vascular claudin-5 in the neuron rich region, but not in fibre rich region. We confirmed higher permeability of the blood-DRG-barrier within the neuron rich region compared to the fibre rich region for Hoechst reagent, a small molecule of ~533 Da, and fluorescein dextran, with an average molecular weight of ~4,000 Da. The permeability for large and small molecules was unaltered after CCI, but macrophage invasion in the neuron rich region was increased in the neuron rich region.

4.1 Characterization of *Adgrl1/3* Expression in Rats Lumbar Dorsal Root Ganglia Before and After Traumatic Nerve Injury

4.1.1 Muscle Tissue Shows Low *Adgrl1/3* mRNA Expression

Cerebral cortex, liver, and muscle tissue were selected for RT-qPCR screening, with cortex being the most researched tissue regarding *Adgrl1/3* expression. As **Figure 6** demonstrates, muscle tissue is a suitable negative control, expressing only 2.9% *Adgrl1* and 1.4% *Adgrl3* compared to cortex mRNA levels. Later, I used muscle tissue as negative control for the RNA*ish* experiment.

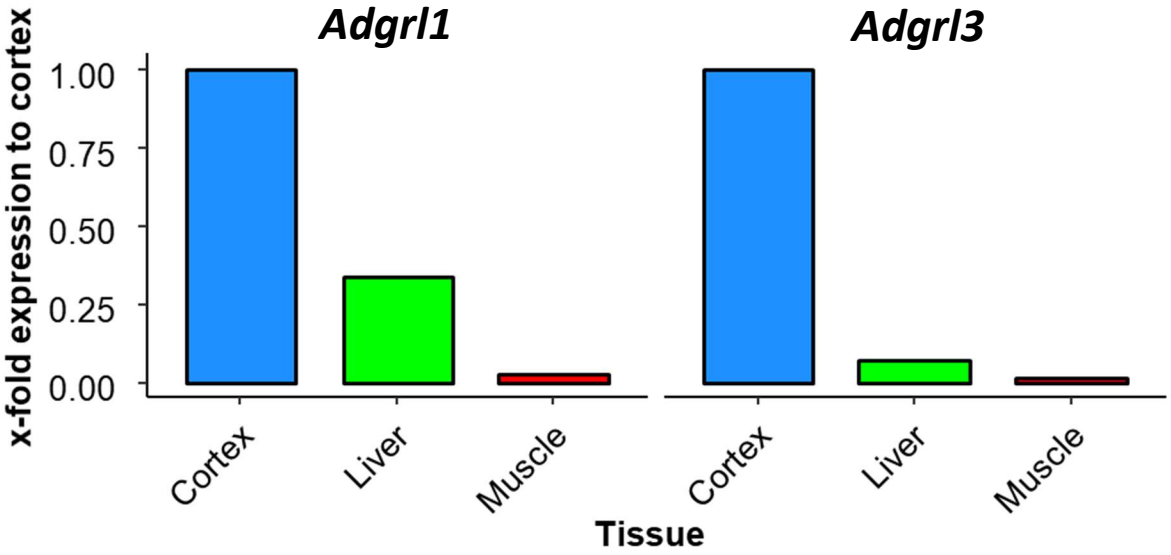

Figure 6. Muscle tissue expresses low *Adgrl1/3* mRNA levels. Therefore, it is suitable as negative control for further experiments. Immediately after sacrificing a male Wistar rat, tissues were extracted and snap frozen in liquid nitrogen. After RNA extraction using TRIZOL™ reagents and cDNA transcription, mRNA levels were quantified using GAPDH as household gene and n-fold expression compared to cortex was calculated. (n = 3)

4.1.2 Immunohistochemical Markers Distinguish Neuronal Subpopulations of the Dorsal Root Ganglion

Our results confirm specific signal for the anti-NF200, anti-CGRP and IB4 stainings after performing RNAscope pre-treatment (**Figure 7**).

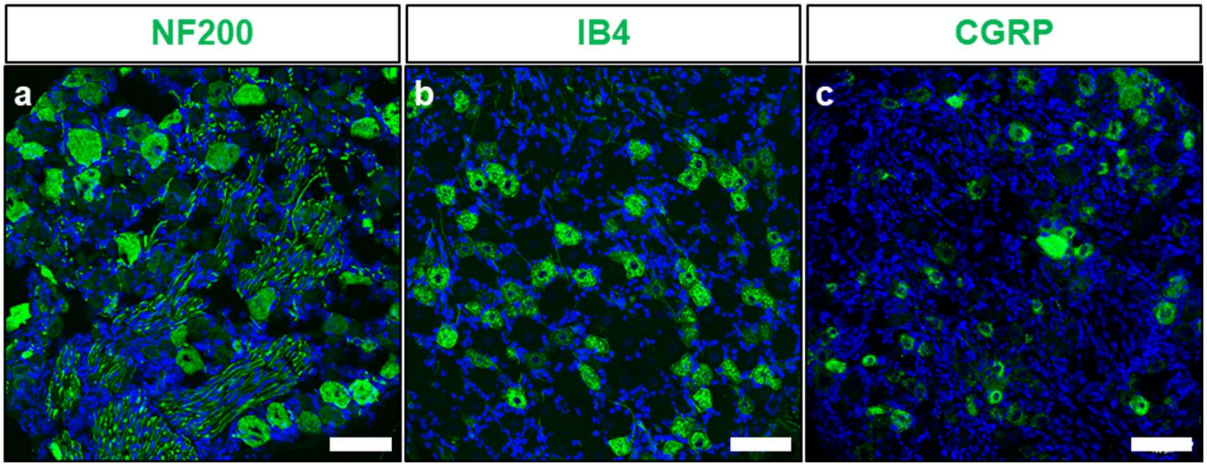

Figure 7. Specific NF200, IB4 and CGRP signal in rats lumbar dorsal root ganglia after RNAscope pre-treatment. Sections of dorsal root ganglia (d = 10 µm) were prepared with a cryostat and stained with antibodies against NF200 (a) and CGRP (c) as well as IB4 after pre-treatment with RNAscope™ reagents. Nuclei were counterstained using DAPI (blue). Scale bars: 100 µm. (n = 3) Representative example.

The cell populations were analysed regarding area distribution in naive animals as well as time course after CCI in contralateral and ipsilateral dorsal root ganglia. ROIs were designated manually or using a convolutional neural network [134] (training with n = 6 per counterstaining). **Figure 8** illustrates the area distribution of $NF200^+$, $IB4^+$, and $CGRP^+$ cells with no obvious alterations over six weeks after CCI: $NF200^+$ mean area was evenly distributed between cells larger/equal and smaller than 900 µm². $IB4^+$ and $CGRP^+$ cells were mostly smaller than 900 µm². The exact area values (mean, median, standard deviation of mean, number of analysed cells, percentage of cells smaller and larger than 900 µm²) are demonstrated in **Supplementary Table 1** and larger cells were mostly $NF200^+$, whereas $IB4^+$ and $CGRP^+$ cells were mostly of small size.

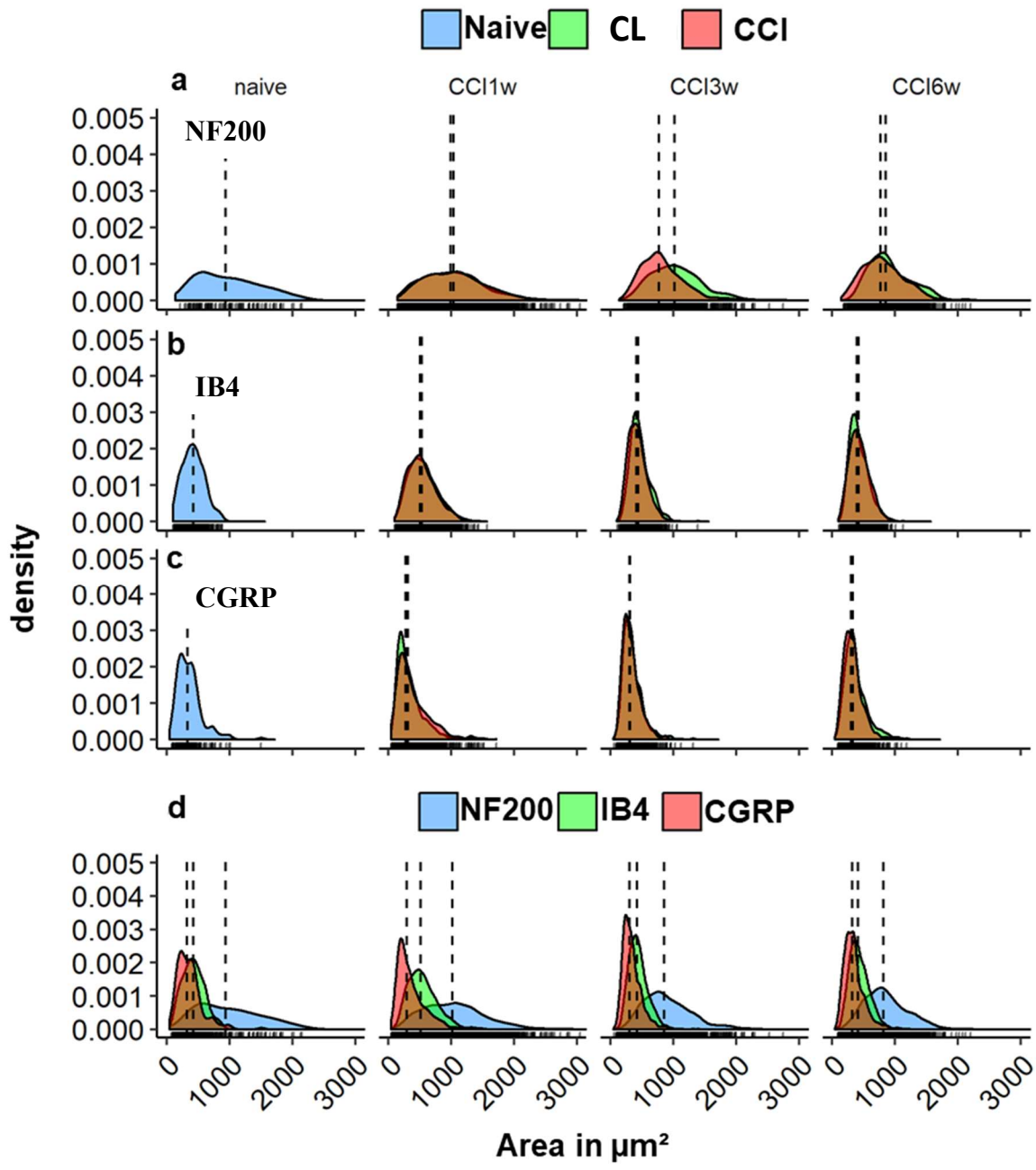

Figure 8. Cell area analysis reveals consistent area distributions over test conditions for NF200⁺, IB4⁺ and CGRP⁺ cells. A Total of over 12,000 cells was manually marked as ROIs in images of male Wistar rats' dorsal root ganglia (n = 18) in naive and CCI treated (ipsi- and contralateral) animals. Cell area distribution was density plotted, lines indicate median values of the area distribution in µm² for NF200⁺ (a), IB4⁺ (b) and CGRP⁺ (c) cells. First column demonstrates naïve (a-c: blue) animals, whereas animals after one (second column), three (third column) and six (fourth column) weeks after operation show animals with sham (a-c: green) and CCI (a-c: red) treatment. Data is summarized with area distribution of NF200⁺ (blue), IB4⁺ (green) and CGRP⁺ (red) cells after the putative timepoints (d). Dashed line indicates mean.

Next, I applied automatic cell segmentation using a convolutional neural network and compared the area distribution with manual segmented data from the same images. **Figure 9** demonstrates

the resulting segmentation process: I observed comparable results for NF200$^+$ cells, but the standard deviation of IB4$^+$ and CGRP$^+$ cells increased by a factor of 4.0, respectively 2.3. For NF200$^+$ cells, the proportion between large and small cells (>= or < than 900 µm²) was constant for both segmentation methods. The other two cell populations' fraction of large cells increased from 0 % to 17.6 % (IB4$^+$) and from 0.9 % to 12.7 % (CGRP$^+$) after computational segmentation (**Figure 9**).

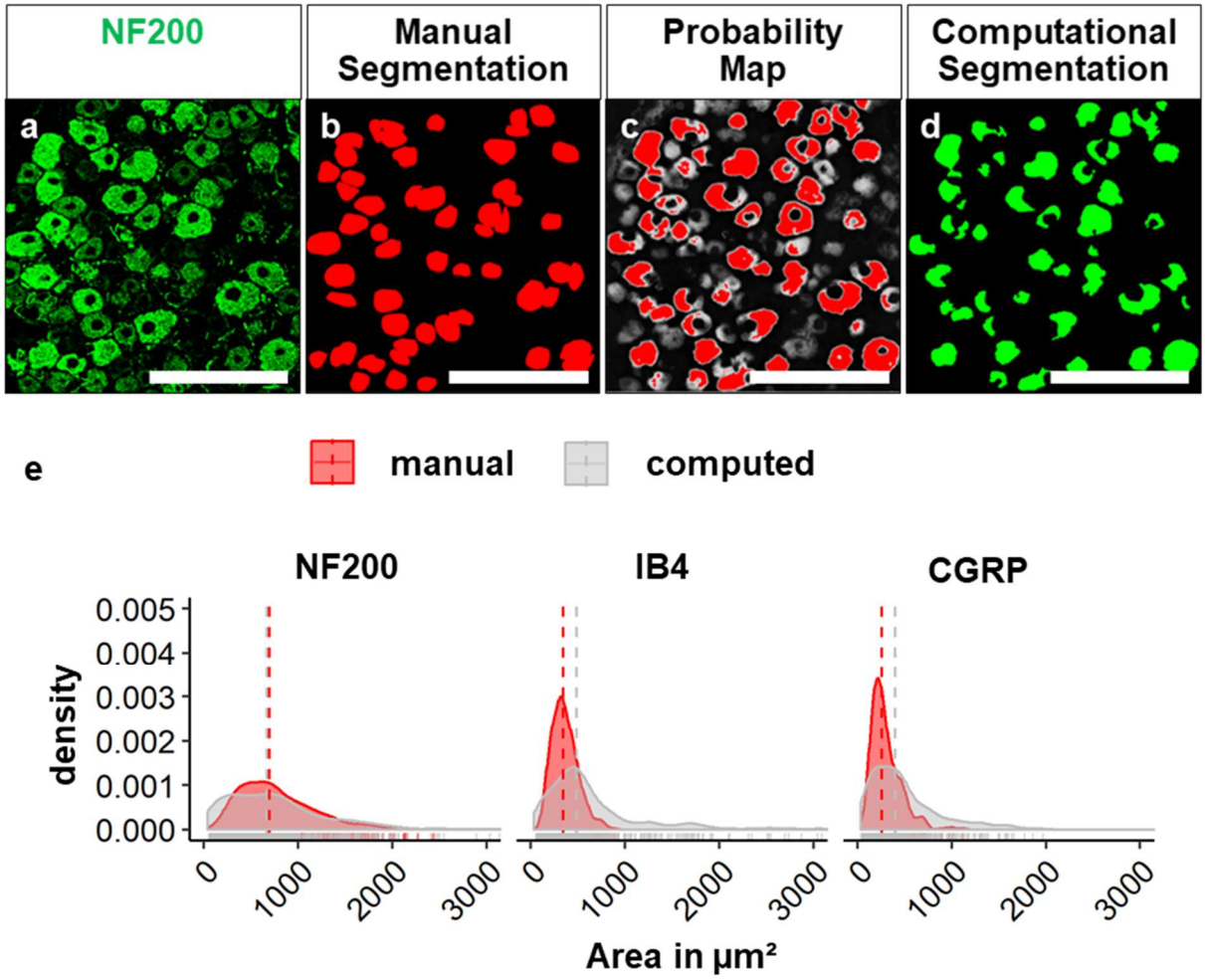

Figure 9. Manual and computational cell segmentation yield comparable results. Cell segmentation of NF200$^+$ cells by a convolutional neural network (CNN) shows wider distributed but similar cross-sectional cell areas compared to manual segmentation. An image of NF200$^+$ (green) cells in a rats' lumbar dorsal root ganglion (a) was manually segmented (b) for comparison and then analyzed by a CNN. The resulting probability map (c) shows calculated areas classified as part of a cell and pixels with a >= 95% confidence were accepted (red overlay). The result was turned into a binary segmentation map (d). The cells cross-sectional areas were density plotted (e). Scale bars: 200 µm (a-d); dotted line: median cross-sectional area (e).

While computational segmentation yielded promising results, nearby cells were sometimes classified as single cell and the nucleus region was not always marked. As a larger training set would be needed to overcome these hurdles, we chose manual segmentation as our primary

evaluation method for further experiments. Computational analysis was still performed to evaluate performance against the manual segmentation gold standard.

Finalizing the subpopulation analysis, we used a dorsal root ganglion section to detect all three subpopulations' signals at once and found that they partially overlapped (**Figure 10**). While we did not quantify the overlap, visual impression showed all combinations were observed but only at a low rate. We did not observe triple positive cells.

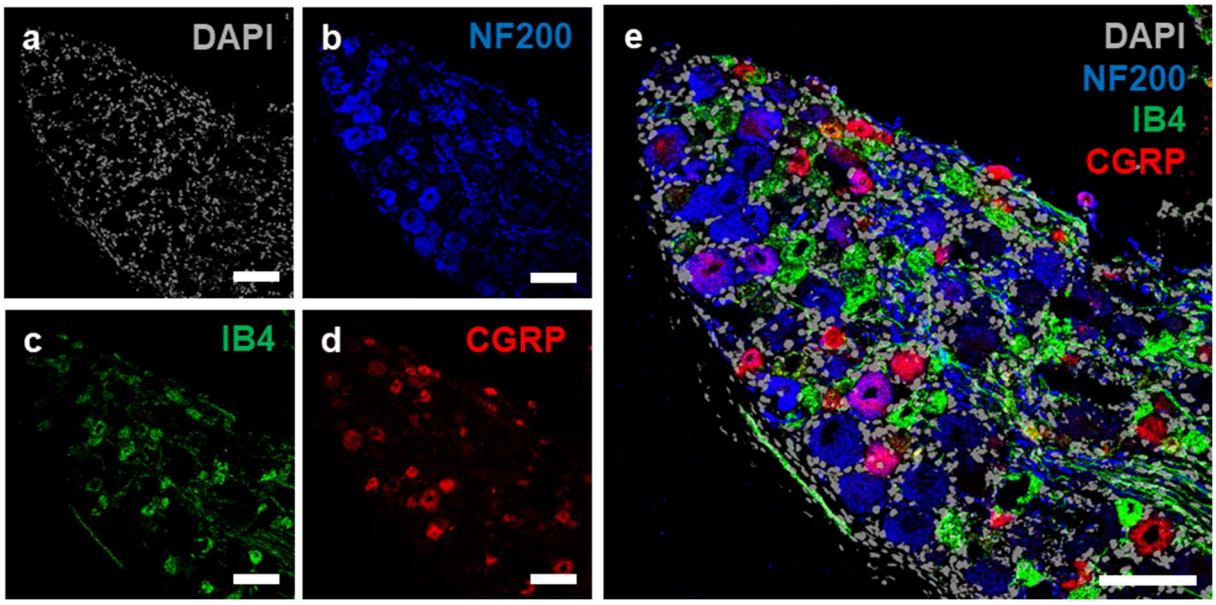

Figure 10. NF200$^+$, IB4$^+$ and CGRP$^+$ cells in rat lumbar dorsal root ganglion. NF200 (blue, pseudocolored), IB4 (green) and CGRP (red) positive neurons and overlap of populations, in the form of double-positive cells, are visible. Nuclear counterstaining was performed using DAPI (grey, pseudocolored). Images (a)-(d) show single channels and (e) the merged image. Scale bars = 100 µm

4.1.3 Chromophore Based RNAish is Highly Sensitive but Interferes with Immunofluorescence Counterstainings

After establishing protocols for the detection and segmentation of neuronal subpopulations, we used two RNAscope™ based methods to detect *Adgrl1/3* via chromophores and fluorophores. The chromogenic kit showed very high sensitivity but interfered with immunofluorescence in other channels. **Figure 11** demonstrates that the red fluorophore inhibits signal detection in the green channel. This resulted in areas with signal extinction in the green channel, resembling holes (a, b) or even completely absent signal (c, d).

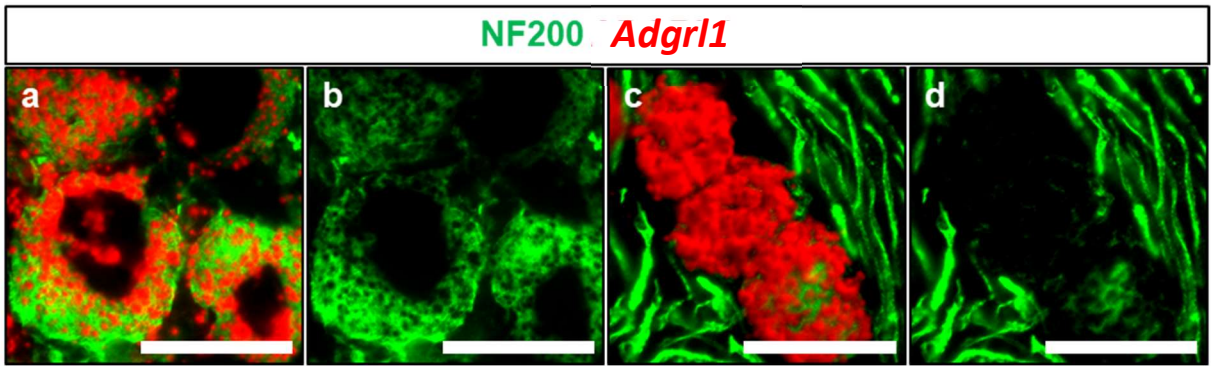

Figure 11. The red chromogenic RNAscope signal inhibits the Alexa488 fluorophore signal. *Adgrl1* mRNA was detected using the RNAscope™ chromogenic assay (red) according to the manufacturer's instructions in rats dorsal root ganglia. Subsequently, $NF200^{+}$ cells (green) were detected with a specific primary antibody and a suitable, Alexa488-conjugated, secondary antibody. Merged images with medium (a) and high (c) *Adgrl1* expression, as well as the putative single-channel images (b, d) demonstrate NF200 signal extinction in areas with *Adgrl1* signal. Scale bars = 25 µm.

The abundance of *Adgrl1/3* in the dorsal root ganglion combined with signal interference in other channels forced us to discard the chromogenic detection kit, despite its supreme sensitivity. Signal detection using the fluorogenic is demonstrated in **Figure 12**: while an intense signal for *Adgrl1/3* is detected (a), the negative control probes yield low signals (b). Surface plots visualize signal-to-noise-ratio and the efficacy of background reduction, which was crucial for further processing.

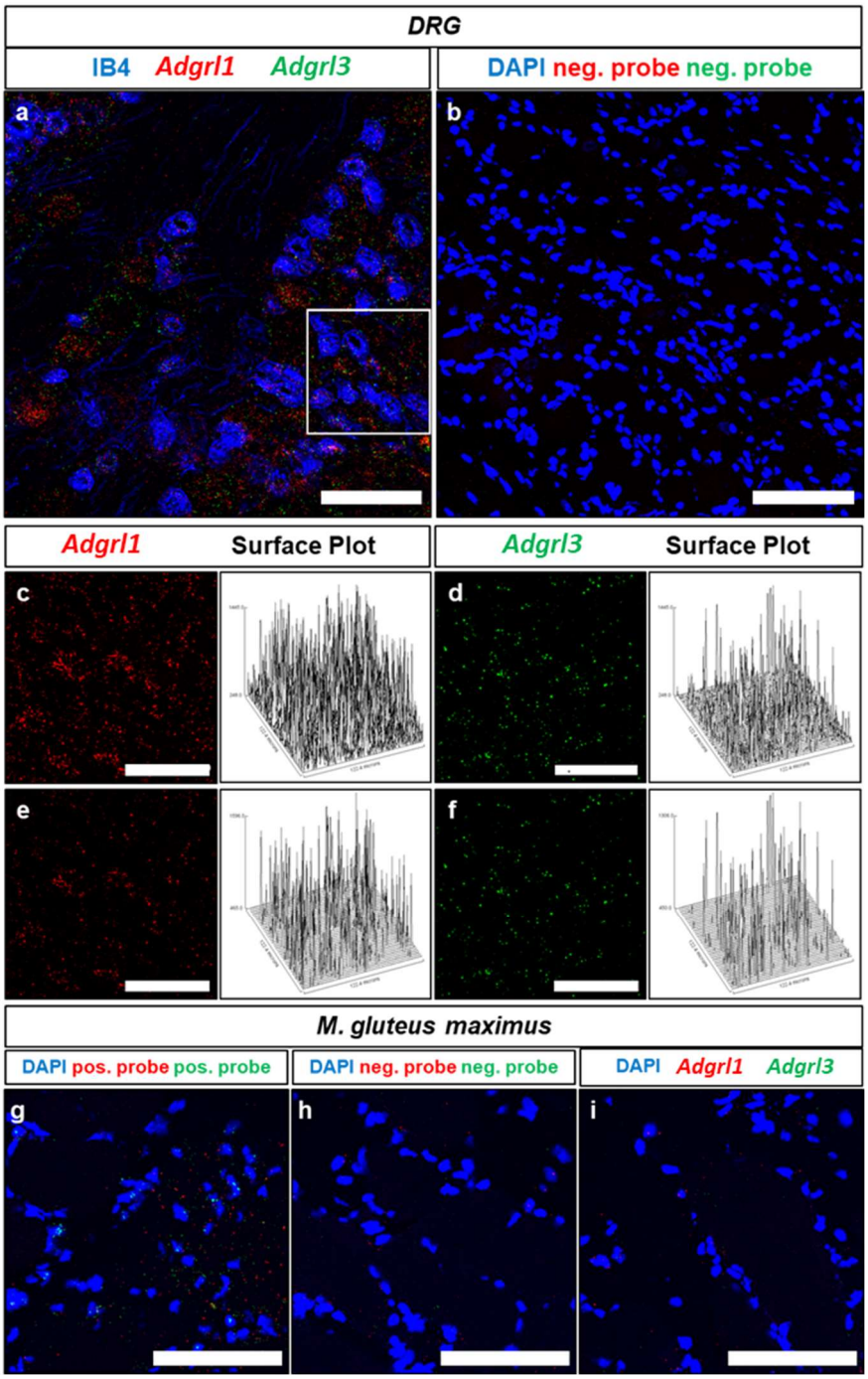

Figure 12. Fluorogenic RNAish specifically detects Adgrl1/3 in rats lumbar dorsal root ganglia. Muscle tissue (*M. gluteus maximus*) and lumbar dorsal root ganglia (DRG) were harvested from naive Wistar rats and RNA*ish* was performed utilizing the fluorophore based RNAscope™ assay following manufacturers' instructions. A costaining of *Adgrl1* (red), *Adgrl3* (green) with IB4 (blue) in the dorsal root ganglion demonstrates (a) abundant signal of both genes while the negative control probes were barely detected (b). The inset is magnified and only *Adgrl1* (c) or *Adgrl3* (d) is displayed. Next to them, the signal was surface plotted to visualize signal-to-noise-ratio, which is improved after background subtraction (mean grey value of three representative background regions plus mean value of their standard deviation was subtracted from every pixel). Muscle tissue expressed low *Adgrl1/3* mRNA levels in our rt-qPCR study and was chosen as control tissue for *Adgrl1/3*-probes. Positive control probes' signal is detected (g), neither the negative control (h) or *Adgrl1/3* (i) probes' signal is apparent. Scale bars: 100 µm (a. b, g, h, i), 50 µm (c, d, e, f).

4.1.4 Semi-quantification of Detected RNAish Signal

To semi-quantify the target genes mRNA expression reliably, we established an automated dot quantification algorithm utilizing the image analysis program *ImageJ's* macro function (script is documented in the appendix, chapter 8.1.1). We were able to achieve reproducible, unbiased, and image-specific semi-quantification by automatically recognizing mainly single dots based on size, circularity, and signal strength. Consecutively, we calculated the mean brightness per dot for each individual image. **Figure 13** demonstrates the results of this procedure in digitally magnified cells of the earlier introduced image of *Adgrl1/3* in IB4^{+} cells. Manual and computed dot count (*Adgrl1*: mean dpc_{manual} = 38 vs mean $dpc_{computed}$ = 32; *Adgrl3*: mean dpc_{manual} = 20 vs mean $dpc_{computed}$ = 19) were slightly different.

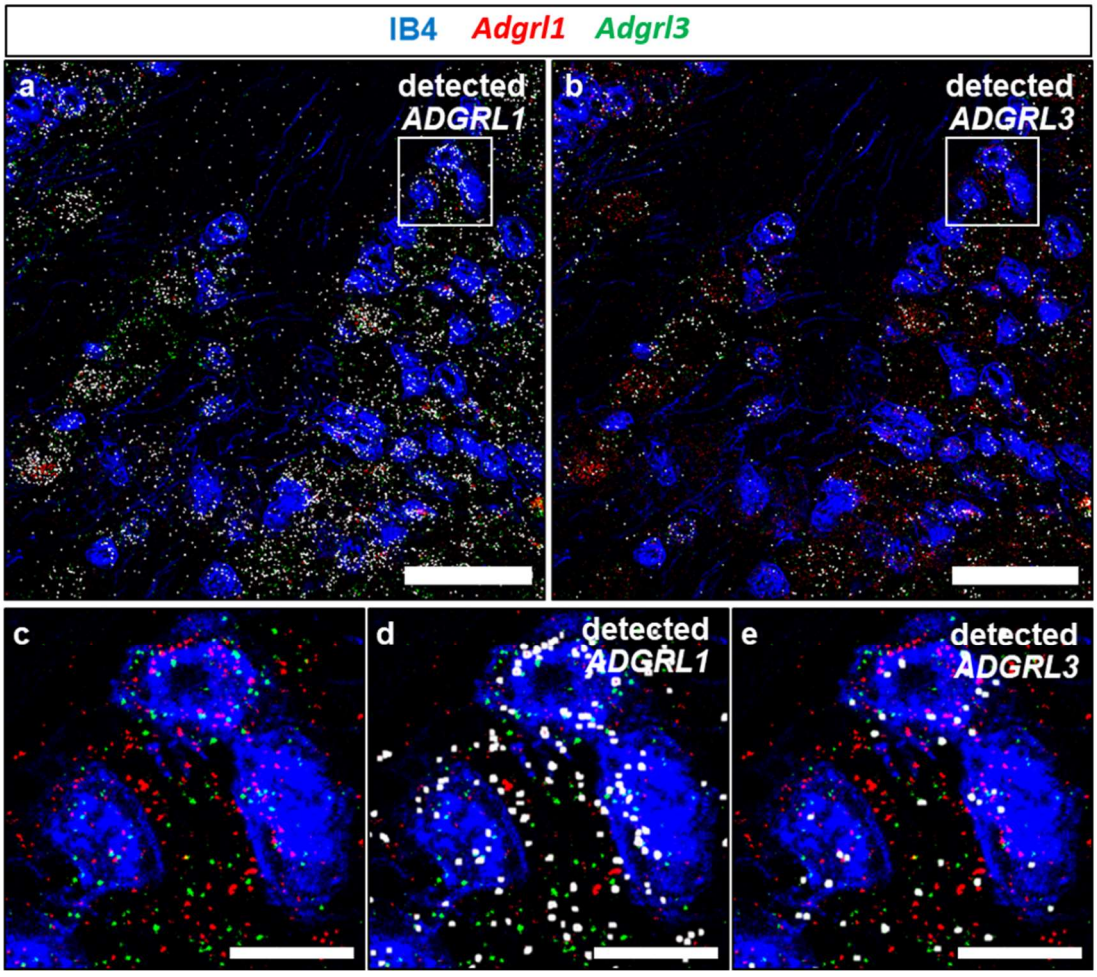

Figure 13. Computer assisted dot-recognition is utilized for fast, unbiased, and reproducible semi-quantification after RNA*ish*. Processing by an algorithm allowed us to detect signal peaks, marked in white (a, b, d, e), after RNA*ish* (*Adgrl1* (a) and *Adgrl3* (b)). The marked insets are magnified and show the raw insert (c), as well as recognized dots for *Adgrl1* (d) and *Adgrl3* (e). While single dots are identified, clusters are excluded. Scale bars: 100 µm (a, b) and 25 µm (c-e)

4.1.5 *Adgrl1* is Transiently Downregulated in IB4$^+$ and Upregulated in NF200$^+$ Dorsal Root Ganglia Cells Specifically After CCI

Following detection of *Adgrl1/3* mRNA in neuronal subpopulations, we proceeded to semi-quantify its expression over the time course of six weeks (naive, one week, three weeks, six weeks) after introducing traumatic mononeuropathy of the sciatic nerve (CCI model). Representative images from rat lumbar dorsal root ganglion sections after combined RNA*ish* and antibody staining are shown in **Figure 14**.

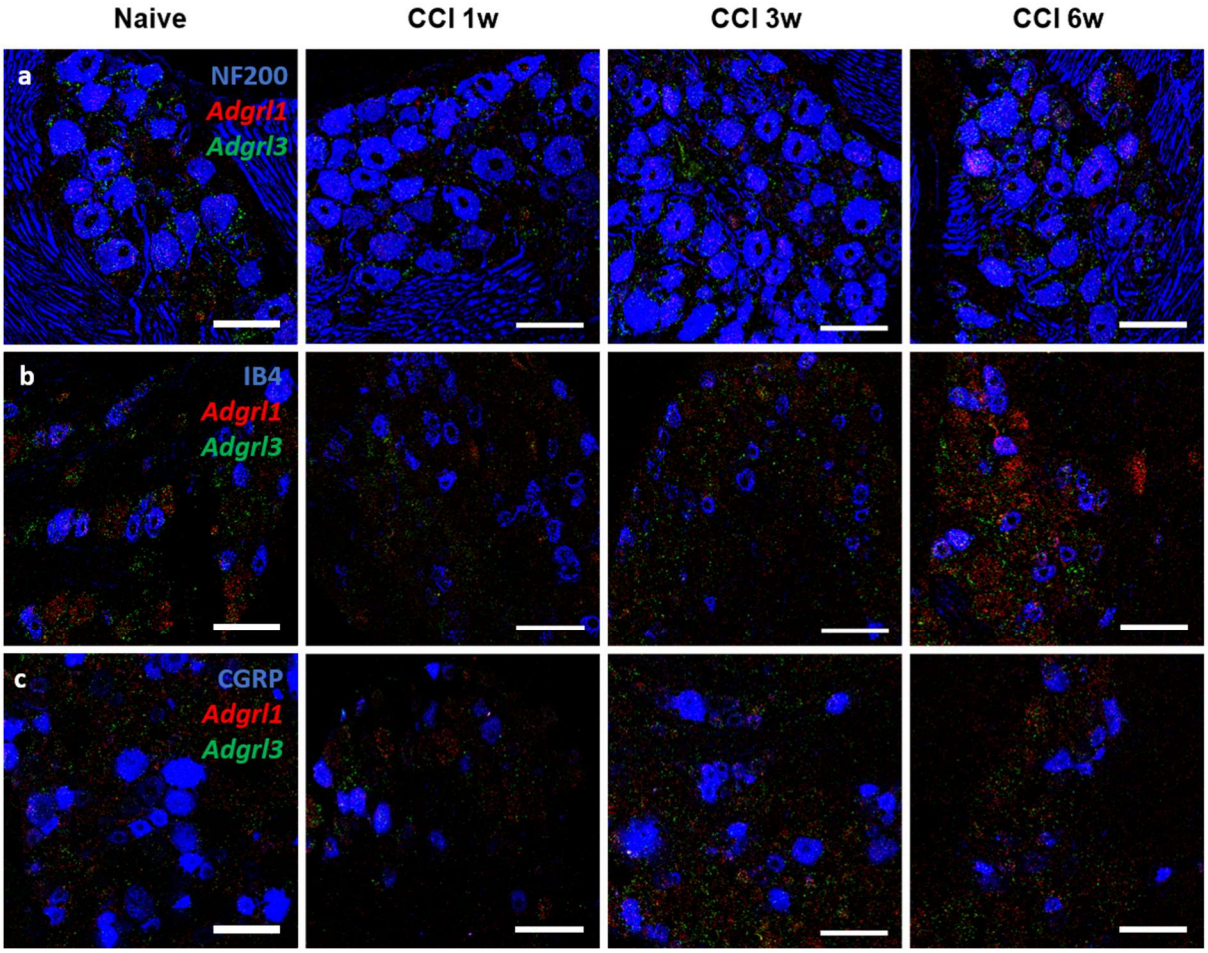

Figure 14. Adgrl1 is more abundant than Adgrl3 in all subpopulations and Adgrl1 expression is reduced in IB4+ cells one week after CCI. Wistar rats were sacrificed at the defined time points and samples were snap frozen in liquid nitrogen immediately after harvesting. Combined RNA*ish* and immunohistochemistry was performed under RNase free conditions as long as necessary to detect *Adgrl1/3* mRNA. One neuronal subpopulation was co-stained per section. The experiment was performed simultaneously for all groups and images were acquired within 24 h after staining. NF200$^+$ (a), IB4$^+$ (b) and CGRP$^+$ (c) neurons expressed *Adgrl1* and *Adgrl3* at all time points. Scale bars: 100 µm

All three neuronal subpopulations have high expression levels of *Adgrl1* and *Adgrl3*. The visual impression confirms higher levels of *Adgrl1* compared to *Adgrl3*. We employed the previously established methods for quantification of mRNA as dots per cell to verify this hypothesis. **Figure 15** visualizes the development of *Adgrl1/3* expression after CCI and revealed a

significant, transient downregulation of *Adgrl1* by 76% in IB4$^+$ cells after one week of CCI. Moreover, NF200$^+$ cells show no downregulation but an overexpression of *Adgrl1* to levels two-fold of naive cells' dots per cells after six weeks. *Adgrl1* expression in CGRP$^+$ cells as well as *Adgrl3* expression in general were unaffected.

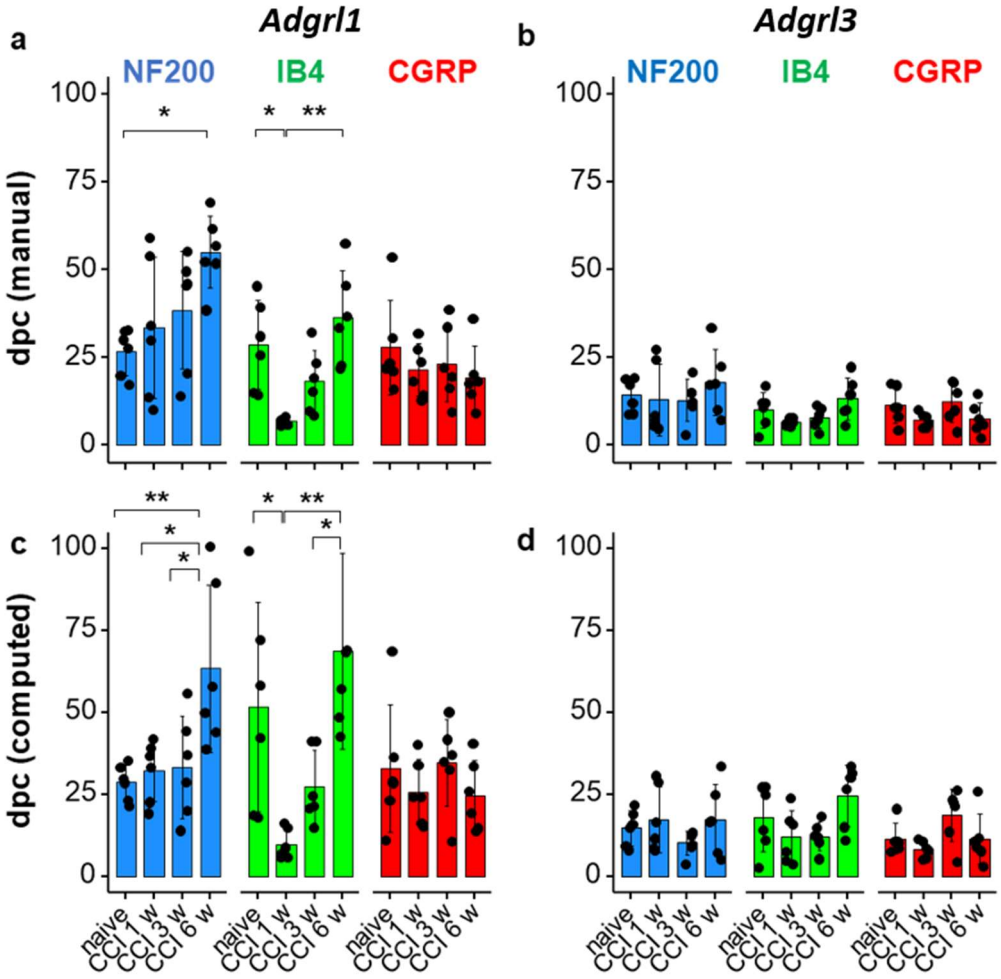

Figure 15. Transient downregulation of *Adgrl1* expression in IB4$^+$ cells early after CCI and upregulation in NF200$^+$ cells during late regeneration in rats lumbar dorsal root ganglia. The dorsal root ganglia were harvested from naive animals as well as one, three and six weeks after CCI. *Adgrl1* and *Adgrl3* expression was detected via *RNAish* and semi-quantified as dots per cell (dpc) in the neuronal subpopulations. Subpopulations were distinguished using immunofluorescence labeling against NF200, CGRP as well as IB4. Segmentation of immunofluorescence signal was performed manually (a: *Adgrl1*, b: *Adgrl3*) as well as computer assisted (c: *Adgrl1*, d: *Adgrl3*). A transient downregulation of *Adgrl1* after one week and consecutive regeneration was detected in IB4$^+$ cells. *Adgrl1* expression is increased six weeks after CCI in NF200$^+$cells. Error bars represent +/- sd, ANOVA and Tukey HSD or Kruskal Wallis and Dunn Tests were performed, depending on data distribution.

Since we detected *Adgrl1* and *Adgrl3* expression simultaneously *in situ*, we could calculate the ratio of mRNA expression within each cell. Initially, cells of all subpopulations expressed 2.2x – 3.2x as much *Adgrl1* compared to *Adgrl3* (NF200: 2.25x, IB4: 3.18x, CGRP: 2.55x). For IB4$^+$ neurons, the ratio is reduced to 1.08 after one week and recovers until week six. In NF200$^+$

neurons on the other hand, the ratio increases until week six (4.59). By analysing large and small cells separately, we evaluated a correlation between cell area and mRNA level. The correlation between *Adgrl* expression and cell size is linear for both Adgrl*1* and *Adgrl3*.

4.1.6 Anti-ADGRL1/3 Antibodies Indicate Expression in Rat and Human Dorsal Root Ganglia

For verification of protein expression, we used antibodies against the putative antigens. Western blot experiments with untreated antibodies resulted in multiple bands. Therefore, we purified the antibodies utilizing a rats' dorsal root ganglion blot (ADGRL1: 100 – 140 kDa, ADGRL3 70 – 100 kDa) to pull down and elute antibodies. The stock and purified antibodies were used for a western blot of a rats' dorsal root ganglia. Even after purification we find strong bands outside of our range used for purification and only barely visible bands at the expected range (Figure 16).

We proceeded staining rats dorsal root ganglia to demonstrate expression in dorsal root ganglia's $IB4^+$ and $CGRP^+$ cells as demonstrated in **Figure 16** b and c. The staining pattern did not vary considerably after purification. Furthermore, we detected ADGRL1/3 signal in light microscopy images of human dorsal root ganglia (**Figure 17**) utilizing immunohistochemistry. Human samples' autofluorescence was too high for regular immunofluorescence even after attempts to reduce it chemically.

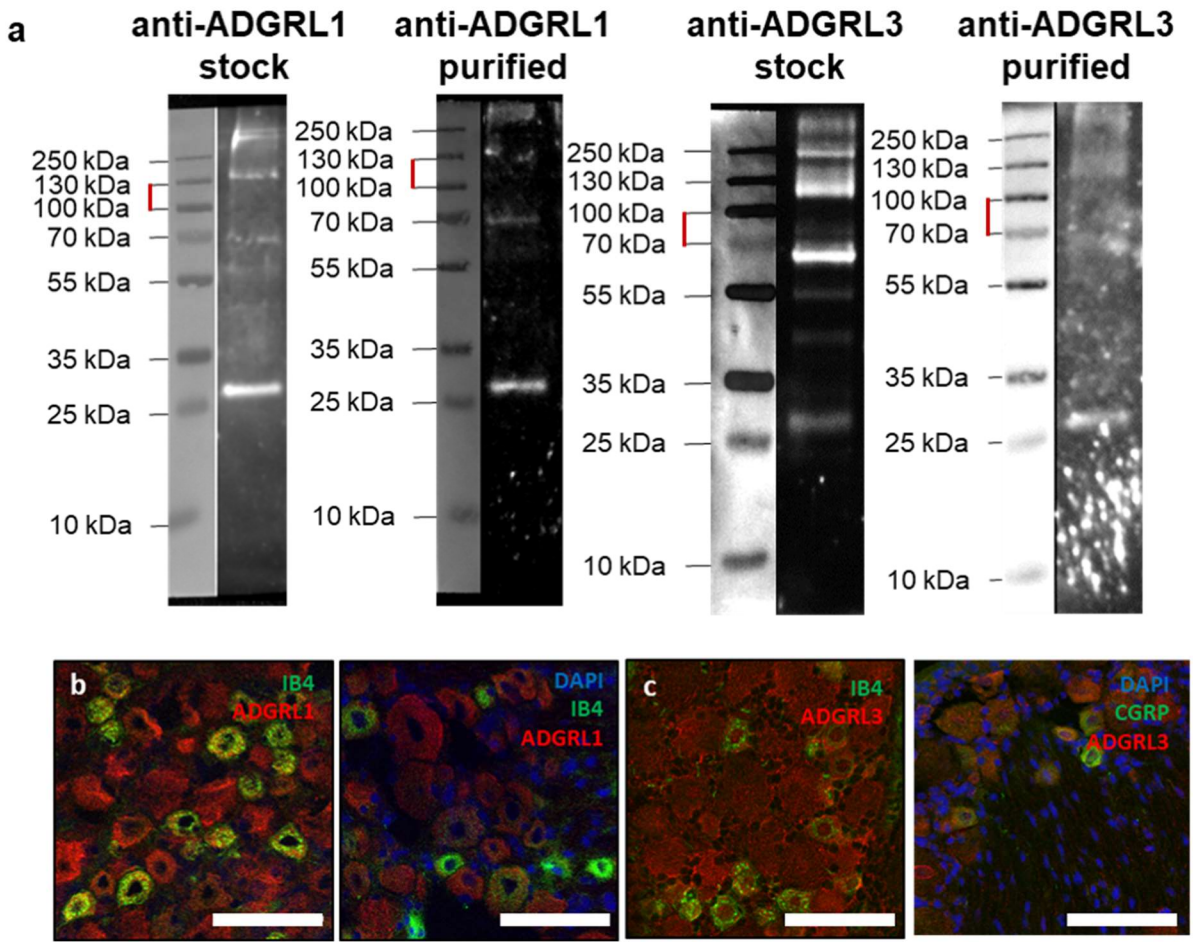

Figure 16. Anti-ADGRL1 and Anti-ADGRL3 antibodies result in multiple bands and ubiquitous immunofluorescence in rats' lumbar dorsal root ganglia. (a) Multiple bands of different molecular weights are visible in western blots of rat dorsal root ganglia before and after antibody purification via pulldown with blotted dorsal root ganglion proteins. Range of expected bands is signified by red bars (ADGRL1: ~120 kDa, ADGRL3 ~85kDa). Immunofluorescence of both (b) ADGRL1 and (c) ADGRL3 is detected in $IB4^+$ and $CGRP^+$ cells. Scale bars: 100 µm.

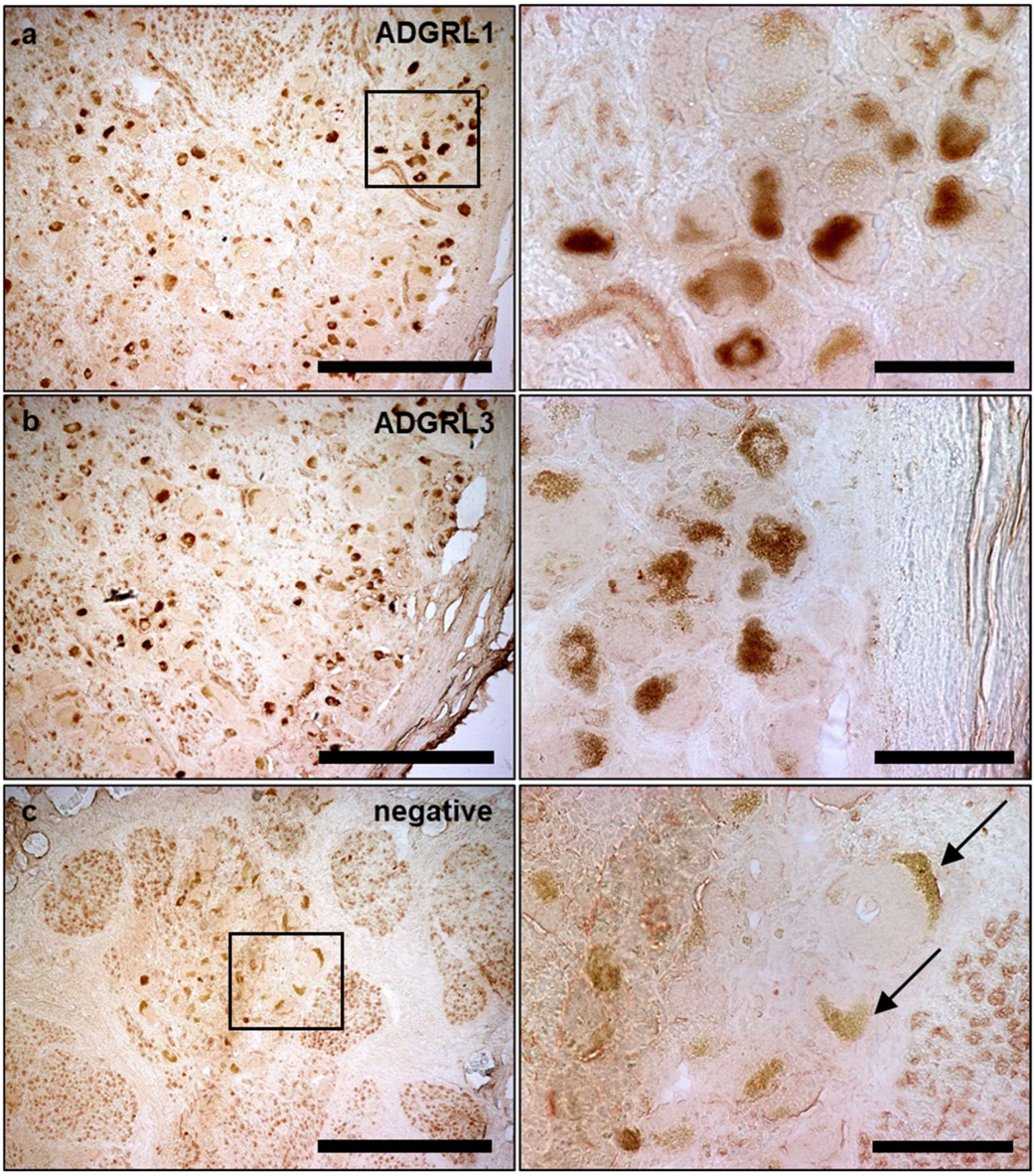

Figure 17. DAB signal of anti-ADGRL1 and anti-ADGRL3 antibodies in human dorsal root ganglia. Cryosections (d = 10 µm) of human dorsal root ganglia were treated with anti-ADGRL1 (a) and anti-ADGRL3 (b) antibodies. The signal was visualized utilizing DAB. Negative control (c) shows less signal. Black boxes indicate areas displayed in higher magnification. For ADGRL3, the magnified area is not visible in the overall view. Black arrows in the negative control indicate areas with pigment depositions. Scale bars: 500 µm (left column), 100 µm (right column).

4.2 In Situ Analysis Reveals Region-specific Tight Junction Proteins Regulation After Traumatic Mononeuropathy in Rats Lumbar Dorsal Root Ganglia

4.2.1 Expression of Claudin-1, Claudin-19 and ZO-1 in Rats Dorsal Root Ganglia is Region-specific

The blood-DRG-barrier was characterized regarding the distribution of claudin-1, claudin-5, claudin-12, claudin-19, and ZO-1 in the neuronal or fibre region and their putative epiperineurium (**Figure 18**). **Figure 19** demonstrates the tight junction proteins' distribution in naive rats: Claudin-12 was the most abundant tight junction protein among all regions. Claudin-1 was strongest in both epiperineural regions. ZO-1's immunoreactivity was highest in the epiperineurium of the fibre region. Claudin-19 immunoreactivity was most prominent in the neuron-rich region. ZO-1 and claudin-1 formed clusters resembling zig-zag patterns in the epiperineurium. Claudin-19 clustered in paranodes of myelinated fibres, as validated by NF200 co-staining (**Supplementary Figure 1**). Claudin-5 colocalized with von Willebrand factor (**Supplementary Figure 2**).

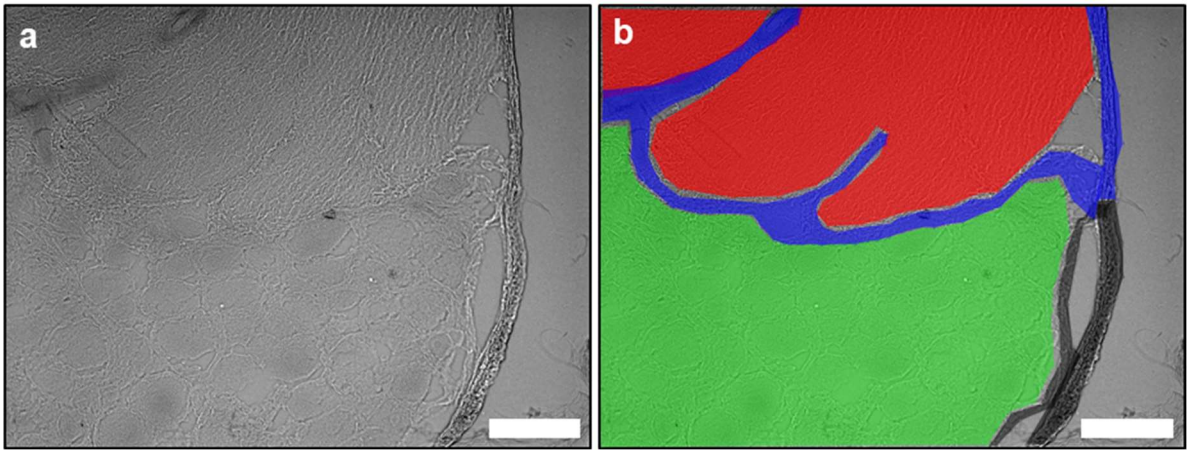

Figure 18. Neuron rich region and fibre rich region of rat dorsal root ganglia were distinguished in a brightfield image. Rats' dorsal root ganglia were sectioned in a cryostat (d = 10 µm) and imaged without further treatment. (a) Raw brightfield image, (b) demonstrates the result after manual image segmentation into neuron rich region (green), fibre rich region (red), neuron rich region's epiperineurium (black) and fibre rich region's epiperineurium (blue). Scale bar: 100 µm.

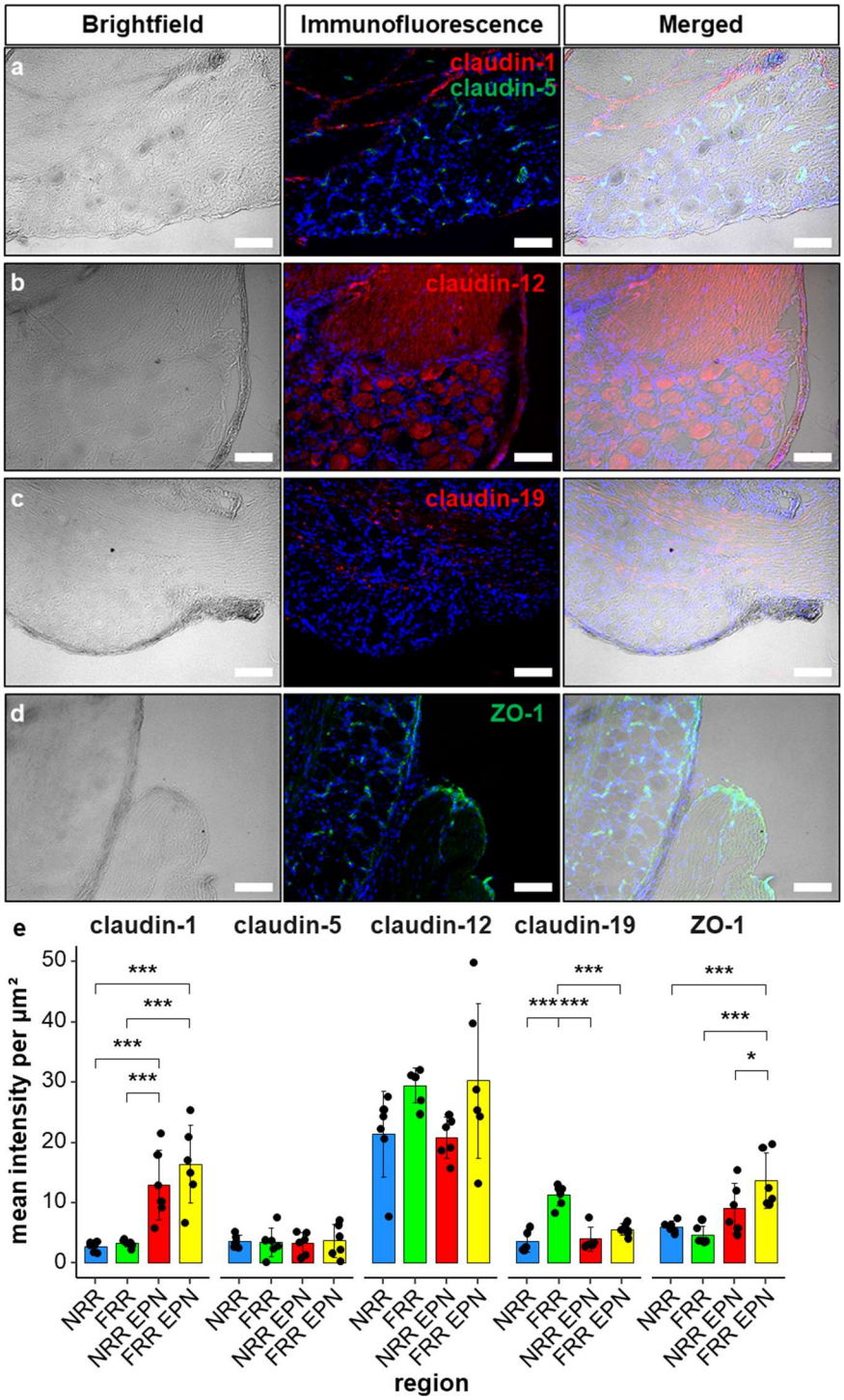

Figure 19. Epi-perineural regions express highest levels of claudin-1 and ZO-1, while most intense claudin-19 signal was in the fibre rich region of naive rats' dorsal root ganglia. Naive rats' dorsal root ganglia were harvested, snap frozen and sectioned using a cryostat (d = 10 µm). After staining, the signal was detected. Image analysis revealed region-specific expression of tight junction proteins in rats' dorsal root ganglia. (a-d): Representative brightfield (left column), immunofluorescence (middle column) and merged (right column) images demonstrating the location of claudin-1 (a, red), claudin-5 (a, green), claudin-12 (b, red), claudin-19 (c, red), ZO-1 (d, green). (e): Statistical analysis confirms differences between specific areas in specified regions of the dorsal root ganglion. Scale bars: 100 µm, ANOVA, Tukey HSD, n = 6.

4.2.2 Decreased Claudin-5 Immunoreactivity in the Neuron Rich Region One Week After Traumatic Nerve Injury

After looking into the spatial distribution of tight junction proteins expression in naive rat dorsal root ganglia, we investigated their expression one week after induction of traumatic nerve injury. **Figure 20** demonstrates representative images of the experiment. To increase sensitivity of our quantification for molecules with small areas of signal, we utilized von Willebrandt factor to assess vascular specific signals within the neuron rich and fibre rich region after CCI. We observed claudin-5 downregulation only in vessels of the neuron rich region (**Figure 21**).

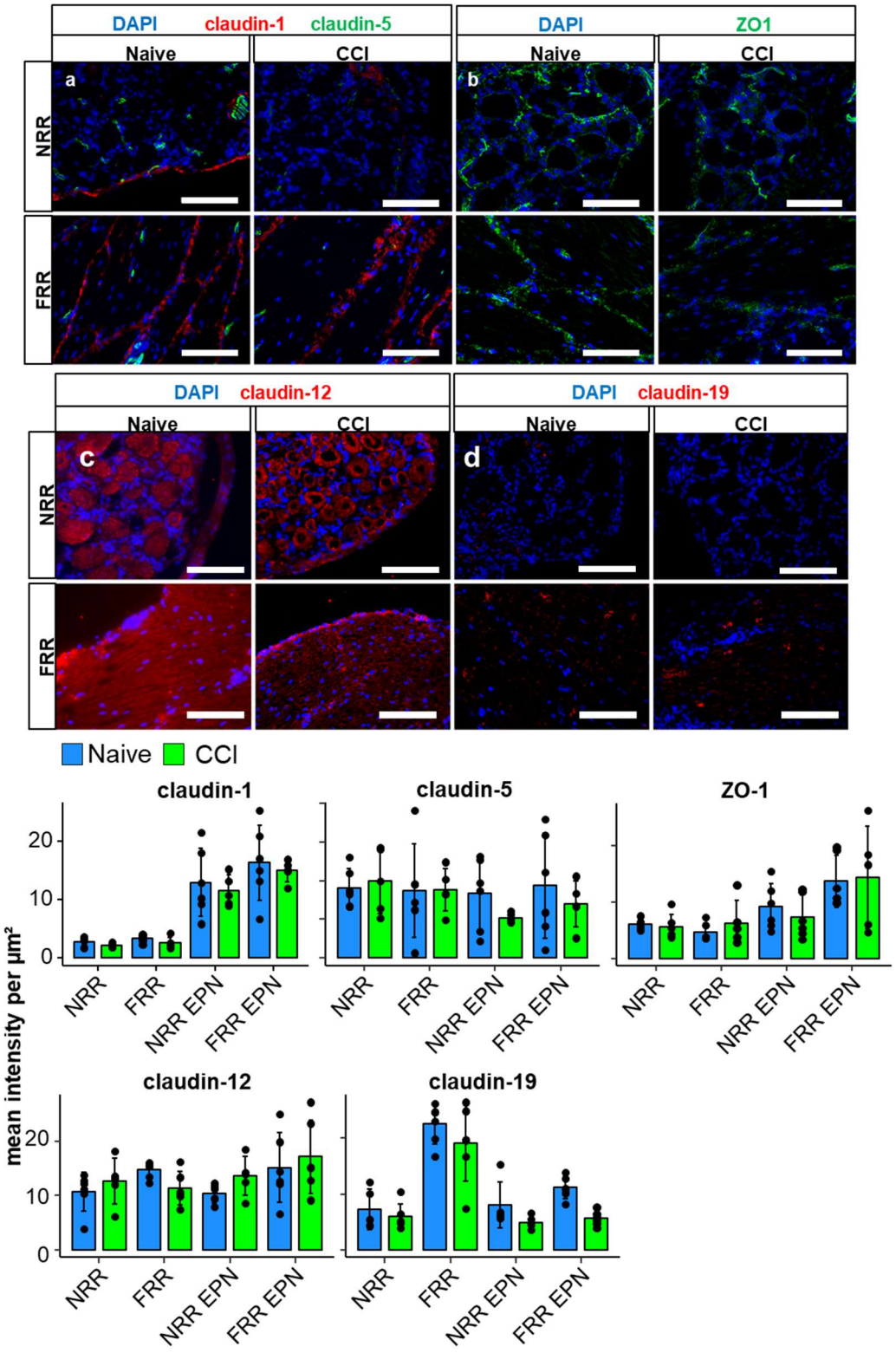

Figure 20. No alteration of tight junction proteins' regional expression in rats' dorsal root ganglia one week after CCI. Wistar rats dorsal root ganglia were harvested and immunostainings against the tight junction proteins claudin-1, claudin-5 (a), ZO-1 (b), claudin-12 (c) and claudin-19 (d) were prepared. Regional tight junction protein expression is unaltered after CCI compared to naive (neuron rich region, NRR; fibre rich region, FRR; epiperineurium, EPN; n = 5-6). Scale bars: 100 µm

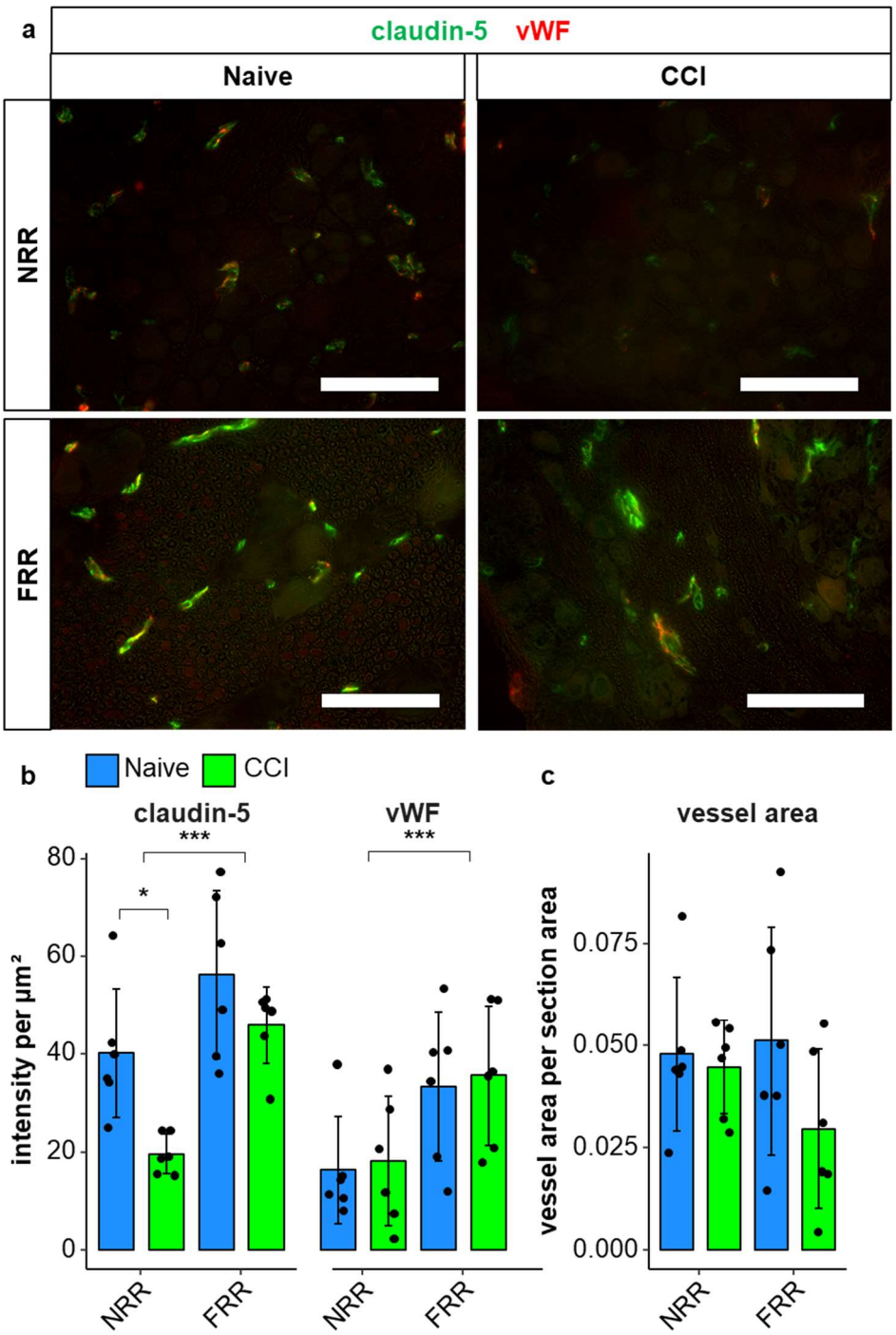

Figure 21. Vessel specific downregulation of claudin-5 one week after CCI only occurs in the neuron rich region. One week after CCI, lumbar dorsal root ganglia were harvested, processed and intravascular claudin-5 (green) immunofluorescence was measured (vessel marker: von Willebrandt Factor (vWF), red). Mean immunoreactivity per µm² in the neuron rich and fibre rich region (NRR, FRR) were compared. (a) Representative images of dorsal root ganglia' neuron rich region (upper row) and fibre rich region (lower row) in naive (left column) and CCI rats are shown. (b): Claudin-5 immunoreactivity was significantly reduced one week after CCI, while von Willebrandt Factor immunoreactivity did not change. Fibre rich region shows more abundant claudin-5 as well as von Willebrandt Factor signal. The area of analysed vessels was not significantly different between test groups (c). Scale bar: 100 µm

4.2.3 Increased Macrophage Invasion in the Neuron Rich Region After Chronic Constriction Injury

To evaluate the biological relevance of the vessel specific claudin-5 downregulation on permeability in the neuron rich region, we conducted perfusion experiments with small molecules, Hoechst (533.88 Da) reagent, as well as with larger molecules, FITC-dextran (average: 4000 Da). While there was a significantly higher immunofluorescence for FITC-Dextran and Hoechst immunofluorescence in the fibre rich region compared to the neuron rich region as demonstrated in **Figure 22**, we found no significant difference regarding immunofluorescence intensity one week after CCI comparing ipsilateral and contralateral dorsal root ganglia for FITC-Dextran and Hoechst reagent.

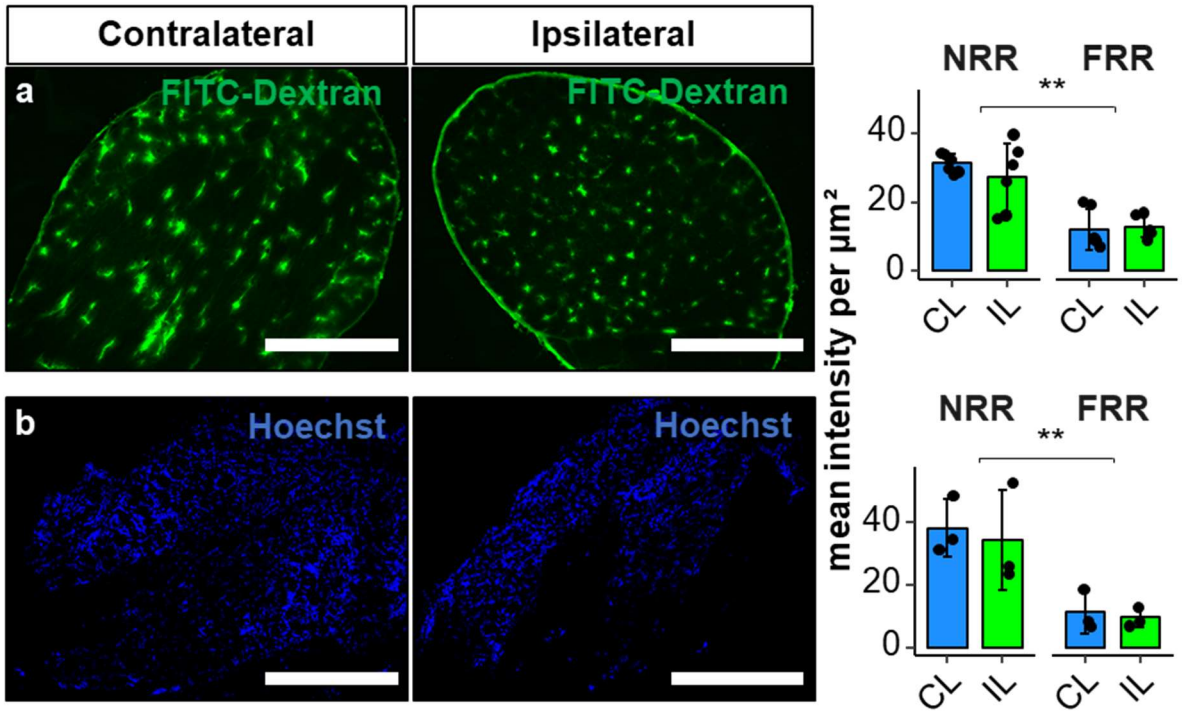

Figure 22. Permeability for small and large molecules is higher in the neuron rich region than the fibre rich region but unaltered after CCI. Male Wistar rats' contralateral (CL) and ipsilateral (IL) lumbar dorsal root ganglia were harvested after perfusion with FITC-Dextran (a) and Hoechst reagent (b) one week after CCI. While permeability for large and small molecules is higher in the neuron rich region (NRR) compared to the fibre rich region (FRR), no increase in permeability was observed after CCI. Scale bars: 100 µm (n = 6 from 3 animals (FITC-Dextran) and n = 3 from 3 animals (Hoechst reagent), 2-way-ANOVA and TukeyHSD test; figure taken from Lux et al. 2019 [135], no explicit permission needed for reuse under Creative Common License)

Furthermore, we quantified the number of $CD68^+$ cells and CD68 immunoreactivity in naive rats' dorsal root ganglia, as well as ipsi- and contralateral dorsal root ganglia of animals one week after CCI (**Figure 23**). The number of $CD68^+$ cells per µm² in ipsilateral dorsal root ganglia

after CCI significantly increased in comparison to contralateral. Compared to naïve dorsal root ganglia, we only observed a tendency (p = 0.065).

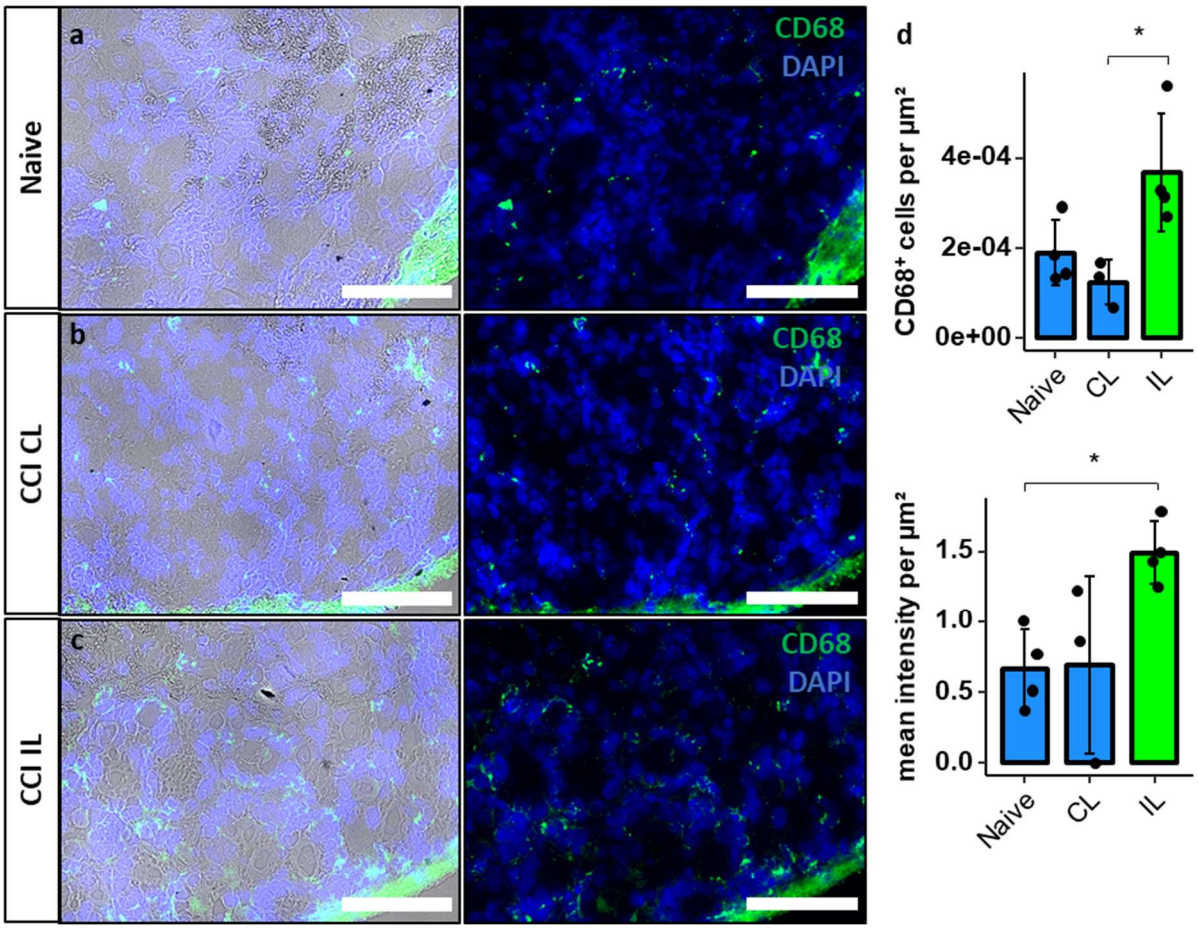

Figure 23. Increased macrophage invasion in the neuron rich region after CCI. Dorsal root ganglia of naïve rats (a) and the contralateral (CL, b) and ipsilateral (IL, c) dorsal root ganglia of rats 7d after CCI were harvested and stained. DAPI (blue) and anti-CD68 (green) antibodies were used (left: immunofluorescence with brightfield; right: only immunofluorescence). $CD68^+$ cells were counted manually in the neuron rich region and signal intensity was measured. Both were quantified per µm² (d). (n = 3 or 4; CD68+ cells per µm²: CL versus IL, p = 0.024; mean intensity per µm²: Naive versus IL, p = 0.038. Two-way ANOVA, Tukey HSD; scale bars = 100 µm; * $p < 0.05$, Figure taken from Lux et al. 2019 [135], no explicit permission needed for reuse under Creative Common License)

5 Discussion

5.1 Summary of Results

In my thesis, I observed high *Adgrl1/3* expression in all analysed neural subpopulations ($NF200^+$, $IB4^+$ and $CGRP^+$ neurons) in the dorsal root ganglion and detected a downregulation of *Adgrl1* in $IB4^+$ neurons one week after CCI as well as an upregulation in $NF200^+$ neurons six weeks after CCI. Reduced expression of the antinociceptive *Adgrl1* occurred at a timepoint of maximal mechanical hypersensitivity.

Secondly, I demonstrated high resemblance of the blood-DRG-barrier to the blood-nerve-barrier regarding claudin-1, -5, -12, -19 and ZO1 distribution. The fibre rich region resembled the blood-nerve-barrier in tight junction composition and sealing against diffusion of small and large molecules. The neuron rich region on the other hand was highly permeable for small and large molecules. The vessel specific analysis of claudin-5 was higher expressed in the vessels of the fibre rich compared to the neuron rich region. Since *Cldn5* knockdown increases blood-brain-barrier permeability selectively for molecules smaller than 800 Da, this explanation alone does explain the leakiness. Therefore, further analyses into the origin of the blood-DRG-barriers leakiness in healthy state is necessary. Seven days after CCI, claudin-5 was downregulated in the neuron rich region's vessels. This was accompanied by an increased migration of $CD68^+$ cells into the neuron rich region but unchanged permeability.

5.2 Discussion of Methods

5.2.1 Chronic Constriction Injury: Modelling Traumatic Mononeuropathy

CCI is a widely accepted animal model of nerve injury [135-141]. One of its weaknesses is the discrimination of post-operative and nerve-injury associated pain [142]. To overcome this weakness, we performed experiments with contralateral samples as well as samples of sham operated and naive animals if required. Secondly, "loose ligations" might vary between surgeons. To minimize this, operations were performed by a single investigator. Lastly, the phenotype invoked by CCI is transient. Therefore, it is possible to assess the acute phase, as well as the recovery to normal nociceptive thresholds over six weeks. Since the model is well-established and very standardized in the group, we refrained from assessing pain behaviour in the animals used for tissue analysis.

5.2.2 Immunofluorescence to Detect mRNA and Protein Expression in the Dorsal Root Ganglion

The detection of specific immunoreactivity is widely used for qualitative and quantitative evaluation of proteins. Nevertheless, this method poses many variables ranging from antibody concentration used during preparation to acquisition parameters used during imaging. We kept all parameters as constant as possible to get reliable results during quantification. For new and unestablished antibodies and probes, we tested negative controls to evaluate risk of unspecific staining. We established stable and standardized protocols for immunofluorescence quantification *in situ*. Inter-experiment errors were prevented by only comparing parallelly executed experiments. For images we compared, detection parameters during image acquisition were always the same. If signal-quantification was performed, we minimized signal saturation during image acquisition.

By distinguishing specific regions of the dorsal root ganglion, we achieved a high sensitivity for expression changes and were able to construct a precise hypothesis to follow up on. In our case, limiting factors included the availability of specific antibodies and tissue auto-fluorescence. Indeed, the immunoreactivity signals on the human dorsal root ganglia were not suitable for analysis due to autofluorescence even after applying chemical bleaching or photo bleaching (data not shown). This factor forced us to use non-fluorescent immunohistochemistry. Immunofluorescence imaging captures light with a different wavelength than the microscope emits. This enables us to specifically measure and quantify signal intensity of labelled antibodies or probes. In immunohistochemistry experiments, we capture coloured images which are less suitable for quantification. Western blot and qPCR are suitable for protein and RNA quantification but lack spatial resolution. Single cell qPCR or fluorescence-activated cell scanning may quantify RNA or respectively proteins with spatial resolution. These methods are not yet established in our group, highly complex and expensive. Furthermore, tissue preparation is highly complex and might distort results. Therefore, we decided not to use these methods for our initial study. Nevertheless, follow-up studies should consider the use of single cell qPCR or fluorescence-activated cell scanning to further specify our results.

Neuronal subpopulations were discriminated using the markers NF200, IB4, and CGRP. More elaborate combinations of immunohistochemistry markers are available as proposed by Usoskin et al. (2014). These provide a better correlation between physiological function as well as higher sensitivity [35]. While NF200, IB4 and CGRP distinguish neuron populations,

Usoskin et al. described distinct subpopulations for each of these groups. Therefore, even significant expression alterations might not be detected if the change only occurs in a subpopulation. Consequently, follow-up studies further specifying distinct physiological subpopulations and confirming our results should be performed.

5.2.2.1 Valid and Reliable Quantification of Immunofluorescence Studies

Despite standardized protocols, there are some pitfalls during evaluation of microscopy images. Some of which may be prevented easily, others remain unsolved problems to this day. Dunn et al. (2011) published a review of immunofluorescence quantification, focussing on preventing such errors [143]. The acquisition and evaluation of immunofluorescence data involves many manual processing steps. These include choosing a representative section, choosing the acquisition parameters, and marking the regions of interest. In most setups, each of these steps involves a partly subjective decision and is therefore an error source. To address this, the development of semi-automated and automated image analysis tools is subject of extensive research. Nevertheless, manual image evaluation is still the most commonly used method. Hence, multiple cryosections were prepared for each sample and we chose randomly from them. Furthermore, we evaluated the acquisition parameters in a test experiment to prevent pixel saturation in channels we planned on quantifying. Lastly, we chose a setup with the investigator being blind to the condition and automated as many steps as possible: By acquiring a z-stack and converting it into a maximum projection image, we lost some spatial resolution but minimized the error evoked by incorrect focus during image acquisition. We determined ROIs manually, but we evaluated the use of a convolutional neural network for image segmentation and achieved comparable as well as easily reproducible results. Furthermore, the correlation of light intensity and amount of probe is not linear. Therefore, one must keep in mind quantifying light intensity is not the same as quantifying amounts of molecules.

For tight junction protein and permeability studies, we quantified the light intensity per area after background correction to account for sample specific inhomogeneities. In the case of our *Adgrl1/3* mRNA study, we achieved semi-quantification of mRNA expression by calculating the number of gene copies utilizing the RNAscope™ kits' properties [144-146]. This kit labels each mRNA copy with one molecule of the probe. After an "amplification" process, each probe has many binding sites for fluorophores and may be measured as one dot-shaped light signal. Therefore, not only semi-quantification but quantification is possible. High *Adgrl1/3* expression in the dorsal root ganglion made it impossible to consistently differentiate between single dots and dot-clusters. We utilized computer-assisted dot segmentation to evaluate mean dot light

intensity and calculate a semi-quantitative dot per cell count of *Adgrl1/3*. The semi-automated segmentation is based on parameters which are, in a reasonable margin of error, equal for all samples' dots: size and circularity. This method introduces a systemic error possibly neglecting some dots or including clusters. Nevertheless, it is a consistent method, free from subjective bias and led us to reliable and reproducible results. The results were comparable to a count by eye.

In the future, artificial intelligence assisted image segmentation and even image acquisition could standardize the field of quantitative immunofluorescence studies. This would make faster as well as more reliable results possible.

5.2.2.2 RNAish: Chromophores vs. Fluorophores

The RNA*ish* protocols were established using fluorophore- and chromophore-conjugated probes. While we found the chromophore probes to possess excellent sensitivity, they absorbed light necessary for the counter-stainings' fluorophores to emit light. The high expression of *Adgrl1/3* combined with this light extinction was not suitable for our experiment which forced us to omit the chromophore conjugated probes and to use the slightly less sensitive and less stable fluorophore-conjugated probes instead.

5.3 Discussion of Results

5.3.1 Neural Subpopulations of the Dorsal Root Ganglion

We analysed the cross-sectional area of $NF200^+$, $CGRP^+$ and $IB4^+$ neurons in naive, sham operated, and CCI male Wistar rats. While not observed in most literature regarding neuropathy models, phenotype switching neurons in a model of diabetic neuropathy and after nerve compression have been reported [147, 148]. While we did not detect significant differences regarding size distribution or cell counts within the subpopulations, our study design does not exclude the possibility of altered marker expression after CCI. Further studies utilizing a pan-neural marker might exclude this possibility. For $NF200^+$ neurons, we observed large cells with a broad area distribution, while $CGRP^+$ and $IB4^+$ neurons' areas were narrowly distributed. These results align with previously published data.

Image segmentation was performed twice: manually and computer assisted. For the latter, we trained a convolutional neural network to perform the task. This allowed us to obtain a comparable outcome for the $NF200^+$ cell population, even with little training (n = 6 for each staining). Regarding $IB4^+$ and $CGRP^+$ cells, the convolutional neural network assisted segmentation had problems to distinguish between adjacent cells, recognizing them as one large

cell. This might be due to the differences in staining quality and exact staining patterns. $NF200^+$ cells for example feature a contrast rich signal for the cells outer limit combined with a homogenous signal within the cell, while $IB4^+$ and $CGRP^+$ cells' stainings are more heterogenous. Nevertheless, the nucleus area was often neglected since it was not stained. With an increased training data size, the neural network would probably adapt to these features. Therefore, we recommend the usage of a convolutional neural network with a large training data set labelled by multiple experts for experiments which are performed frequently. This excludes bias, combines the expertise of multiple researchers, and yields fast as well as easily reproducible results.

5.3.2 Spatial Distribution of *Adgrl1/3* in the Dorsal Root Ganglion

Adgrl1 and *Adgrl3* are expressed in all neural subpopulations in naive animals as well as after CCI. Existing studies observed *Adgrl1* and *Adgrl3* expression in neurons of the peripheral nervous system and central nervous system [74, 87, 149]. This aligns with our data in this regard. For further verification, *Adgrl1/3* expression in satellite cells should also be evaluated – especially because we observed many dots seemingly outside of neurons and satellite glia and neurons have a common origin. Since we only evaluated one neural subpopulation at once and did not use a satellite cell marker, our observations regarding *Adgrl1/3* expression in glial cells should be confirmed in a future study.

During CCI, *Adgrl3* expression remained unchanged. *Adgrl1* expression in $IB4^+$ neurons was transiently downregulated one week after CCI. Furthermore, $NF200^+$ neurons overexpressed *Adgrl1* mRNA six weeks after CCI. The deletion of *dCirl* in *Drosophila* causes a higher threshold for detecting light and a lower threshold for detecting coarse mechanical stimuli. Both mechanisms are mediated by downregulation of cAMP production but result in different physiological outcomes. This likely due to cell-type specific adjustments of the proteins affected by cAMP-signalling and differences between *Stachel*-dependent and *Stachel*-independent receptor activation. The downregulation in $IB4^+$ neurons, potential nociceptors, one week after CCI coincides with severe hyperalgesia. Therefore, a similar mechanism as in *Drosophila* seems possible: If *Adgrl1* reduces nociceptor response to mechanical stimuli, its absence might be involved in the development of hyperalgesia or even spontaneous pain. Therefore, our observations suggest for the first time that *Adgrl1* plays a significant role in the pathogenesis of neuropathy in rats. Next steps, following up on this hypothesis, include verification of our results on a protein level, conditional knockout experiments in healthy and neuropathic animals, or stimulation/inhibition of ADGRL1 during neuropathy. Our own

follow-up study on *Adgrl1/3* protein expression utilizing antibodies showed expression in $IB4^+$ and $CGRP^+$ neurons in rats and unspecified neurons in human dorsal root ganglia. During the verification of antibody specificity in western blot experiments, Adgrl1 and Adgrl3 antibodies stained multiple bands before and after affinity purification. Furthermore, the expected bands were barely visible. This might be the result of faulty antibodies or an unsuitable purification protocol. Therefore, specificity must be verified, for example in ko or genetically tagged animals, to validate these results. Furthermore, the site of ADGRL expression must also be verified: Are the receptors located in the cell body's, the axon's, or the synapse's membrane? Does protein the expression correlate with our findings on the mRNA level? Our promising results justify more elaborate studies into the interaction of the latrophilins' with the sensory system of vertebrates.

5.3.3 Spatial Distribution of Tight Junction Proteins in the Dorsal Root Ganglion

To evaluate the spatial distribution of tight junction proteins in the dorsal root ganglion of rats, we took claudin-1, claudin-5, claudin-12, claudin-19, and ZO-1 as the representatives and examined their expression in the neuron rich region, the fibre rich region, and the putative epiperineurium. Our study revealed regional differences for claudin-1, claudin-5, claudin-19, and ZO-1 in naive rats' dorsal root ganglia. Regarding morphology and tight junction proteins composition, our study revealed the blood-DRG-barrier to be very similar compared with the blood-nerve-barrier. As we decided to evaluate the most prominent tight junction proteins of the blood-nerve-barrier, differences regarding other tight junction proteins are not represented in our study. While the fibre rich region's blood barrier is similar in composition and permeability, the neuron rich region's blood barrier is marked by lower claudin-5 expression in vessels. In contrast to the blood-nerve-barrier, the blood-DRG-barrier in the neuron rich region is highly permeable for small and large molecules. A major sealing tight junction protein of the blood-nerve-barrier, claudin-1, is primarily expressed in the neuron rich region's epiperineurium and fibre rich region. *Cldn1* ko is lethal, as the animals die from dehydration due to its key function in the epidermal barrier. Despite its vital function in the skin, it is also expressed in the in the blood-nerve-barrier and the blood-brain-barrier [123, 139]. In the blood-nerve-barrier, it is highly expressed in the perineurium but also found in paranodal loops of myelinating Schwann cells, the Mesaxon and Schmidt-Lanterman incisures [40, 138, 139, 150, 151]. We observed no obviously different distribution of *Cldn1* in the blood-DRG-barrier and assume similar claudin-1 functionality in the blood-nerve and blood-DRG-barrier.

Claudin-12 is expressed in the blood-brain-barrier and blood-nerve-barrier [152-154]. In our study of the dorsal root ganglion, we observed claudin-12 within neurons *somata* and in or around nerve fibres. While small and intense signal areas in the fibre rich region correlate to findings auf claudin-12 in the paranodal region, the signal within the neurons poses a mystery. Firstly, specificity of this signal should be validated. If verified, further studies should then evaluate the physiological function of claudin-12 in neurons.

Previously, claudin-19 was detected in myelinating glial cells of the peripheral nervous system but not the central nervous system. Without claudin-19, the formation of tight junctions in these cells is impaired [110, 155]. While *Cldn19* ko mice are able to reproduce and vital, they exhibit the phenotype of a peripheral neuropathy, leading to motor deficits [155]. Our study revealed highest claudin-19 immunoreactivity in the fibre rich region. The signal was arranged in small clusters of high signal intensity. Furthermore, claudin-19 is expressed in between neurons *somata* in the neuron rich region, but no organized signal was detected in vessels or the epiperineural regions. This correlates with previous findings in the sciatic nerve and these clusters might correspond to paranodal regions of myelinated fibres like in the sciatic nerve [41, 154]. Our findings indicate no relevant deviation of claudin-19's expression comparing the dorsal root ganglion and the sciatic nerve.

Correct tight junction formation in the sciatic nerve often requires ZO-1 as tight junction associated protein forming complexes with claudin-1 [110]. ZO-1 ko animals are not vital and Katsuno et al. associated ZO-deficiency with neurological disorders [156]. Expression of ZO-1 in the sciatic nerve is mostly observed in vessels, perineurium and myelinated Schwann cells [154, 157]. In the dorsal root ganglion, our study detected ZO-1 immunoreactivity predominantly in the fibre rich region's epiperineurium, but also the neuron rich region's epiperineurium as well as in small clusters in the neuron rich region and fibre rich region. The clusters in the neuron rich region and fibre rich region colocalized with claudin-5, indicating expression in vascular endothelial cells. ZO-1 expression levels were not lower in the neuron rich region compared to the fibre rich region. Since ZO-1 signal in these regions was distributed in small clusters and we evaluated large areas, our method might not have been sensible enough to detect a difference. Therefore, ZO-1's involvement in the blood-DRG-barrier's leakiness should be considered and evaluated further.

Cldn5 is believed to be the most important tight junction protein of the blood brain barrier. Its mRNA expression in endothelial cells of the brain exceeds the 100-fold of other tight junction proteins [128]. *Cldn5* ko mice are vital after birth but die within 10 days after birth. In these

animals, Nitta et al. observed that molecules smaller than 800 Da penetrate the blood-brain-barrier in these animals [126]. In the sciatic nerve, *Cldn5* is expressed in myelinating Schwann cells and endoneural vessels. The site-specific expression of claudin-5 immunoreactivity revealed higher density in vessels of the fibre rich region than in the neuron rich region [135]. Follow up studies should evaluate the connection between high vessel permeability and low claudin-5 expression in the neuron rich area of the dorsal root ganglion. Since previous studies associated claudin-5 downregulation with a permeability increase for small but not large molecular substances, involvement of other tight junction proteins is probable.

5.3.4 Tight Junction Protein Alterations After Chronic Constriction Injury

Since traumatic neuropathy causes blood-nerve-barrier and blood-spinal-cord-barrier breakdown, we also expected an opening of blood-DRG-barrier with tight junction protein downregulation. However, only vessels of the neuron rich region had a lowered claudin-5 expression. Expression studies in the sciatic nerve revealed *Cldn1* mRNA downregulation after CCI [14, 116, 135, 139]. *Cldn1* downregulation in the sciatic nerve after CCI starts as early as 3 h after CCI and mRNA levels reach a minimum after 7 d [14]. After CCI, mRNA levels of *Cldn1*, *Cldn5*, *Cldn19*, *Tjp1*, *Ocln* and *MarvelD2* are also decreased in the spinal cord. Furthermore, vessels of the spinal cord express lower levels of ZO-1 and claudin-5 after CCI [158]. This signifies, that the traumatic nerve injury's effect extends beyond a local reaction. The dorsal root ganglion is the connection between sensory peripheral nerves and the spinal cord, but its barrier is significantly more permeable. Does it break down further after CCI? How does further breakdown affect it?

In accordance with published mRNA data in rats, we observed no difference in claudin-1 immunoreactivity in rat's dorsal root ganglia one week after CCI. As claudin-1 is the major sealing protein of the sciatic nerve's perineural barrier, we conclude that epiperineural disruption after CCI is unlikely in rats' blood-DRG-barrier. The effect of nerve injury on claudin-12 expression is yet unclear, but assessment of mRNA expression in rodents dorsal root ganglia revealed *Cldn12* downregulation one week after CCI [135]. This aligns with spinal cord and peripheral nerve data. We were unable to verify a reduced protein expression in rats dorsal root ganglia after CCI. This might indicate that this change in mRNA expression is not biologically relevant for protein expression, or that our method was not sensitive enough to detect these alterations. Nevertheless, the morphology of claudin-12 immunoreactivity changed from a uniform to a clustered distribution one week after inflicting nerve injury. A follow-up study on altered claudin-12 expression must be strongly considered, regarding the evidence on

the mRNA level and the hints on changed expression morphology. For *Cldn19* mRNA, no regulatory changes after CCI in the sciatic nerve or the dorsal root ganglion have been observed so far. We also did not observe alterations of claudin-19 expression pattern or quantity after CCI. While *Tjp1* downregulation after CCI was observed on mRNA and protein level in the sciatic nerve as well as on a mRNA level in the dorsal root ganglion [135], our study did not find ZO-1 immunoreactivity to be altered after CCI. ZO-1 expression is reduced in vessels of the spinal cord after CCI. Furthermore, ZO-1 is upregulated in the blood-brain-barrier after claudin-5 downregulation and limits permeability for large molecules. Therefore, our observation should be confirmed with a more sensitive method. *Cldn5* mRNA in dorsal root ganglia is downregulated after CCI in rats and we confirmed lower protein expression, but only in the vessels of the neuron rich region. Since the neuron rich regions barrier is highly permeable for small substances even before claudin 5 downregulation, the physiological function of this downregulation should be further evaluated.

5.3.5 Blood-DRG-barrier Permeability Before and After Chronic Constriction Injury

Current literature of traumatic and other peripheral neuropathies focuses on the blood-nerve-barrier. The blood-DRG-barrier is mostly neglected and only few studies exist. Studies of the dorsal root ganglion hint to a filter function in relation to sensation as well as a source of ectopic signal generation. Furthermore, involvement in the inflammatory reaction during some neuropathic conditions has been suggested. To elucidate the role of the blood-DRG-barrier we also examined its permeability during CCI and performed permeability assays for both large and small molecules. Similar to previous data, we found the neuron rich region to be 2-3x more permeable for intravenously injected small and large molecules compared to the fibre rich region. This is very peculiar as the assessed tight junction proteins' distribution is similar in both regions as well as in the blood-nerve-barrier. Since tight junction proteins barrier function is highly flexible and depends on the exact composition, other tight junction proteins than our selection should be evaluated for significant differences to the blood-nerve-barrier. The vessel specific downregulation of claudin-5 after CCI in the neuron rich region suggests increased permeability of the blood-DRG-barrier after CCI. While we did not observe increased permeability, this might be due to the fact, that the barrier is very leaky even in healthy state. Furthermore, involvement of tight junction proteins not evaluated in our study should be considered. This leakiness might be favourable for pain treatment as drugs, opioids for example, may easily reach their target receptors, but undesirable as noxious substances like neuropathy-inducing chemotherapeutics also easily reach the neurons. Another implication of a leaky

blood-DRG-barrier is a concept of the dorsal root ganglion, in which it is more than a relay-station, but a modulator reacting to endogenous and exogenous stimuli. This function might be comparable to other areas of the nervous system in which the barrier is particularly leaky, like the *area postrema* [159]. While satellite glia cells are not known to express tight junctions, they surround the neurons' somata and act as mediator between neuron and environment. We suggest that satellite glia cells' role as filter or mediator should be topic of further studies to elucidate the physiological function of the blood-DRG-barriers' leakiness. Other than molecules, cell migration is also limited by the blood-DRG-barrier. Macrophage invasion during neuropathic conditions has been observed in the nerve and the dorsal root ganglion [160, 161]. While increased permeation of small molecules accompanies claudin-5 downregulation in the blood-brain-barrier, the neuron rich region's permeability for small molecules is unaltered despite claudin-5 downregulation [126, 135]. This is puzzling at first, but the naturally high permeability of the blood-DRG-barrier in the neuron rich region might prevent further, claudin-5 associated, increase. Also, upregulation of tight junction proteins not analysed in our study must be considered. In contrast to the unaltered permeability, we observed an increased migration of macrophages into the neuron rich region after CCI. Macrophage invasion might indicate a breakdown of the blood-DRG-barrier; thus, the origin of this phenomenon needs to be evaluated further.

We observed only slight differences regarding the expression of tight junction proteins comparing the neuron rich region and fibre rich region but could not fully explain the neuron rich region's high permeability for intravenously injected small and large molecules. Other tight junction proteins as well as the exact interaction and arrangement of tight junction proteins must be considered as possible explanation. Additionally, the utilized permeability assays were established to evaluate permeability of the blood-brain-barrier and blood-nerve-barrier, which both show very low base permeability and have therefore high sensitivity in low permeability scenarios and not necessarily under high permeability conditions. Other than this, claudin-5 downregulation might have other biologically relevant implications like increased macrophage invasion, which has been observed after nerve injury [160, 161]. Lastly, possible compensatory mechanisms preventing further permeability increase must be considered. Future studies should address these questions and possible experiments include long-term CCI and immune cell migration studies [135].

5.4 Perspective

Emerging studies of aGPCRs have identified the latrophilins shaping mechanosensation in *Drosophila*: increasing the signal response to subtle touch and reducing the response to noxious or harsh stimulation [70, 88, 89]. Previously, mutations of latrophilins were already associated with diseases like attention deficit hyperactivity disorder as well as addiction and leukaemia [96, 102, 105, 162, 163]. Similarly, cohort studies with chronic pain patients might reveal mutated *ADGRL* variants. This field of research is young; nevertheless, evidence from association studies and strong evidence in invertebrates pushed it forward. The unique role of *dCirl* in shaping *Drosophila's* mechanosensation, combining the characteristics of a metabotropic receptor and mechanical interaction, identified this receptor family as an interesting target for further research: *dCirl* ko causes a higher threshold for light mechanical stimuli, while the animals have a decreased threshold for coarse mechanical stimuli. This resembles features like hypaesthesia and allodynia, conditions frequently observed in neuropathies [4]. Nevertheless, studies in *Drosophila* require verification in vertebrates to further evaluate the potential therapeutic value. While research of latrophilins, primarily *Adgrl1* and *Adgrl3*, in the central nervous system progressed in recent years, the peripheral nervous system has been neglected. Our study confirmed *Adgrl1*/*3* expression in $NF200^+$, $CGRP^+$ and $IB4^+$ neurons and demonstrated regulatory changes during traumatic neuropathy. What are the clinical implications? The dorsal root ganglion's role in neuropathy includes impaired filter function and ectopic signal generation. These features combined with regulatory changes of *Adgrl1*, a receptor previously shown to interact with somatosensation, point to the question if they interact pathophysiologically. If so, a metabotropic receptor in the dorsal root ganglion is an easily accessible target due to the demonstrated permeability of the blood-DRG-barrier in the neuron rich region. Follow-up studies regarding the basic physiology of these receptors and their role in the peripheral nervous system should be performed. These include the verification of our study on a protein level, the exact characterisation of the spatial distribution, studies of ko animals with traumatic neuropathy and a characterization of neuropathic animals after stimulating *Adgrl1*.

Little is known about the dorsal root ganglion and its structural features. Even though studies show the physiological importance as filter for sensations, alterations during diseases, and successful therapeutic targeting of the dorsal root ganglion, its full physiological function is not clear yet [45, 46, 48, 58]. For example, the precise function of pseudounipolar neurons' T-stem structure is unknown. Furthermore, cross-activation exists within the dorsal root ganglion, but

its role in painful, other diseases of the sensory system or even in healthy state is unclear. What physiological, pathophysiological, and therapeutic implications lie in the leakiness of the blood-DRG-barrier? Our and other studies showed not only high permeability of the dorsal root ganglion's vessels, but also that substances might access the neurons *somata* [164]. Other areas of the nervous system with high base permeability, like the *area postrema* in the brain stem, function as chemo sensor. Therefore, a possible role of the dorsal root ganglion as chemo sensor directly reacting to the body's internal milieu must be considered and evaluated in the future. Hypersensitivity in neuropathy could partly originate from proalgesic molecules bypassing the blood-DRG-barrier. This is supported by reduction of hypersensitivity after application of low-dose local anaesthetics, selectively silencing ectopic activity in the dorsal root ganglion [165]. The absence of objective measures and suitable biomarkers of pain, particularly detecting malfunctions of the primary afferent neuron, poses a problem in pain research and diagnostics [166]. If noxious substances in the blood permeate the blood-DRG-barrier and cause sensory impairment, these should be identified and evaluated in future studies. These substances might be possible biomarkers and expand clinical diagnostics for diseases of the sensory system. Furthermore, Godel et al. reported changes of dorsal root ganglion volume in genetic diseases like *M. Fabry* and neurofibromatosis, as well as chemotherapy induced neuropathy [36-38, 167]. In Fabry's disease glycolipids accumulate, which might be a result of altered permeation in the dorsal root ganglion [37, 167]. Therefore, MRI of the dorsal root ganglion and blood-DRG-barrier permeability are potential early *in vivo* markers for peripheral nervous system involvement in neuropathy. If blood-DRG-barrier breakdown contributes to pain generation, barrier stabilization poses a potential therapeutic target for pain relief, as already demonstrated for the blood-nerve-barrier [14, 41]. Lastly, understanding the blood-DRG-barrier's characteristics could improve understanding the dorsal root ganglia role in anaesthesia involving systemic and local drugs [135].

With our findings we elucidated the physiology of the blood-DRG-barrier and its potential value as biomarker and therapeutic target in neuropathy. Furthermore, we were able to confirm *Adgrl1* affection in rats, the first step in translating the valuable findings of *dCirl* to mammals.

6 Summary

In my thesis, I characterized aGPCRs *Adgrl1* and *Adgrl3,* tight junction proteins and the blood-DRG-barrier in rats' lumbar dorsal root ganglions after traumatic neuropathy. In contrast to the otherwise tightly sealed barriers shielding neural tissues, the dorsal root ganglion's neuron rich region is highly permeable in its healthy state. Furthermore, the DRG is a source of ectopic signal generation during neuropathy; the exact origin of which is still unclear. I investigated two characteristics of dorsal root ganglia: 1. Which neural subpopulations of the dorsal root ganglion express *Adgrl1/3*? Does the *Adgrl1/3* expression change over the time course of six weeks after CCI? 2. How are the evaluated tight junction proteins distributed in the dorsal root ganglion? Are there regional differences? Does traumatic nerve injury influence the blood-DRG-barrier regarding composition or permeability?

I documented expression of *Adgrl1* and *Adgrl3* in $NF200^+$, $CGRP^+$ and $IB4^+$ neurons. One week after CCI I observed transient downregulation of *Adgrl1* in non-peptidergic nociceptors ($IB4^+$). In the context of previous data, *dCirl* deletion causing an allodynia-like state in *Drosophila*, our research hints to a possible role of *Adgrl1* nociceptive signal processing and pain resolution in neuropathy.

Furthermore, I demonstrated similar claudin-1, claudin-12, claudin-19, and ZO-1 expression of the dorsal root ganglion's neuron rich and fibre rich region. Claudin-5 expression in vessels of the neuron rich region was lower compared to the fibre rich region. This could partly explain the neuron rich regions high permeability for intravenously injected substances. However, previous studies of the blood-brain-barrier reported claudin-5 deficiency to cause permeation for small molecules only, while both small and large molecules penetrate the blood-DRG-barrier. Therefore, the lower claudin-5 expression alone does not explain the constitutive barriers leakiness for small and large intravenously injected molecules.

Claudin-5 expression was decreased one week after nerve injury in vessels of the neuron rich region while permeability for small and large injected molecules remained unchanged. Nevertheless, we detected more $CD68^+$ cells in the neuron rich region one week after CCI. Therefore, the claudin-5 downregulation might allow for increased immune cell migration.

As clinically relevant conclusion, we verified the high permeability of the neuron rich regions barrier as well as a vessel specific claudin-5 downregulation after CCI. Similar to the blood-spinal-cord-barrier, we observed increased macrophage invasion into the neuron rich region after CCI. A possible clinical application could be diagnostic imaging of the dorsal root ganglion. Furthermore, we identified aGPCR as potential target for further research and

possible treatments for neuropathy, which should be easily accessible due to the blood-DRG-barriers leaky nature. Its precise function in peripheral tissues, its mechanisms of activation, and its role in pain resolution should be evaluated further.

7 Zusammenfassung

Die vorliegende Arbeit charakterisiert die aGPCR *Adgrl1* und *Adgrl3,* repräsentative Tight Junction Proteine, sowie die Blut-Spinalganglion-Schranke in lumbalen Spinalganglien von Ratten mit und ohne traumatische Neuropathie. Die hohe Permeabilität der zellulären, neuronenreichen Region von Spinalganglien in naiven Tieren ist eine der wenigen Ausnahmen der sonst sehr dichten Barrieren des Nervensystems. In Neuropathien kann das Spinalganglion ektopische Signale generieren; der genaue Ursprung dieser Aktionspotentiale ist jedoch unklar. Daher habe ich zwei Charakteristika der Spinalganglia von naiven Ratten und nach einer traumatischen Nervenverletzung untersucht: 1. Welche Neuronen Populationen exprimieren *Adgrl1/3*? Verändert sich die Expression über den Zeitraum von bis zu 6 Wochen nach CCI? 2. Wie sind die untersuchten Tight Junction Proteine im Spinalganglion verteilt? Gibt es regionale Unterschiede? Beeinflusst die traumatische Nervenverletzung die Blut-Spinalganglion-Schranke bzgl. Komposition und Permeabilität für Moleküle und Makrophagen?

Ich konnte die Expression von *Adgrl1* und *Adgrl3* in $NF200^+$, $CGRP^+$ und $IB4^+$ Neuronen nachweisen. Eine Woche nach CCI war die *Adgrl1* Expression in nicht-peptidergen Nozizeptoren ($IB4^+$) vorübergehend herabreguliert. Im Zusammenhang mit verstärktem nozizeptiven Verhalten nach *dCirl* knockout in *Drosophila* weist dies auf eine potenzielle antinozizeptive Funktion von *Adgrl1* sowie eine Rolle in nozizeptiven Signalverarbeitung hin.

Zusätzlich konnten wir eine ähnliche Expression von Claudin-1, Claudin-12, Claudin-19 und ZO-1 in der neuronenreichen sowie der faserreichen Region zeigen. Claudin-5 ist in Gefäßen der neuronenreichen Region niedriger exprimiert als in Gefäßen der faserreichen Region. In der Blut-Hirn-Schranke ist Claudin-5 für die Abdichtung gegen Diffusion kleiner Moleküle verantwortlich. Daher erklärt die niedrige Claudin-5 Expression der Blut-Spinalganglion-Schranke in der neuronenreichen Region die hohe Permeabilität zwar für kleine, aber nicht gut für große applizierte Moleküle. Nach Nervenläsion war die Claudin-5 Immunoreaktivität in Gefäßen der neuronenreichen Region reduziert, die Permeabilität für große und kleine Moleküle jedoch unverändert. Allerdings konnten wir nach traumatischer Nervenverletzung vermehrt Makrophagen in der neuronenreichen Region nachweisen. Daher könnte die verminderte Claudin-5 Expression zum Beispiel eine erhöhte Migration von Immunzellen wie Monozyten/Makrophagen ermöglichen.

Unabhängig von einer direkten Öffnung der Nervenbarriere ist auch proximal die Claudin-5 gesteuerte Blut-Spinalganglion-Schranke durchlässiger für Makrophagen – ähnlich der

vermehrten Durchlässigkeit der Blut-Rückenmarks-Schranke. Diese Veränderungen könnten klinisch-diagnostisch beispielsweise in der Bildgebung genutzt werden.
Weiterhin haben wir einen neuen endogenen antinozizeptiven Rezeptor, *Adrlg1*, ähnlich den Opioidrezeptoren, als potenzielles, und aufgrund der permeablen Blut-Spinalganglion-Schranke therapeutisch gut erreichbares, Target für die antineuropathische Therapie identifiziert. Seine genaue Funktion im peripheren Gewebe, seine Aktivierungsmechanismen sowie seine Rolle bei der Schmerzauflösung sollten weiter untersucht werden.

8 Appendix

8.1 ImageJ Scripts

The following code snippets are written in the ImageJ macro language.

8.1.1 Automated Dot Segmentation

```
#@ File (label = "Input directory", style = "directory") dir                //defining input directory
#@ File (label = "Output directory", style = "directory") output        //defining output directory
#@ String (label = "File suffix", value = ".oib") suffix //defining file type

processFolder(dir);
print("Finished");
function processFolder(dir) {
	list = getFileList(dir);
	list = Array.sort(list);

	for (i = 0; i < list.length; i++) {
		if(endsWith(list[i], suffix))
			print(dir + File.separator + list[i]);
			processFile(dir, output, list[i]);
			print(i);
	}
}

function processFile(input, output, file) {
	 run("Bio-Formats Importer", "open=[" + input + File.separator + file + "]  autoscale
color_mode=Custom rois_import=[ROI manager] view=Hyperstack stack_order=XYCZT
series_0_channel_0_red=0 series_0_channel_0_green=0 series_0_channel_0_blue=255
series_0_channel_1_red=0 series_0_channel_1_green=255 series_0_channel_1_blue=0
series_0_channel_2_red=255 series_0_channel_2_green=0 series_0_channel_2_blue=0");
	Img = getTitle();
	Name = replace( Img , ".oib" , "" );

	run("Z Project...", "projection=[Max Intensity]");
	ImgZ = getTitle();
	close(Img);

//Cy3
	run("Duplicate...", "duplicate channels=2");
	ImgRNA1 = getTitle();
	title = getImageID();
	run("Clear Results");
	selectWindow(ImgRNA1);
	run("Duplicate...", "duplicate channels=1");
	ImgRNA2 = getTitle();
	setThreshold(1200, 65535);
	run("Create Mask");
	mask = getTitle();
	setOption("BlackBackground", true);
	run("Analyze Particles...", "size=3-22 pixel display exclude clear add");
```

```
        run("Clear Results");
        close(mask);
        close(ImgRNA2);
        run("Clear Results");
        selectWindow(ImgRNA1);
        roiManager("Deselect");
        roiManager("Measure");
        saveAs("Results", output + File.separator + "Dot_Cy3_" + Name + ".csv");
        roiManager("Save", output + File.separator + "ROIs_Dot_Cy3_" + Name + ".zip");
        roiManager("Deselect");
        roiManager("Deselect");
        roiManager("Reset");
        run("Clear Results");
        close(ImgRNA1);

//Cy5
        selectWindow(ImgZ);
        run("Duplicate...", "duplicate channels=3");
        ImgRNA1 = getTitle();
        title = getImageID();
        run("Clear Results");
        selectWindow(ImgRNA1);
        run("Duplicate...", "duplicate channels=1");
        ImgRNA2 = getTitle();
        setThreshold(1150, 65535);
        run("Create Mask");
        mask = getTitle();
        setOption("BlackBackground", true);
        run("Analyze Particles...", "size=3-22 pixel display exclude clear add");
        run("Clear Results");
        close(mask);
        close(ImgRNA2);
        close(ImgZ);
        run("Clear Results");
        selectWindow(ImgRNA1);
        roiManager("Deselect");
        roiManager("Measure");
        saveAs("Results", output + File.separator + "Dot_Cy5_" + Name + ".csv");
        roiManager("Save", output + File.separator + "ROIs_Dot_Cy5_" + Name + ".zip");
        roiManager("Deselect");
        roiManager("Deselect");
        roiManager("Reset");
        run("Clear Results");
        close(ImgRNA1);
}
```

8.2 Supplementary Data

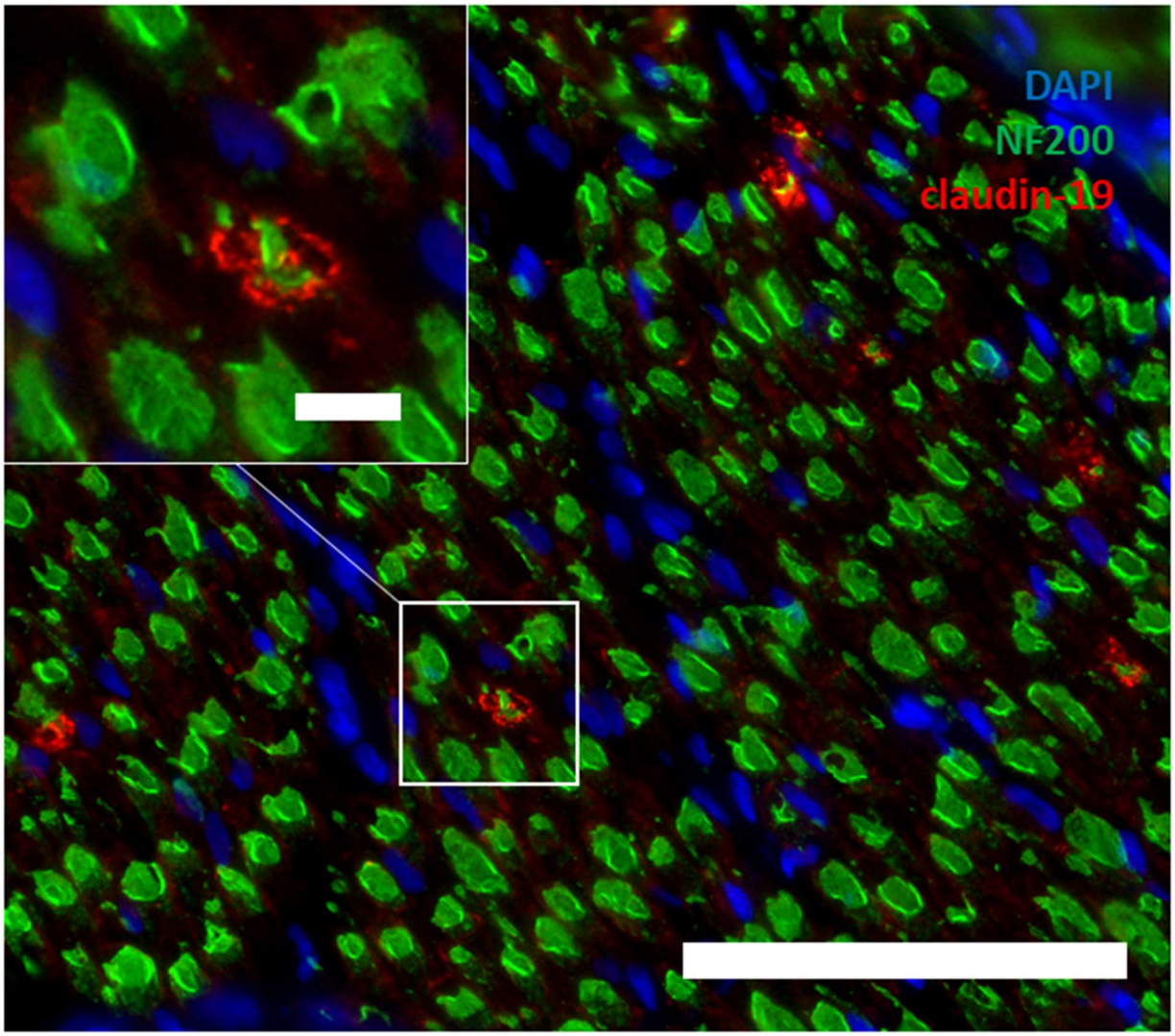

Supplementary Figure 1. Co-Staining of claudin-19 and NF200 in the fibre rich region of a rat's DRG reveals anti-claudin-19 immunoreactivity at incisures of myelinated fibres. A DRG section (d = 10 µm) of a male Wistar rats' lumbar DRG was prepared with anti-NF200 (green) and anti claudin-19 (red) antibodies. Nuclear counterstaining with DAPI visualizes high cell density in suspected epi-/perineural regions. Scale bars: 100 µm in large image, 10 µm in inset

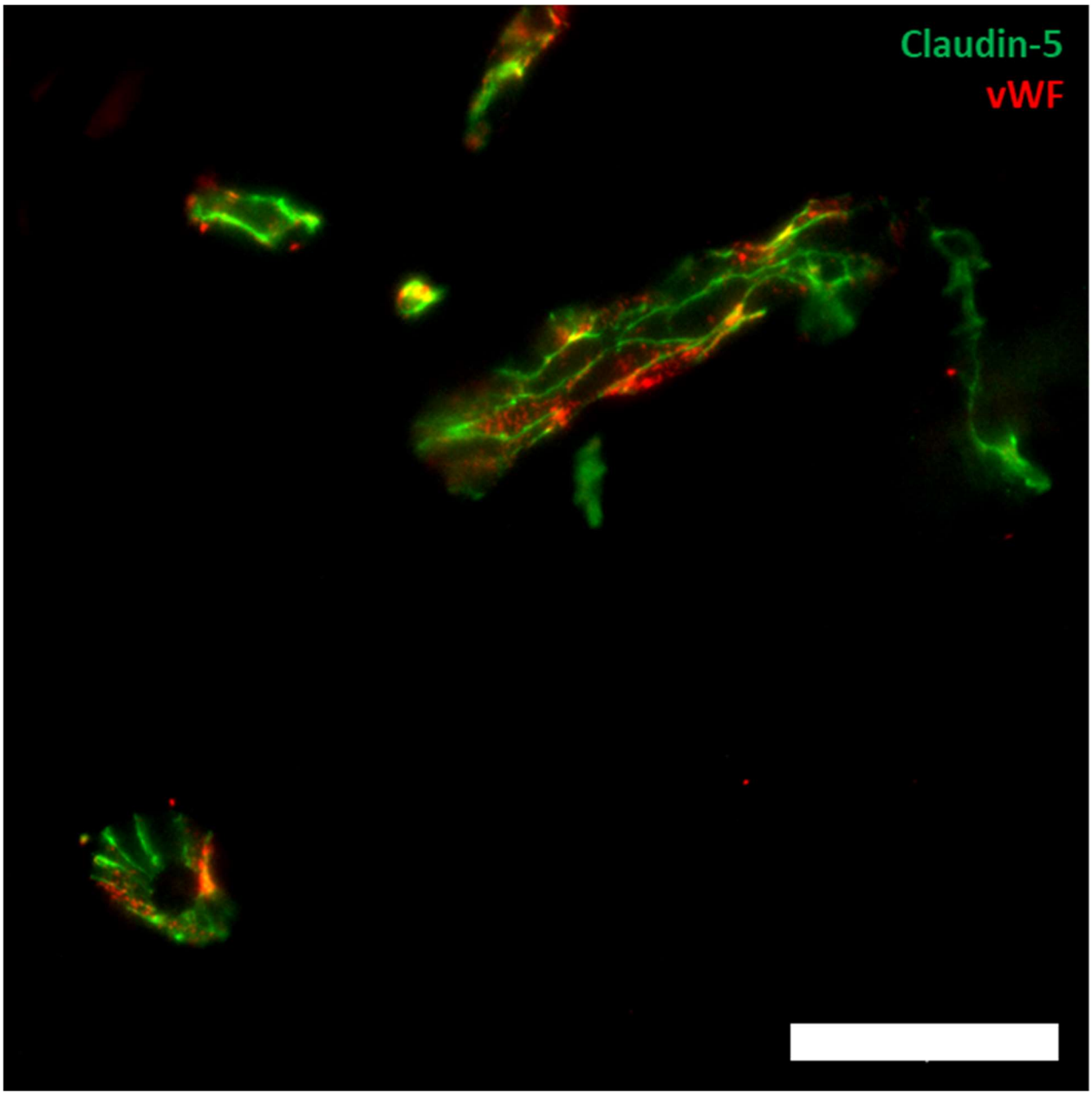

Supplementary Figure 2. Claudin-5 colocalizes with von Willebrandt Factor in rats DRGs indicating expression in endothelial cells. Naïve male Wistar Rats DRGs were sectioned with a cryostat (d = 10 µm), Subsequently, von Willebrandt Factor (red) and claudin-5 (green) immunoreactivity were detected. Both antigens immunofluorescence colocalize. Scale bar: 50 µm.

Supplementary Table 1. Analysis of IB4+, CGRP+ and NF200+ cells' areas. Naive rats' dorsal root ganglia as well as dorsal root ganglia after one, three and six weeks after CCI were harvested, stained, and segmented (man.: manual segmentation; comp.: computational segmentation).

Staining	Group	Mean cell area in µm² (man.)	Median cell area in µm² (man.)	standard deviation (man.)	Mean cell area in µm² (comp.)	Median cell area in µm² (comp.)	standard deviation (comp.)
NF200	naive	986.782	937.7	494.756	1022.53	965.2	640.802
NF200	CCI1w	669.608	631.95	386.739	714.157	643.5	510.670
NF200	CCI3w	792.282	727.4	369.882	632.070	558.6	480.101
NF200	CCI6w	689.537	646.95	354.132	799.159	733.1	527.832
IB4	naive	329.169	319.6	145.548	581.770	462.9	510.224
IB4	CCI1w	340.610	315.95	132.547	524.781	424.1	376.219
IB4	CCI3w	412.525	396.3	144.415	732.109	513.25	682.623
IB4	CCI6w	333.889	321.8	107.823	662.335	527.8	514.634
CGRP	naive	315.076	278.5	169.713	485.759	402	391.340
CGRP	CCI1w	301.485	253.75	163.945	409.881	374.5	250.302
CGRP	CCI3w	332.146	279.7	169.153	533.183	418.7	395.483
CGRP	CCI6w	228.763	218.05	89.8493	475.221	398.9	389.922

9 Abbreviations

Adgrl1, adhesion G protein-coupled receptor latrophilin-1

Adgrl3, adhesion G protein-coupled receptor latrophilin-3

aGPCR, adhesion G protein-coupled receptor

APS, ammonium persulfate

blood-DRG-barrier, blood-dorsal-root-ganglion-barrier

CCI, chronic constriction injury

CGRP, calcitonin gene-related peptide

DEPC, diethyl pyrocarbonate

dpc, dots per cell

GPCR, G protein-coupled receptor

IB4, isolectin B4

ko, knockout

NF200, neurofilament heavy polypeptide

PBS, phosphate buffer solution

PFA, paraformaldehyde

ROI, region of interest

RT, room temperature

sd, standard deviation

SDS, sodium dodecyl sulfate

10 Curriculum vitae

Persönliche Daten		
Name	Thomas Joachim Lux	
Geburtsdatum	21.03.1994	
Geburtsort	Frankfurt am Main	
Ausbildung		
2004 – 2013	Allgemeine Hochschulreife	Humboldtschule, Bad Homburg v.d.H
2014 – 2020	Studium Humanmedizin	Julius-Maximilians-Universität Würzburg
2014 – 2020	Studium Translational Medicine	Julius-Maximilians-Universität Würzburg
Klinik		
2013	Zentraler Sanitätsdienst der Bundeswehr	Bundeswehr
2013	Pflegepraktikum	Bundeswehrzentral-Krankenhaus, Koblenz
2014	Pflegepraktikum	Hochtaunuskliniken, Usingen
2016	Famulatur	Hochtaunuskliniken, Usingen
2017	Famulatur	Praxis Dres. Vescovi & Schiel, Würzburg
2017	Famulatur	Universitätsklinikum Würzburg
2018	Famulatur	Machame Hospital, Machame, Tansania
Forschung		
2014	Forschungspraktikum	Institut für Neurophysiologie, Universität Würzburg
2015	Forschungspraktikum	Institut für Tissue Engineering, Universität Würzburg
2017	Forschungspraktikum	Zentrum für Experimentelle Molekulare Medizin, Universität Würzburg
2018 – 2021	Promotion	AG Molekulare Schmerzforschung, Universitätsklinikum Würzburg
Förderungen und Auszeichnungen		
2017 – 2020	Max-Weber-Programm	
2017 – 2020	Studienstiftung des Deutschen Volkes	
2018 – 2021	Graduated School of Life Sciences	Universität Würzburg
2020	Nachwuchsförderpreis Schmerz 2020	Deutsche Schmerzgesellschaft e.V.

_____, Würzburg, 15.02.2021

11 Publication List

1. *Quantitative and Microstructural Changes of the Blood-Nerve Barrier in Peripheral Neuropathy*; AK Reinhold, Joachim Schwabe, **TJ Lux**, E Salvador, HL Rittner; 2018 Frontiers in Neuroscience 12:936, doi: 10.3389/fnins.2018.00936
2. *Regional Differences in Tight Junction Protein Expression in the Blood-DRG Barrier and Their Alterations after Nerve Traumatic Injury in Rats*; **TJ Lux**, X Hu, A Ben-Kraiem, R Blum, JTC Chen, HL Rittner; 2019, International Journal of Molecular Sciences 21(1):270, doi: 10.3390/ijms21010270
3. *Antinociceptive modulation by the adhesion GPCR CIRL promotes mechanosensory signal discrimination*; S Dannhäuser, **TJ Lux**, C Hu, M Selcho, JTC Chen, N Ehmann, D Sachidanandan, S Stopp, D Pauls, M Pawlak, T Langenhan, P Soba, HL Rittner, RJ Kittel; 2020, eLife 2020;9:e56738, doi: 10.7554/eLife.56738

12 Literature

1. Finnerup, Attal, Haroutounian, Mcnicol, Baron, Dworkin, et al., *Pharmacotherapy for Neuropathic Pain in Adults: A Systematic Review and Meta-Analysis.* Lancet Neurol, 2015. **14**(2): p. 162-73.
2. Sommer, Geber, Young, Forst, Birklein and Schoser, *Polyneuropathies.* Dtsch Arztebl Int, 2018. **115**(6): p. 83-90.
3. Cruccu, Sommer, Anand, Attal, Baron, Garcia-Larrea, et al., *Efns Guidelines on Neuropathic Pain Assessment: Revised 2009.* Eur J Neurol, 2010. **17**(8): p. 1010-8.
4. Van Hecke, Austin, Khan, Smith and Torrance, *Neuropathic Pain in the General Population: A Systematic Review of Epidemiological Studies.* Pain, 2014. **155**(4): p. 654-62.
5. Maier, Baron, Tolle, Binder, Birbaumer, Birklein, et al., *Quantitative Sensory Testing in the German Research Network on Neuropathic Pain (Dfns): Somatosensory Abnormalities in 1236 Patients with Different Neuropathic Pain Syndromes.* Pain, 2010. **150**(3): p. 439-50.
6. Scholz, Mannion, Hord, Griffin, Rawal, Zheng, et al., *A Novel Tool for the Assessment of Pain: Validation in Low Back Pain.* PLoS Med, 2009. **6**(4): p. e1000047.
7. Phillips, *The Cost and Burden of Chronic Pain.* Rev Pain, 2009. **3**(1): p. 2-5.
8. Yam, Loh, Tan, Khadijah Adam, Abdul Manan and Basir, *General Pathways of Pain Sensation and the Major Neurotransmitters Involved in Pain Regulation.* Int J Mol Sci, 2018. **19**(8).
9. Cox, Reimann, Nicholas, Thornton, Roberts, Springell, et al., *An Scn9a Channelopathy Causes Congenital Inability to Experience Pain.* Nature, 2006. **444**(7121): p. 894-8.
10. Baron, Binder and Wasner, *Neuropathic Pain: Diagnosis, Pathophysiological Mechanisms, and Treatment.* Lancet Neurol, 2010. **9**(8): p. 807-19.
11. Bannister and Dickenson, *What the Brain Tells the Spinal Cord.* Pain, 2016. **157**(10): p. 2148-51.
12. Dubin and Patapoutian, *Nociceptors: The Sensors of the Pain Pathway.* J Clin Invest, 2010. **120**(11): p. 3760-72.
13. Gaudet, Popovich and Ramer, *Wallerian Degeneration: Gaining Perspective on Inflammatory Events after Peripheral Nerve Injury.* J Neuroinflammation, 2011. **8**: p. 110.
14. Moreau, Mauborgne, Bourgoin, Couraud, Romero, Weksler, et al., *Early Alterations of Hedgehog Signaling Pathway in Vascular Endothelial Cells after Peripheral Nerve Injury Elicit Blood-Nerve Barrier Disruption, Nerve Inflammation, and Neuropathic Pain Development.* Pain, 2016. **157**(4): p. 827-39.
15. Joshi and Honore, *Animal Models of Pain for Drug Discovery.* Expert Opin Drug Discov, 2006. **1**(4): p. 323-34.
16. Seltzer, Dubner and Shir, *A Novel Behavioral Model of Neuropathic Pain Disorders Produced in Rats by Partial Sciatic Nerve Injury.* Pain, 1990. **43**(2): p. 205-18.
17. Vadakkan, Jia and Zhuo, *A Behavioral Model of Neuropathic Pain Induced by Ligation of the Common Peroneal Nerve in Mice.* J Pain, 2005. **6**(11): p. 747-56.
18. Wall, Devor, Inbal, Scadding, Schonfeld, Seltzer, et al., *Autotomy Following Peripheral Nerve Lesions: Experimental Anaesthesia Dolorosa.* Pain, 1979. **7**(2): p. 103-13.
19. Bennett and Xie, *A Peripheral Mononeuropathy in Rat That Produces Disorders of Pain Sensation Like Those Seen in Man.* Pain, 1988. **33**(1): p. 87-107.
20. Reinhold, Batti, Bilbao, Buness, Rittner and Heppenstall, *Differential Transcriptional Profiling of Damaged and Intact Adjacent Dorsal Root Ganglia Neurons in Neuropathic Pain.* PLoS One, 2015. **10**(4): p. e0123342.
21. Puigdellivol-Sanchez, Prats-Galino, Ruano-Gil and Molander, *Sciatic and Femoral Nerve Sensory Neurones Occupy Different Regions of the L4 Dorsal Root Ganglion in the Adult Rat.* Neurosci Lett, 1998. **251**(3): p. 169-72.
22. Gemes, Koopmeiners, Rigaud, Lirk, Sapunar, Bangaru, et al., *Failure of Action Potential Propagation in Sensory Neurons: Mechanisms and Loss of Afferent Filtering in C-Type Units after Painful Nerve Injury.* J Physiol, 2013. **591**(4): p. 1111-31.
23. Kent, Min, Hogan and Kramer, *Mechanisms of Dorsal Root Ganglion Stimulation in Pain Suppression: A Computational Modeling Analysis.* Neuromodulation, 2018. **21**(3): p. 234-46.
24. Sundt, Gamper and Jaffe, *Spike Propagation through the Dorsal Root Ganglia in an Unmyelinated Sensory Neuron: A Modeling Study.* J Neurophysiol, 2015. **114**(6): p. 3140-53.
25. Haller and Low, *The Fine Structure of the Peripheral Nerve Root Sheath in the Subarachnoid Space in the Rat and Other Laboratory Animals.* Am J Anat, 1971. **131**(1): p. 1-19.
26. Hirakawa, Okajima, Nagaoka, Kubo, Takamatsu and Oyamada, *Regional Differences in Blood-Nerve Barrier Function and Tight-Junction Protein Expression within the Rat Dorsal Root Ganglion.* Neuroreport, 2004. **15**(3): p. 405-8.

27. Jimenez-Andrade, Herrera, Ghilardi, Vardanyan, Melemedjian and Mantyh, *Vascularization of the Dorsal Root Ganglia and Peripheral Nerve of the Mouse: Implications for Chemical-Induced Peripheral Sensory Neuropathies.* Mol Pain, 2008. **4**: p. 10.
28. Kobayashi, Yoshizawa, Hachiya, Ukai and Morita, *Vasogenic Edema Induced by Compression Injury to the Spinal Nerve Root. Distribution of Intravenously Injected Protein Tracers and Gadolinium-Enhanced Magnetic Resonance Imaging.* Spine (Phila Pa 1976), 1993. **18**(11): p. 1410-24.
29. H. S. Gasser, *The Role Played by the Sizes of the Constituent Fibers of a Nerve Trunk in Determining the Form of Its Action Potential Wave.* Am J Physiol, 1927. **80**(3): p. 522-47.
30. Djouhri and Lawson, *Abeta-Fiber Nociceptive Primary Afferent Neurons: A Review of Incidence and Properties in Relation to Other Afferent a-Fiber Neurons in Mammals.* Brain Res Brain Res Rev, 2004. **46**(2): p. 131-45.
31. Wang, Belanger, Cote, Desrosiers, Prescott, Cote, et al., *Sensory Afferents Use Different Coding Strategies for Heat and Cold.* Cell Rep, 2018. **23**(7): p. 2001-13.
32. Tandrup, *Unbiased Estimates of Number and Size of Rat Dorsal Root Ganglion Cells in Studies of Structure and Cell Survival.* J Neurocytol, 2004. **33**(2): p. 173-92.
33. Lawson and Waddell, *Soma Neurofilament Immunoreactivity Is Related to Cell Size and Fibre Conduction Velocity in Rat Primary Sensory Neurons.* J Physiol, 1991. **435**(1): p. 41-63.
34. Ruscheweyh, Forsthuber, Schoffnegger and Sandkuhler, *Modification of Classical Neurochemical Markers in Identified Primary Afferent Neurons with Abeta-, Adelta-, and C-Fibers after Chronic Constriction Injury in Mice.* J Comp Neurol, 2007. **502**(2): p. 325-36.
35. Usoskin, Furlan, Islam, Abdo, Lonnerberg, Lou, et al., *Unbiased Classification of Sensory Neuron Types by Large-Scale Single-Cell Rna Sequencing.* Nat Neurosci, 2015. **18**(1): p. 145-53.
36. Godel, Pham, Heiland, Bendszus and Baumer, *Human Dorsal-Root-Ganglion Perfusion Measured in-Vivo by Mri.* Neuroimage, 2016. **141**: p. 81-7.
37. Godel, Baumer, Pham, Kohn, Muschol, Kronlage, et al., *Human Dorsal Root Ganglion in Vivo Morphometry and Perfusion in Fabry Painful Neuropathy.* Neurology, 2017. **89**(12): p. 1274-82.
38. Apostolidis, Schwarz, Xia, Weiler, Heckel, Godel, et al., *Dorsal Root Ganglia Hypertrophy as in Vivo Correlate of Oxaliplatin-Induced Polyneuropathy.* PLoS One, 2017. **12**(8): p. e0183845.
39. Zhang, Li, De Carvalho-Barbosa, Kavelaars, Heijnen, Albrecht, et al., *Dorsal Root Ganglion Infiltration by Macrophages Contributes to Paclitaxel Chemotherapy-Induced Peripheral Neuropathy.* J Pain, 2016. **17**(7): p. 775-86.
40. Pummi, Heape, Grenman, Peltonen and Peltonen, *Tight Junction Proteins Zo-1, Occludin, and Claudins in Developing and Adult Human Perineurium.* J Histochem Cytochem, 2004. **52**(8): p. 1037-46.
41. Sauer, Krug, Hackel, Staat, Konasin, Yang, et al., *Safety, Efficacy, and Molecular Mechanism of Claudin-1-Specific Peptides to Enhance Blood-Nerve-Barrier Permeability.* J Control Release, 2014. **185**: p. 88-98.
42. Akert, Sandri, Weibel, Peper and Moor, *The Fine Structure of the Perineural Endothelium.* Cell Tissue Res, 1976. **165**(3): p. 281-95.
43. Reinhold and Rittner, *Barrier Function in the Peripheral and Central Nervous System-a Review.* Pflugers Arch, 2017. **469**(1): p. 123-34.
44. Devor, *Unexplained Peculiarities of the Dorsal Root Ganglion.* Pain, 1999. **Suppl 6**: p. S27-S35.
45. Deer, Levy, Kramer, Poree, Amirdelfan, Grigsby, et al., *Dorsal Root Ganglion Stimulation Yielded Higher Treatment Success Rate for Complex Regional Pain Syndrome and Causalgia at 3 and 12 Months: A Randomized Comparative Trial.* Pain, 2017. **158**(4): p. 669-81.
46. Liem, Russo, Huygen, Van Buyten, Smet, Verrills, et al., *A Multicenter, Prospective Trial to Assess the Safety and Performance of the Spinal Modulation Dorsal Root Ganglion Neurostimulator System in the Treatment of Chronic Pain.* Neuromodulation, 2013. **16**(5): p. 471-82; discussion 82.
47. Soresi, *Control of Intractable Pain by Spinal Ganglia Block.* Am J Surg, 1949. **77**(1): p. 72-8.
48. Liem, Russo, Huygen, Van Buyten, Smet, Verrills, et al., *One-Year Outcomes of Spinal Cord Stimulation of the Dorsal Root Ganglion in the Treatment of Chronic Neuropathic Pain.* Neuromodulation, 2015. **18**(1): p. 41-8; discussion 8-9.
49. Hu and Mclachlan, *Distinct Functional Types of Macrophage in Dorsal Root Ganglia and Spinal Nerves Proximal to Sciatic and Spinal Nerve Transections in the Rat.* Exp Neurol, 2003. **184**(2): p. 590-605.
50. Hu, Bembrick, Keay and Mclachlan, *Immune Cell Involvement in Dorsal Root Ganglia and Spinal Cord after Chronic Constriction or Transection of the Rat Sciatic Nerve.* Brain Behav Immun, 2007. **21**(5): p. 599-616.
51. Krames, *The Role of the Dorsal Root Ganglion in the Development of Neuropathic Pain.* Pain Med, 2014. **15**(10): p. 1669-85.

52. Liem, Van Dongen, Huygen, Staats and Kramer, *The Dorsal Root Ganglion as a Therapeutic Target for Chronic Pain.* Reg Anesth Pain Med, 2016. **41**(4): p. 511-9.
53. Xiao, Huang, Zhang, Bao, Lu, Guo, et al., *Identification of Gene Expression Profile of Dorsal Root Ganglion in the Rat Peripheral Axotomy Model of Neuropathic Pain.* Proc Natl Acad Sci U S A, 2002. **99**(12): p. 8360-5.
54. Suseki, Takahashi, Takahashi, Chiba, Yamagata and Moriya, *Sensory Nerve Fibres from Lumbar Intervertebral Discs Pass through Rami Communicantes. A Possible Pathway for Discogenic Low Back Pain.* J Bone Joint Surg Br, 1998. **80**(4): p. 737-42.
55. Huygen, Liem, Cusack and Kramer, *Stimulation of the L2-L3 Dorsal Root Ganglia Induces Effective Pain Relief in the Low Back.* Pain Pract, 2018. **18**(2): p. 205-13.
56. Devor and Wall, *Cross-Excitation in Dorsal Root Ganglia of Nerve-Injured and Intact Rats.* J Neurophysiol, 1990. **64**(6): p. 1733-46.
57. Eldabe, Burger, Moser, Klase, Schu, Wahlstedt, et al., *Dorsal Root Ganglion (Drg) Stimulation in the Treatment of Phantom Limb Pain (Plp).* Neuromodulation, 2015. **18**(7): p. 610-6; discussion 6-7.
58. Esposito, Malayil, Hanes and Deer, *Unique Characteristics of the Dorsal Root Ganglion as a Target for Neuromodulation.* Pain Med, 2019. **20**(Suppl 1): p. S23-S30.
59. Lynch, Mcjunkin, Eross, Gooch and Maloney, *Case Report: Successful Epiradicular Peripheral Nerve Stimulation of the C2 Dorsal Root Ganglion for Postherpetic Neuralgia.* Neuromodulation, 2011. **14**(1): p. 58-61; discussion
60. Feirabend, Choufoer, Ploeger, Holsheimer and Van Gool, *Morphometry of Human Superficial Dorsal and Dorsolateral Column Fibres: Significance to Spinal Cord Stimulation.* Brain, 2002. **125**(Pt 5): p. 1137-49.
61. Shen, Wang, Chen and Liang, *Morphologic Analysis of Normal Human Lumbar Dorsal Root Ganglion by 3d Mr Imaging.* AJNR Am J Neuroradiol, 2006. **27**(10): p. 2098-103.
62. Hayflick, *A Family of Heptahelical Receptors with Adhesion-Like Domains: A Marriage between Two Super Families.* J Recept Signal Transduct Res, 2000. **20**(2-3): p. 119-31.
63. Davenport, Alexander, Sharman, Pawson, Benson, Monaghan, et al., *International Union of Basic and Clinical Pharmacology. Lxxxviii. G Protein-Coupled Receptor List: Recommendations for New Pairings with Cognate Ligands.* Pharmacol Rev, 2013. **65**(3): p. 967-86.
64. Hauser, Chavali, Masuho, Jahn, Martemyanov, Gloriam, et al., *Pharmacogenomics of Gpcr Drug Targets.* Cell, 2018. **172**(1-2): p. 41-54 e19.
65. Hauser, Attwood, Rask-Andersen, Schioth and Gloriam, *Trends in Gpcr Drug Discovery: New Agents, Targets and Indications.* Nat Rev Drug Discov, 2017. **16**(12): p. 829-42.
66. Conn, Ulloa-Aguirre, Ito and Janovick, *G Protein-Coupled Receptor Trafficking in Health and Disease: Lessons Learned to Prepare for Therapeutic Mutant Rescue in Vivo.* Pharmacol Rev, 2007. **59**(3): p. 225-50.
67. Meza-Aguilar and Boucard, *Latrophilins Updated.* Biomol Concepts, 2014. **5**(6): p. 457-78.
68. Bjarnadottir, Fredriksson, Hoglund, Gloriam, Lagerstrom and Schioth, *The Human and Mouse Repertoire of the Adhesion Family of G-Protein-Coupled Receptors.* Genomics, 2004. **84**(1): p. 23-33.
69. Fredriksson, Lagerstrom, Lundin and Schioth, *The G-Protein-Coupled Receptors in the Human Genome Form Five Main Families. Phylogenetic Analysis, Paralogon Groups, and Fingerprints.* Mol Pharmacol, 2003. **63**(6): p. 1256-72.
70. Langenhan, Aust and Hamann, *Sticky Signaling—Adhesion Class G Protein–Coupled Receptors Take the Stage.* Sci Signal, 2013. **6**(276): p. re3-re.
71. Monk, Hamann, Langenhan, Nijmeijer, Schoneberg and Liebscher, *Adhesion G Protein-Coupled Receptors: From in Vitro Pharmacology to in Vivo Mechanisms.* Mol Pharmacol, 2015. **88**(3): p. 617-23.
72. Krasnoperov, Bittner, Beavis, Kuang, Salnikow, Chepurny, et al., *Alpha-Latrotoxin Stimulates Exocytosis by the Interaction with a Neuronal G-Protein-Coupled Receptor.* Neuron, 1997. **18**(6): p. 925-37.
73. Hamann, Hartmann and Van Lier, *Structure of the Human Cd97 Gene: Exon Shuffling Has Generated a New Type of Seven-Span Transmembrane Molecule Related to the Secretin Receptor Superfamily.* Genomics, 1996. **32**(1): p. 144-7.
74. Hamann, Aust, Arac, Engel, Formstone, Fredriksson, et al., *International Union of Basic and Clinical Pharmacology. Xciv. Adhesion G Protein-Coupled Receptors.* Pharmacol Rev, 2015. **67**(2): p. 338-67.
75. Trzaskowski, Latek, Yuan, Ghoshdastider, Debinski and Filipek, *Action of Molecular Switches in Gpcrs--Theoretical and Experimental Studies.* Curr Med Chem, 2012. **19**(8): p. 1090-109.
76. Promel, Frickenhaus, Hughes, Mestek, Staunton, Woollard, et al., *The Gps Motif Is a Molecular Switch for Bimodal Activities of Adhesion Class G Protein-Coupled Receptors.* Cell Rep, 2012. **2**(2): p. 321-31.
77. Yona, Lin, Siu, Gordon and Stacey, *Adhesion-Gpcrs: Emerging Roles for Novel Receptors.* Trends Biochem Sci, 2008. **33**(10): p. 491-500.

78. Langenhan, Promel, Mestek, Esmaeili, Waller-Evans, Hennig, et al., *Latrophilin Signaling Links Anterior-Posterior Tissue Polarity and Oriented Cell Divisions in the C. Elegans Embryo.* Dev Cell, 2009. **17**(4): p. 494-504.
79. Luo, Jeong, Jin, Strokes, Li and Piao, *G Protein-Coupled Receptor 56 and Collagen Iii, a Receptor-Ligand Pair, Regulates Cortical Development and Lamination.* Proc Natl Acad Sci U S A, 2011. **108**(31): p. 12925-30.
80. Krasnoperov, Bittner, Holz, Chepurny and Petrenko, *Structural Requirements for Alpha-Latrotoxin Binding and Alpha-Latrotoxin-Stimulated Secretion. A Study with Calcium-Independent Receptor of Alpha-Latrotoxin (Cirl) Deletion Mutants.* J Biol Chem, 1999. **274**(6): p. 3590-6.
81. Gray, Haino, Roth, Maguire, Jensen, Yarme, et al., *Cd97 Is a Processed, Seven-Transmembrane, Heterodimeric Receptor Associated with Inflammation.* J Immunol, 1996. **157**(12): p. 5438-47.
82. Chang, Stacey, Kwakkenbos, Hamann, Gordon and Lin, *Proteolytic Cleavage of the Emr2 Receptor Requires Both the Extracellular Stalk and the Gps Motif.* FEBS Lett, 2003. **547**(1-3): p. 145-50.
83. Hsiao, Cheng, Chen, Chou, Stacey, Chang, et al., *Site-Specific N-Glycosylation Regulates the Gps Auto-Proteolysis of Cd97.* FEBS Lett, 2009. **583**(19): p. 3285-90.
84. Krasnoperov, Lu, Buryanovsky, Neubert, Ichtchenko and Petrenko, *Post-Translational Proteolytic Processing of the Calcium-Independent Receptor of Alpha-Latrotoxin (Cirl), a Natural Chimera of the Cell Adhesion Protein and the G Protein-Coupled Receptor. Role of the G Protein-Coupled Receptor Proteolysis Site (Gps) Motif.* J Biol Chem, 2002. **277**(48): p. 46518-26.
85. Lin, Chang, Davies, Stacey, Harris and Gordon, *Autocatalytic Cleavage of the Emr2 Receptor Occurs at a Conserved G Protein-Coupled Receptor Proteolytic Site Motif.* J Biol Chem, 2004. **279**(30): p. 31823-32.
86. Promel, Waller-Evans, Dixon, Zahn, Colledge, Doran, et al., *Characterization and Functional Study of a Cluster of Four Highly Conserved Orphan Adhesion-Gpcr in Mouse.* Dev Dyn, 2012. **241**(10): p. 1591-602.
87. Langenhan, Piao and Monk, *Adhesion G Protein-Coupled Receptors in Nervous System Development and Disease.* Nat Rev Neurosci, 2016. **17**(9): p. 550-61.
88. Scholz, Gehring, Guan, Ljaschenko, Fischer, Lakshmanan, et al., *The Adhesion Gpcr Latrophilin/Cirl Shapes Mechanosensation.* Cell Rep, 2015. **11**(6): p. 866-74.
89. Scholz, Guan, Nieberler, Grotemeyer, Maiellaro, Gao, et al., *Mechano-Dependent Signaling by Latrophilin/Cirl Quenches Camp in Proprioceptive Neurons.* eLife, 2017. **6**.
90. Matsushita, Lelianova and Ushkaryov, *The Latrophilin Family: Multiply Spliced G Protein-Coupled Receptors with Differential Tissue Distribution.* FEBS Lett, 1999. **443**(3): p. 348-52.
91. Silva and Ushkaryov, *The Latrophilins, "Split-Personality" Receptors.* Adv Exp Med Biol, 2010. **706**: p. 59-75.
92. Silva, Lelianova, Hopkins, Volynski and Ushkaryov, *Functional Cross-Interaction of the Fragments Produced by the Cleavage of Distinct Adhesion G-Protein-Coupled Receptors.* J Biol Chem, 2009. **284**(10): p. 6495-506.
93. Volynski, Silva, Lelianova, Atiqur Rahman, Hopkins and Ushkaryov, *Latrophilin Fragments Behave as Independent Proteins That Associate and Signal on Binding of Ltx(N4c).* EMBO J, 2004. **23**(22): p. 4423-33.
94. Davletov, Shamotienko, Lelianova, Grishin and Ushkaryov, *Isolation and Biochemical Characterization of a Ca2+-Independent Alpha-Latrotoxin-Binding Protein.* J Biol Chem, 1996. **271**(38): p. 23239-45.
95. Sugita, Ichtchenko, Khvotchev and Sudhof, *Alpha-Latrotoxin Receptor Cirl/Latrophilin 1 (Cl1) Defines an Unusual Family of Ubiquitous G-Protein-Linked Receptors. G-Protein Coupling Not Required for Triggering Exocytosis.* J Biol Chem, 1998. **273**(49): p. 32715-24.
96. Arcos-Burgos, Jain, Acosta, Shively, Stanescu, Wallis, et al., *A Common Variant of the Latrophilin 3 Gene, Lphn3, Confers Susceptibility to Adhd and Predicts Effectiveness of Stimulant Medication.* Mol Psychiatry, 2010. **15**(11): p. 1053-66.
97. Tobaben, Sudhof and Stahl, *Genetic Analysis of Alpha-Latrotoxin Receptors Reveals Functional Interdependence of Cirl/Latrophilin 1 and Neurexin 1 Alpha.* J Biol Chem, 2002. **277**(8): p. 6359-65.
98. Bonaglia, Marelli, Novara, Commodaro, Borgatti, Minardo, et al., *Genotype-Phenotype Relationship in Three Cases with Overlapping 19p13.12 Microdeletions.* Eur J Hum Genet, 2010. **18**(12): p. 1302-9.
99. Niiro, Azuma, Tanago, Matsumura, Shikata, Tachibana, et al., *(3z)-2-Acetylamino-3-Octadecen-1-Ol as a Potent Apoptotic Agent against Hl-60 Cells.* Bioorg Med Chem, 2004. **12**(1): p. 45-51.
100. Nazarko, Kibrom, Winkler, Leon, Stoveken, Salzman, et al., *A Comprehensive Mutagenesis Screen of the Adhesion Gpcr Latrophilin-1/Adgrl1.* iScience, 2018. **3**: p. 264-78.
101. O'sullivan, De Wit, Savas, Comoletti, Otto-Hitt, Yates, et al., *Flrt Proteins Are Endogenous Latrophilin Ligands and Regulate Excitatory Synapse Development.* Neuron, 2012. **73**(5): p. 903-10.

102. Wallis, Hill, Mendez, Abbott, Finnell, Wellman, et al., *Initial Characterization of Mice Null for Lphn3, a Gene Implicated in Adhd and Addiction.* Brain Res, 2012. **1463**: p. 85-92.
103. Jackson, Del Toro, Carrasquero, Roversi, Harlos, Klein, et al., *Structural Basis of Latrophilin-Flrt Interaction.* Structure, 2015. **23**(4): p. 774-81.
104. Jackson, Mehmood, Chavent, Roversi, Carrasquero, Del Toro, et al., *Super-Complexes of Adhesion Gpcrs and Neural Guidance Receptors.* Nat Commun, 2016. **7**: p. 11184.
105. Lange, Froc, Grunwald, Norton and Bally-Cuif, *Pharmacological Analysis of Zebrafish Lphn3.1 Morphant Larvae Suggests That Saturated Dopaminergic Signaling Could Underlie the Adhd-Like Locomotor Hyperactivity.* Prog Neuropsychopharmacol Biol Psychiatry, 2018. **84**(Pt A): p. 181-9.
106. Lange, Norton, Coolen, Chaminade, Merker, Proft, et al., *The Adhd-Susceptibility Gene Lphn3.1 Modulates Dopaminergic Neuron Formation and Locomotor Activity During Zebrafish Development.* Mol Psychiatry, 2012. **17**(9): p. 946-54.
107. Domene, Stanescu, Wallis, Tinloy, Pineda, Kleta, et al., *Screening of Human Lphn3 for Variants with a Potential Impact on Adhd Susceptibility.* Am J Med Genet B Neuropsychiatr Genet, 2011. **156B**(1): p. 11-8.
108. Ribases, Ramos-Quiroga, Sanchez-Mora, Bosch, Richarte, Palomar, et al., *Contribution of Lphn3 to the Genetic Susceptibility to Adhd in Adulthood: A Replication Study.* Genes Brain Behav, 2011. **10**(2): p. 149-57.
109. Kan, Jaiswal, Stinson, Janakiraman, Bhatt, Stern, et al., *Diverse Somatic Mutation Patterns and Pathway Alterations in Human Cancers.* Nature, 2010. **466**(7308): p. 869-73.
110. Gunzel and Yu, *Claudins and the Modulation of Tight Junction Permeability.* Physiol Rev, 2013. **93**(2): p. 525-69.
111. Mineta, Yamamoto, Yamazaki, Tanaka, Tada, Saito, et al., *Predicted Expansion of the Claudin Multigene Family.* FEBS Lett, 2011. **585**(4): p. 606-12.
112. Duffy, John, Lee, Brosnan and Spray, *Reciprocal Regulation of the Junctional Proteins Claudin-1 and Connexin43 by Interleukin-1beta in Primary Human Fetal Astrocytes.* J Neurosci, 2000. **20**(23): p. RC114.
113. Romanitan, Popescu, Spulber, Bajenaru, Popescu, Winblad, et al., *Altered Expression of Claudin Family Proteins in Alzheimer's Disease and Vascular Dementia Brains.* J Cell Mol Med, 2010. **14**(5): p. 1088-100.
114. Watson, Rowland and Warhurst, *Functional Modeling of Tight Junctions in Intestinal Cell Monolayers Using Polyethylene Glycol Oligomers.* Am J Physiol Cell Physiol, 2001. **281**(2): p. C388-97.
115. Knipp, Ho, Barsuhn and Borchardt, *Paracellular Diffusion in Caco-2 Cell Monolayers: Effect of Perturbation on the Transport of Hydrophilic Compounds That Vary in Charge and Size.* J Pharm Sci, 1997. **86**(10): p. 1105-10.
116. Hirakawa, Okajima, Nagaoka, Takamatsu and Oyamada, *Loss and Recovery of the Blood-Nerve Barrier in the Rat Sciatic Nerve after Crush Injury Are Associated with Expression of Intercellular Junctional Proteins.* Exp Cell Res, 2003. **284**(2): p. 196-210.
117. Nunbhakdi-Craig, Machleidt, Ogris, Bellotto, White and Sontag, *Protein Phosphatase 2a Associates with and Regulates Atypical Pkc and the Epithelial Tight Junction Complex.* J Cell Biol, 2002. **158**(5): p. 967-78.
118. D'souza, Agarwal and Morin, *Phosphorylation of Claudin-3 at Threonine 192 by Camp-Dependent Protein Kinase Regulates Tight Junction Barrier Function in Ovarian Cancer Cells.* J Biol Chem, 2005. **280**(28): p. 26233-40.
119. Van Itallie, Tietgens, Logrande, Aponte, Gucek and Anderson, *Phosphorylation of Claudin-2 on Serine 208 Promotes Membrane Retention and Reduces Trafficking to Lysosomes.* J Cell Sci, 2012. **125**(Pt 20): p. 4902-12.
120. Soma, Chiba, Kato-Mori, Wada, Yamashita, Kojima, et al., *Thr(207) of Claudin-5 Is Involved in Size-Selective Loosening of the Endothelial Barrier by Cyclic Amp.* Exp Cell Res, 2004. **300**(1): p. 202-12.
121. Yamamoto, Ramirez, Sato, Kiyota, Cerny, Kaibuchi, et al., *Phosphorylation of Claudin-5 and Occludin by Rho Kinase in Brain Endothelial Cells.* Am J Pathol, 2008. **172**(2): p. 521-33.
122. Gong, Renigunta, Himmerkus, Zhang, Renigunta, Bleich, et al., *Claudin-14 Regulates Renal Ca(+)(+) Transport in Response to Casr Signalling Via a Novel Microrna Pathway.* EMBO J, 2012. **31**(8): p. 1999-2012.
123. Furuse, Hata, Furuse, Yoshida, Haratake, Sugitani, et al., *Claudin-Based Tight Junctions Are Crucial for the Mammalian Epidermal Barrier: A Lesson from Claudin-1-Deficient Mice.* J Cell Biol, 2002. **156**(6): p. 1099-111.
124. Hadj-Rabia, Baala, Vabres, Hamel-Teillac, Jacquemin, Fabre, et al., *Claudin-1 Gene Mutations in Neonatal Sclerosing Cholangitis Associated with Ichthyosis: A Tight Junction Disease.* Gastroenterology, 2004. **127**(5): p. 1386-90.

125. Gunzel and Fromm, *Claudins and Other Tight Junction Proteins.* Compr Physiol, 2012. **2**(3): p. 1819-52.
126. Nitta, Hata, Gotoh, Seo, Sasaki, Hashimoto, et al., *Size-Selective Loosening of the Blood-Brain Barrier in Claudin-5-Deficient Mice.* J Cell Biol, 2003. **161**(3): p. 653-60.
127. Sirotkin, Morrow, Saint-Jore, Puech, Das Gupta, Patanjali, et al., *Identification, Characterization, and Precise Mapping of a Human Gene Encoding a Novel Membrane-Spanning Protein from the 22q11 Region Deleted in Velo-Cardio-Facial Syndrome.* Genomics, 1997. **42**(2): p. 245-51.
128. Ohtsuki, Sato, Yamaguchi, Kamoi, Asashima and Terasaki, *Exogenous Expression of Claudin-5 Induces Barrier Properties in Cultured Rat Brain Capillary Endothelial Cells.* J Cell Physiol, 2007. **210**(1): p. 81-6.
129. Mcgrath and Lilley, *Implementing Guidelines on Reporting Research Using Animals (Arrive Etc.): New Requirements for Publication in Bjp.* Br J Pharmacol, 2015. **172**(13): p. 3189-93.
130. Sauer, Rittner, Roewer, Sohajda, Shityakov, Brack, et al., *A Novel Approach for the Control of Inflammatory Pain: Prostaglandin E2 Complexation by Randomly Methylated Beta-Cyclodextrins.* Anesth Analg, 2017. **124**(2): p. 675-85.
131. Gerke and Plenderleith, *Binding Sites for the Plant Lectin Bandeiraea Simplicifolia I-Isolectin B(4) Are Expressed by Nociceptive Primary Sensory Neurones.* Brain Res, 2001. **911**(1): p. 101-4.
132. Fang, Djouhri, Mcmullan, Berry, Waxman, Okuse, et al., *Intense Isolectin-B4 Binding in Rat Dorsal Root Ganglion Neurons Distinguishes C-Fiber Nociceptors with Broad Action Potentials and High Nav1.9 Expression.* J Neurosci, 2006. **26**(27): p. 7281-92.
133. Hou, Renigunta, Gomes, Hou, Paul, Waldegger, et al., *Claudin-16 and Claudin-19 Interaction Is Required for Their Assembly into Tight Junctions and for Renal Reabsorption of Magnesium.* Proc Natl Acad Sci U S A, 2009. **106**(36): p. 15350-5.
134. Segebarth, Griebel, Stein, Von Collenberg, Martin, Fiedler, et al., *Deepflash, a Deep Learning Pipeline for Segmentation of Fluorescent Labels in Microscopy Images.* bioRxiv, 2020: p. 473199.
135. Lux, Hu, Ben-Kraiem, Blum, Chen and Rittner, *Regional Differences in Tight Junction Protein Expression in the Blood-Drg Barrier and Their Alterations after Nerve Traumatic Injury in Rats.* Int J Mol Sci, 2019. **21**(1).
136. Austin, Wu and Moalem-Taylor, *Chronic Constriction of the Sciatic Nerve and Pain Hypersensitivity Testing in Rats.* J Vis Exp, 2012(61).
137. Dowdall, Robinson and Meert, *Comparison of Five Different Rat Models of Peripheral Nerve Injury.* Pharmacol Biochem Behav, 2005. **80**(1): p. 93-108.
138. Ramer and Bisby, *Rapid Sprouting of Sympathetic Axons in Dorsal Root Ganglia of Rats with a Chronic Constriction Injury.* Pain, 1997. **70**(2-3): p. 237-44.
139. Reinhold, Schwabe, Lux, Salvador and Rittner, *Quantitative and Microstructural Changes of the Blood-Nerve Barrier in Peripheral Neuropathy.* Front Neurosci, 2018. **12**: p. 936.
140. Sommer, Schmidt and George, *Hyperalgesia in Experimental Neuropathy Is Dependent on the Tnf Receptor 1.* Exp Neurol, 1998. **151**(1): p. 138-42.
141. Wagner, Janjigian and Myers, *Anti-Inflammatory Interleukin-10 Therapy in Cci Neuropathy Decreases Thermal Hyperalgesia, Macrophage Recruitment, and Endoneurial Tnf-Alpha Expression.* Pain, 1998. **74**(1): p. 35-42.
142. Challa, *Surgical Animal Models of Neuropathic Pain: Pros and Cons.* Int J Neurosci, 2015. **125**(3): p. 170-4.
143. Dunn, Kamocka and Mcdonald, *A Practical Guide to Evaluating Colocalization in Biological Microscopy.* Am J Physiol Cell Physiol, 2011. **300**(4): p. C723-42.
144. Grabinski, Kneynsberg, Manfredsson and Kanaan, *A Method for Combining Rnascope in Situ Hybridization with Immunohistochemistry in Thick Free-Floating Brain Sections and Primary Neuronal Cultures.* PLoS One, 2015. **10**(3): p. e0120120.
145. Pharris, Wu, Chen, Wang, Umulis, Weake, et al., *An Automated Workflow for Quantifying Rna Transcripts in Individual Cells in Large Data-Sets.* MethodsX, 2017. **4**: p. 279-88.
146. Wang, Flanagan, Su, Wang, Bui, Nielson, et al., *Rnascope: A Novel in Situ Rna Analysis Platform for Formalin-Fixed, Paraffin-Embedded Tissues.* J Mol Diagn, 2012. **14**(1): p. 22-9.
147. Chao, Pham, Steward and Gupta, *Chronic Nerve Compression Injury Induces a Phenotypic Switch of Neurons within the Dorsal Root Ganglia.* J Comp Neurol, 2008. **506**(2): p. 180-93.
148. Li, Guo, Liu, Sun, Chen and Zhao, *Association of Down-Regulation of Calcitonin Gene-Related Peptide and Substance P with Increase of Myocardial Vulnerability in Diabetic Neuropathic Rats.* Peptides, 2017. **96**: p. 1-7.

149. Wangzhou, Mcilvried, Paige, Barragan-Iglesias, Shiers, Ahmad, et al., *Pharmacological Target-Focused Transcriptomic Analysis of Native Vs Cultured Human and Mouse Dorsal Root Ganglia.* Pain, 2020. **161**(7): p. 1497-517.
150. Hackel, Krug, Sauer, Mousa, Bocker, Pflucke, et al., *Transient Opening of the Perineurial Barrier for Analgesic Drug Delivery.* Proc Natl Acad Sci U S A, 2012. **109**(29): p. E2018-27.
151. Parmantier, Lynn, Lawson, Turmaine, Namini, Chakrabarti, et al., *Schwann Cell-Derived Desert Hedgehog Controls the Development of Peripheral Nerve Sheaths.* Neuron, 1999. **23**(4): p. 713-24.
152. Haseloff, Dithmer, Winkler, Wolburg and Blasig, *Transmembrane Proteins of the Tight Junctions at the Blood-Brain Barrier: Structural and Functional Aspects.* Semin Cell Dev Biol, 2015. **38**: p. 16-25.
153. Obermeier, Daneman and Ransohoff, *Development, Maintenance and Disruption of the Blood-Brain Barrier.* Nat Med, 2013. **19**(12): p. 1584-96.
154. Alanne, Pummi, Heape, Grenman, Peltonen and Peltonen, *Tight Junction Proteins in Human Schwann Cell Autotypic Junctions.* J Histochem Cytochem, 2009. **57**(6): p. 523-9.
155. Miyamoto, Morita, Takemoto, Takeuchi, Kitano, Miyakawa, et al., *Tight Junctions in Schwann Cells of Peripheral Myelinated Axons: A Lesson from Claudin-19-Deficient Mice.* J Cell Biol, 2005. **169**(3): p. 527-38.
156. Katsuno, Umeda, Matsui, Hata, Tamura, Itoh, et al., *Deficiency of Zonula Occludens-1 Causes Embryonic Lethal Phenotype Associated with Defected Yolk Sac Angiogenesis and Apoptosis of Embryonic Cells.* Mol Biol Cell, 2008. **19**(6): p. 2465-75.
157. Morita, Sasaki, Furuse and Tsukita, *Endothelial Claudin: Claudin-5/Tmvcf Constitutes Tight Junction Strands in Endothelial Cells.* J Cell Biol, 1999. **147**(1): p. 185-94.
158. Sauer, Kirchner, Yang, Hu, Leinders, Sommer, et al., *Blood-Spinal Cord Barrier Breakdown and Pericyte Deficiency in Peripheral Neuropathy.* Ann N Y Acad Sci, 2017. **1405**(1): p. 71-88.
159. Bendszus and Stoll, *Technology Insight: Visualizing Peripheral Nerve Injury Using Mri.* Nat Clin Pract Neurol, 2005. **1**(1): p. 45-53.
160. Simeoli, Montague, Jones, Castaldi, Chambers, Kelleher, et al., *Exosomal Cargo Including Microrna Regulates Sensory Neuron to Macrophage Communication after Nerve Trauma.* Nat Commun, 2017. **8**(1): p. 1778.
161. Dubovy, Tuckova, Jancalek, Svizenska and Klusakova, *Increased Invasion of Ed-1 Positive Macrophages in Both Ipsi- and Contralateral Dorsal Root Ganglia Following Unilateral Nerve Injuries.* Neurosci Lett, 2007. **427**(2): p. 88-93.
162. Bruxel, Salatino-Oliveira, Akutagava-Martins, Tovo-Rodrigues, Genro, Zeni, et al., *Lphn3 and Attention-Deficit/Hyperactivity Disorder: A Susceptibility and Pharmacogenetic Study.* Genes Brain Behav, 2015. **14**(5): p. 419-27.
163. Sumbayev, Goncalves Silva, Blackburn, Gibbs, Yasinska, Garrett, et al., *Expression of Functional Neuronal Receptor Latrophilin 1 in Human Acute Myeloid Leukaemia Cells.* Oncotarget, 2016. **7**(29): p. 45575-83.
164. Shinder and Devor, *Structural Basis of Neuron-to-Neuron Cross-Excitation in Dorsal Root Ganglia.* J Neurocytol, 1994. **23**(9): p. 515-31.
165. Yatziv and Devor, *Suppression of Neuropathic Pain by Selective Silencing of Dorsal Root Ganglion Ectopia Using Nonblocking Concentrations of Lidocaine.* Pain, 2019. **160**(9): p. 2105-14.
166. Tracey, Woolf and Andrews, *Composite Pain Biomarker Signatures for Objective Assessment and Effective Treatment.* Neuron, 2019. **101**(5): p. 783-800.
167. Godel, Mautner, Farschtschi, Pham, Schwarz, Kronlage, et al., *Dorsal Root Ganglia Volume Differentiates Schwannomatosis and Neurofibromatosis 2.* Ann Neurol, 2018. **83**(4): p. 854-7.